BURIED GLACIAL GEOMORPHIC FEATURES IDENTIFIED USING 3D-SEISMIC DATA IN THE SOUTHWESTERN BARENTS SEA, ARCTIC NORWAY

A Thesis Presented to

the Faculty of the Department of Earth and Atmospheric Sciences

University of Houston

In Partial Fulfillment

of the Requirements for the Degree

Master of Science

By

Janet Kong

May 2018

BURIED GLACIAL GEOMORPHIC FEATURES

IDENTIFIED USING 3D-SEISMIC DATA IN THE

SOUTHWESTERN BARENTS SEA, ARCTIC NORWAY

Janet Kong

APPROVED:

Dr. Julia S. Wellner
Chair of Committee
University of Houston

Dr. Paul Mann
University of Houston

Dr. Alejandro Escalona
University of Stavanger

Dean, College of Natural Sciences and Mathematics

Acknowledgements

First and foremost, I would like to extend my sincerest gratitude to my advisor Dr. Julia S. Wellner for the opportunity of working with her for this degree. Her support, feedback, and advice have been fundamental to this project, and I am immensely grateful for all her help. I would also like to thank Dr. Alejandro Escalona, whose advice at the University of Stavanger in Norway has been invaluable, and the LoCrA project, which provided the data for this study. Special thanks to Dr. Paul Mann for all the resources and feedback in developing this thesis. I am very grateful to Andreas Habel, who graciously handled all connectivity issues between the University of Houston and the University of Stavanger, and Dr. Heather Bedle, who helped in many aspects regarding seismic data and interpretation.

I would like to thank all of my classmates and friends in Norway, who warmly welcomed me into their lives and homes during my time studying abroad. To my lab mates, thank you for all the feedback throughout the years. To my friends near and far, thank you for lending ears and shoulders when I needed it most, and providing advice, food, and laughter all the other times.

Finally, to my parents, without whom nothing would be possible - you two are my constant and steadfast *rocks* of support and encouragement. Thank you for everything.

BURIED GLACIAL GEOMORPHIC FEATURES IDENTIFIED USING 3D-SEISMIC DATA IN THE SOUTHWESTERN BARENTS SEA, ARCTIC NORWAY

An Abstract of a Thesis Presented to

the Faculty of the Department of Earth and Atmospheric Sciences

University of Houston

In Partial Fulfillment

of the Requirements for the Degree

Master of Science

By

Janet Kong

May 2018

Abstract

The Barents Sea covers one of the world's widest continental shelves, averaging 230 m in water depth. Over the last 3.5 My, the growth and retreat of ice sheets grounded on the shallow shelf and eroded up to 3000 m of sediment in the sea. Glacial erosion was particularly concentrated ~1.0 Ma, when multiple ice sheets converged and completely covered the Barents Sea for the first time. During this period of convergence, flowing ice beneath the ice sheet eroded the substrate and floating icebergs carved features into the sedimentary cover. As the ice sheet retreated, new sediment was deposited over the formerly ice-covered surface, preserving glacial features in the subsurface. Identification and analysis of the features beneath the modern-day seafloor can illustrate past ice-sheet characteristics arising before the last glacial maximum, such as paleo-ice flow direction or changes in flow patterns. This study interprets 3D-seismic grids covering ~2000 km^2 to identify glacial features on the Upper Regional Unconformity, a regional unconformity representing the onset of glaciation. This method of examining glacial history is exclusively possible in areas such as the Barents Sea, which has available 3D-seismic data of glaciated margins for the petroleum industry. A series of parallel, evenly-spaced lineations ranging from 0.5-9 km in minimum length, trending northwest-southeast, has been identified in the subsurface. In comparison to previous seafloor studies, which mark the direction of ice flow from the last glacial maximum (~20 ka), these northwest-southeast oriented lineations, trending ~340°-345°, indicate northwest paleo-ice flow and are interpreted to form parallel to ice flowing towards Bjørnøyrenna Trough, an area of extensive former ice stream activity. The seafloor surface shows

evidence of iceberg scours carved by drifting icebergs following ice-sheet retreat after the last glacial maximum. The subsurface also has evidence of iceberg scours, as well as other features including glacial lineations, erosional grooves, and meltwater depressions. Analysis of glacial geomorphology from seismic data can be used to examine paleo-ice flow and subglacial erosion. By comparison to features found in other glaciated environments, it can lead to a better understanding of current and future ice-sheet behavior.

Table of Contents

1. Introduction

1.1 Objectives

Examining glacial geomorphology in previously glaciated regions can reveal information regarding paleo-ice sheet dynamics and aid in understanding current ice margins. One area where detailed subsurface glacial geomorphology can be analyzed is the Barents Sea, where considerable 3D-seismic data have been collected for industry and academic use. This location is particularly interesting to study glacial geomorphology because many of the geomorphic features that were carved by ice sheets during the onset of glaciation have been preserved beneath the seafloor. The features preserved in the subsurface, such as meltwater-influenced depressions and erosional grooves, may have been directly eroded by ice sheets. In particular, the presence of seafloor iceberg scours and subsurface mega-scale glacial lineations (MSGLs) provides information regarding former ice sheet and ice stream dynamics in the previously-glaciated Barents Sea (Dowdeswell et al., 2007; Andreassen et al., 2008; Dowdeswell and Ottesen, 2013).

There are two primary objectives for this thesis. The first objective is to use industry 3D-seismic data in order to image subsurface glacial geomorphic features carved by formerly grounded ice sheets during glaciation of the Barents Sea. The second objective is to analyze subsurface glacial features in order to determine the direction of paleo-ice flow, and compare those features to similar ones in other glaciated or previously-glaciated margins.

1.2 Study Area

The study area is located within the southwestern portion of the Barents Sea off the northern coast of Norway (Figure 1.1). The Barents Sea is an epicontinental sea of the Arctic Ocean that encompasses 1.4 million km^2, and covers one of the widest continental shelves in the world, a shallow shelf which averages ~230 m in depth (Faleide et al., 1984; Vorren et al., 1989; Loeng, 1991). The sea is bounded by mainland Norway to the south, the Norwegian-Greenland Sea to the west, the Arctic Ocean to the north, and the Kara Sea to the east.

The seafloor of the Barents Sea is characterized by banks, troughs, and channels, influenced by the underlying bedrock and structural trends; the large troughs of the region empty into the Arctic Ocean and Norwegian Sea to the north and west, respectively (Winsborrow et al., 2010; Dowdeswell et al., 2016) (Figure 1.2). Modern water depths average 230-480 m, and large-scale features identified on the seafloor, such as MSGLs, glacial moraines, and iceberg plough marks. These are interpreted to have formed from dynamic ice sheet changes during and after the last glacial maximum (LGM) (Dowdeswell et al., 2007; Andreassen et al., 2008; Knies et al., 2009; Winsborrow et al., 2010).

Repeated cycles of ice-sheet advance and retreat had increased melting through ice streams, areas of fast-flowing ice carrying meltwater and sediment, which carved elongated troughs into the underlying sediments and bedrock (Vorren and Laberg, 1997; Andreassen et al., 2008). The largest and deepest of these troughs in the southwestern Barents Sea is the Bjørnøyrenna Trough, a northwest-southeast trending trough measuring 750 km long, roughly 150-200 km wide, and varying in water depth between 300-500 meters (Solheim and Elverhøi, 1993; Winsborrow et al., 2010; Laberg et al., 2012) (Figure 1.2). This trough, an area of extensive former ice-stream activity, extends past the western continental shelf break into a large trough mouth fan (TMF) known as the Bjørnøya TMF. TMFs are depocenters of sediments from different troughs through which sediment has been transported and ultimately deposited (Vorren et al., 1988; Andreassen et al., 2008). In areas of ice-stream activity, the direction of paleo-ice flow can be examined by identifying MSGLs, which form parallel to the direction of ice flow. Regional seafloor studies have mapped the presence of MSGLs following ice advance and retreat during the LGM (Figure 1.3), but few studies have mapped subsurface MSGLs in the Barents Sea.

The role of ice streams over long timescales is difficult to analyze in present-day ice sheets (e.g., West Antarctic Ice Sheet and Greenland Ice Sheet) because of the shorter timescale of observations (Winsborrow et al., 2010). However, the paleo-record can offer a significant addition of information in previously glaciated areas, such as the Barents Sea, because of the preservation geomorphic features in the subsurface. Analysis of subsurface glacial features, and comparison to seafloor features as well as features in other glaciated margins, can aid in understanding ice-sheet dynamics.

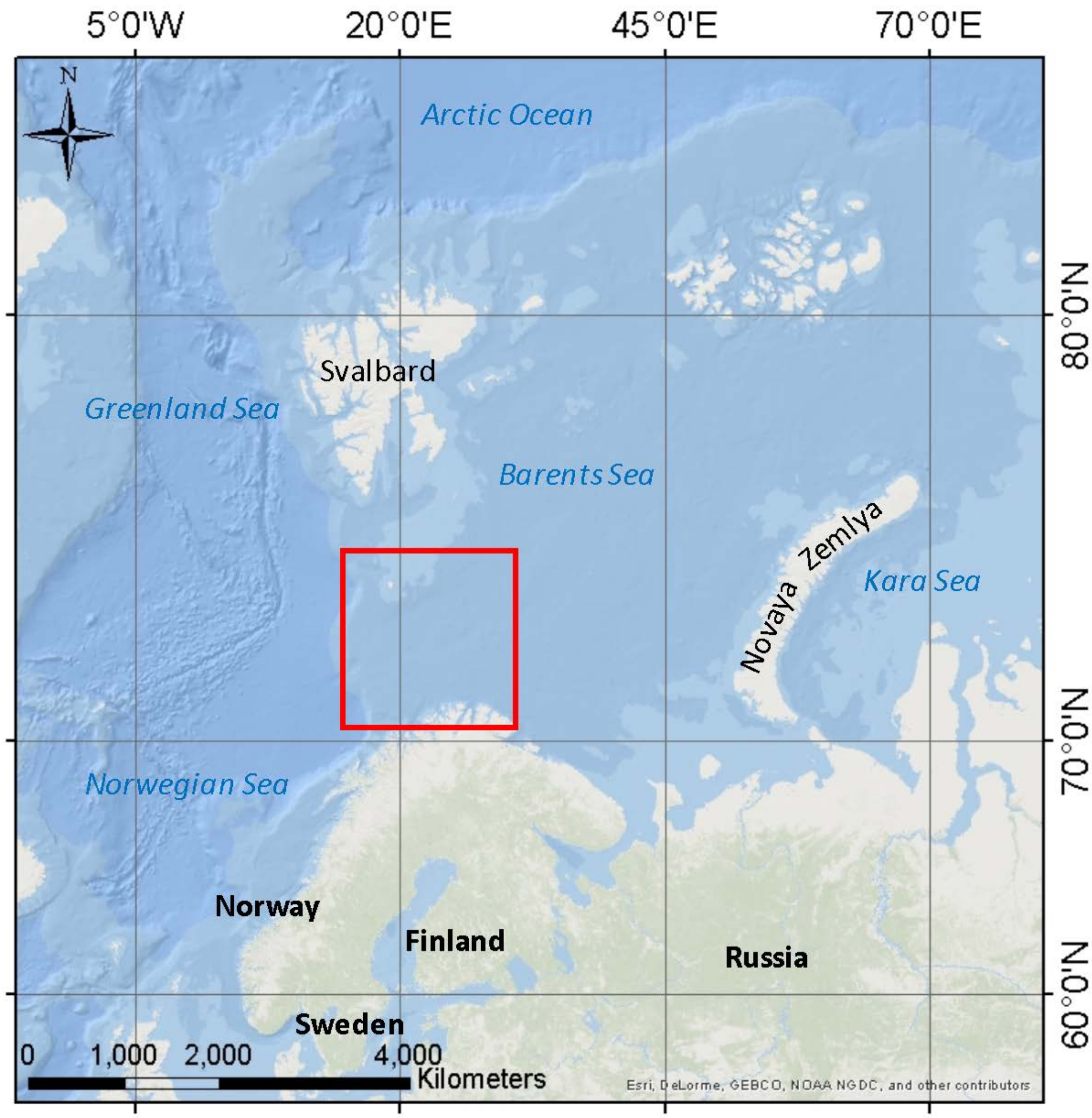

Figure 1.1. *Location map of the Barents Sea. The archipelagos of Svalbard (Norway) and Novaya Zemlya (Russia) delimit the northwest and eastern edge of the Barents Sea. This study focuses on the southwestern Barents Sea, with the study area outlined in red.*

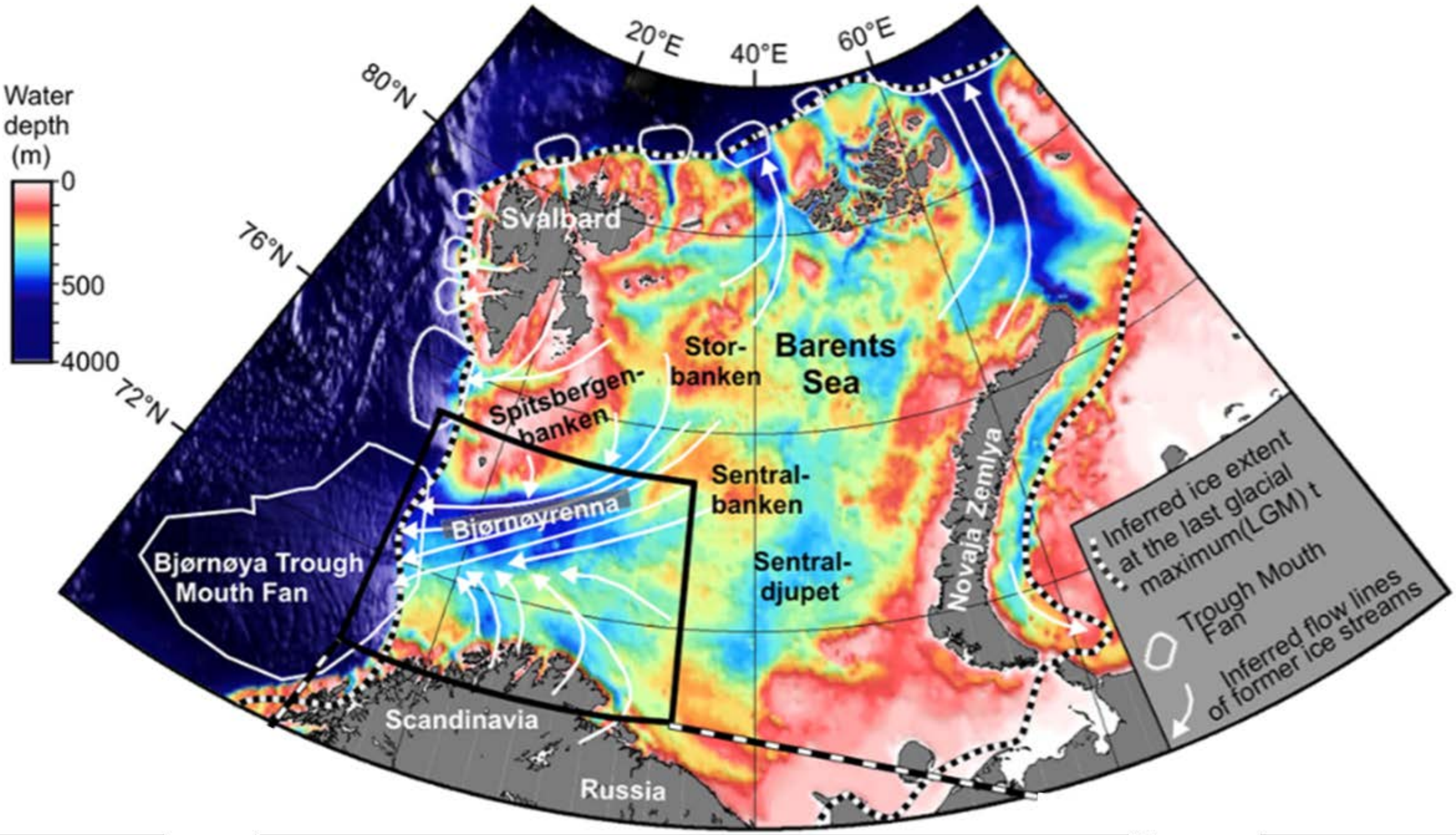

Figure 1.2. *IBCAO bathymetry map showing Bjørnøyrenna Trough and the Bjørnøya TMF in the southwestern Barents Sea (outlined in black). White arrows indicate flow lines of major ice streams that once flowed north into the Arctic Ocean and west into the Norwegian Sea (modified from Andreassen et al., 2008). The black-and-white line represents the inferred ice sheet extent during the LGM ~20,000 years ago.*

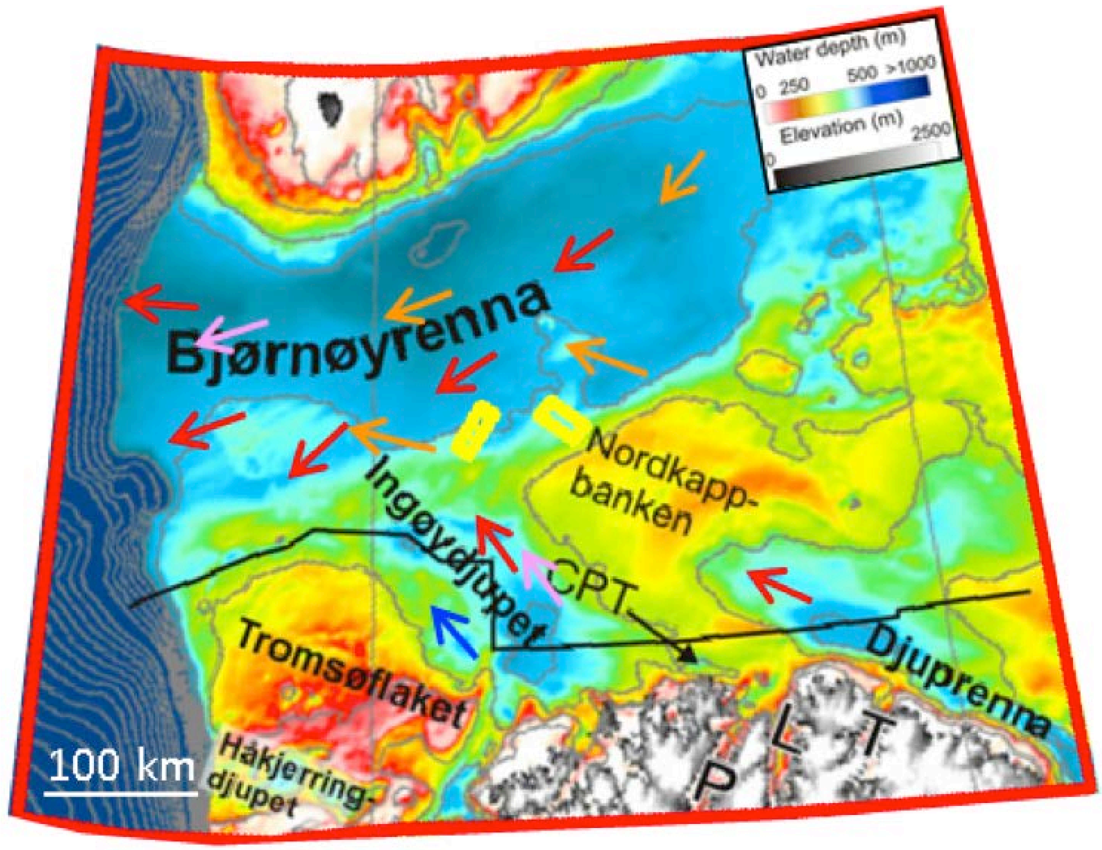

Figure 1.3. *Seafloor studies of MSGLs in the southwestern Barents Sea (insert from Figure 1.2) mapping the direction of ice flow from the LGM. Bathymetry map from Winsborrow et al., 2010. Yellow boxes outline 3D-seismic grids used in this study. Different colored arrows from several different published authors. Dark blue = Ostanin et al., 2005; Red = Winsborrow et al., 2010; Orange = Rebesco et al., 2011; Light pink = Laberg et al., 2012.*

2. Background

2.1 Geologic Background and Structural Setting of the Barents Sea

The Barents Sea continental shelf covers the northwestern corner of the Eurasian continental shelf and encompasses a few of the world's deepest sedimentary basins (Faleide et al., 1984; Faleide et al., 1993; Worsley, 2008). While the eastern part of the Barents Sea is linked to the tectonic history of the Uralian Orogeny (Worsley, 2008;

Smelror et al., 2009), the western portion, the focus of this study, includes a complex tectonic history that led to the development of structural highs, basins, and platforms in the southwestern Barents Sea (Faleide et al., 1984; Smelror et al., 2009) (Figure 2.1).

The western part of the Barents Sea has been affected by several rifting episodes, leading to the break-up of the Eurasian plate, as well as major continental collisions (Smelror et al., 2009). Faleide et al. (1993) have separated the post-Caledonian history of the western Barents Sea into three rift periods: Late Devonian-Carboniferous, Middle Jurassic-Early Cretaceous, and early Tertiary, with tectonic pulses in each phase.

Beginning in the Late Devonian, regional uplift followed by rifting created several half-grabens during a period of regional sea-level rise (Worsley, 2008). This rifting continued through the Early Carboniferous to create extensional basins with syn-rift deposits (Breivik et al., 1998). In the mid-Carboniferous, a major regional uplift followed by renewed rifting led to major subsidence and development of several deep basins, such as the Nordkapp and Tromsø basins (Worsley, 2008).

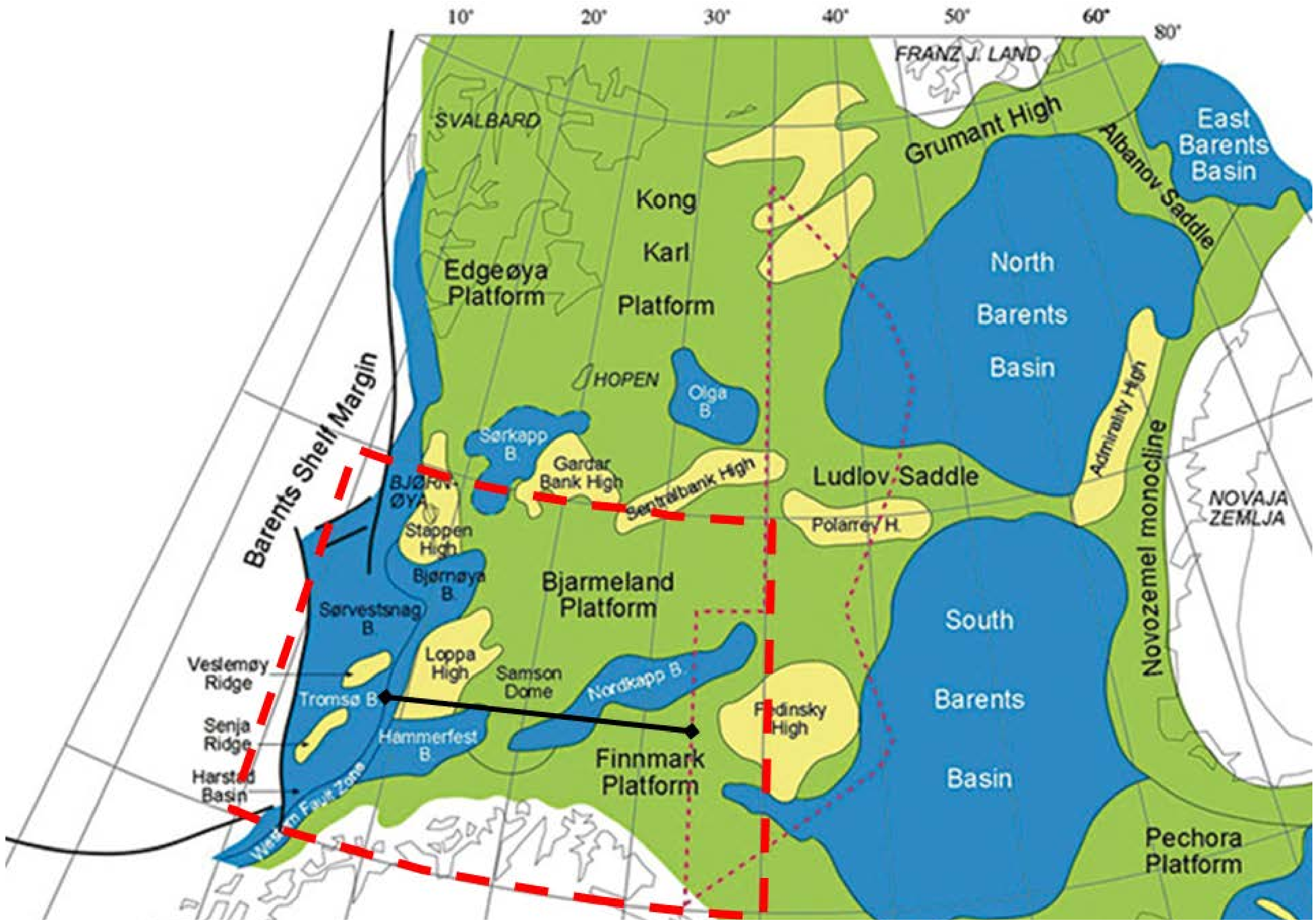

Figure 2.1. *Structural elements map of the Barents Sea. In this map, green indicates platforms, yellow indicates structural highs, and blue indicates basins, with study area of southwestern Barents Sea outlined in dashed red (modified from Worsley, 2008). Solid line (west-east) shows location of lithology (Figure 2.3).*

In the Middle Jurassic-Early Cretaceous, regional extension and strike-slip movement created rift basins such as the Harstad, Tromsø, and Bjørnøya rift basins (Faleide et al., 1993). While this continued rifting occurred, numerous faults arose and separated the structural highs, and the southwestern Barents Sea continued to subside in response to the rifting and faulting motion (Faleide et al., 1993).

During the Late Mesozoic-Early Cenozoic, tectonic events created deep sedimentary basins (Breivik et al., 1998). Young passive margins bordering the Barents Sea were created during the Cenozoic opening of the Norwegian-Greenland Sea to the west and of the Eurasia Basin to the north (Faleide et al., 1984; Faleide et al., 1993). This opening of the Norwegian-Greenland Sea led to considerable uplift in the Barents Sea, and subsequent erosion removed much of the Cenozoic rock record in the southwestern Barents Sea, creating an unconformable boundary between Cretaceous and Paleogene sequences (Dimakis et al., 1998; Faleide et al., 1993).

Within the Neogene, the Plio-Pleistocene uplift and erosion of the western continental shelf caused a rapid increase in erosion (Dimakis et al., 1998; Smelror et al., 2009). The entire Barents Sea shelf was repeatedly eroded as large-scale glaciations moved large amounts of sediment into submarine TMFs (Smelror et al., 2009). Glacial erosion removed roughly 500-600 meters of sediment from the banks, and as much as 1000-1100 meters of sediment in the deeper troughs of the Barents Sea (Laberg et al., 2012). The Barents Sea has been covered by a layer of glacigenic and glaciomarine Quaternary sediments from subsequent glacial and interglacial cycles (Vorren et al., 1989; Faleide et al., 1996). While regional lithology suggests that the upper layer of Quaternary sediments are mostly marine deposits or shale (Figure 2.3), shallow boreholes drilled near the island of Bjørnøya (Figure 2.1) indicate that the layer of unlithified sediments is dominated by diamictons, interpreted as till (Sættem et al., 1992; Faleide et al., 1996). A combination of these interpretations would establish that the uplifted and eroded section separates Cretaceous, shale bedrock from a mix of glaciomarine and marine till and shale. Today, this sea overlies an intracratonic basin system that is bounded by passive continental margins to the west and north, and has been covered with glacigenic and glaciomarine sediments from repeated glacial cycles during the Quaternary (Vorren et al., 1989; Vorren et al., 1991; Winsborrow et al., 2010).

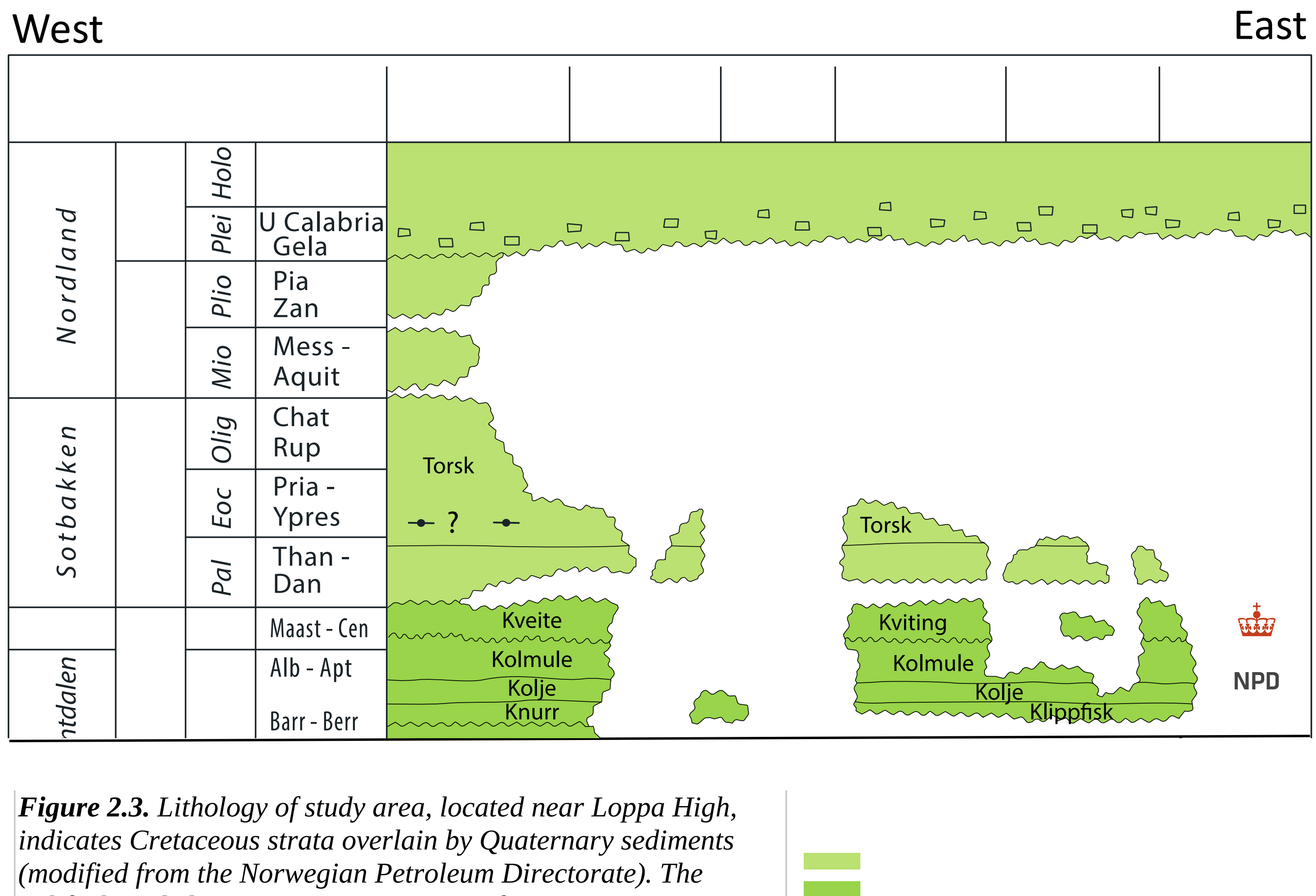

Figure 2.3. *Lithology of study area, located near Loppa High, indicates Cretaceous strata overlain by Quaternary sediments (modified from the Norwegian Petroleum Directorate). The uplifted/eroded area represents an unconformity separating Cretaceous shale bedrock below from a mix of glaciomarine and marine till and shale above (location from Figure 2.1).*

2.2 Glacial History

2.2.1 Glacial-interglacial Cycles

The past 3 My include some of the largest climate variations for glacial-interglacial cycles documented in $\delta^{18}O$ records (Raymo et al., 2006). The cycling between warmer periods (interglacial cycles) and colder periods (glacial cycles) is represented globally by light isotopic events (lower ^{18}O values) and heavy oxygen isotopic events (higher ^{18}O values), respectively (Dokken and Jansen, 1999). Additionally, sediment cores can be examined for pulses of iceberg-rafted debris (IRD), which occur when ice rafting of icebergs deposits additional sediment into the sedimentary record during glacial periods (Tütken et al., 2002). In the marine oxygen isotope curve (Liseicki and Raymo, 2005), each marine isotope stage (MIS), or alternating periods of warmer and cooler periods of Earth's paleoclimate, are numbered: interglacial cycles are odd-numbered and glacial cycles are even-numbered (Figure 2.4). The most recent glaciated period is represented by MIS 2, which documents the $\delta^{18}O$ levels during the LGM roughly 20,000 years ago, when global sea level was roughly 120 m below present-day sea level (Rohling et al., 1998).

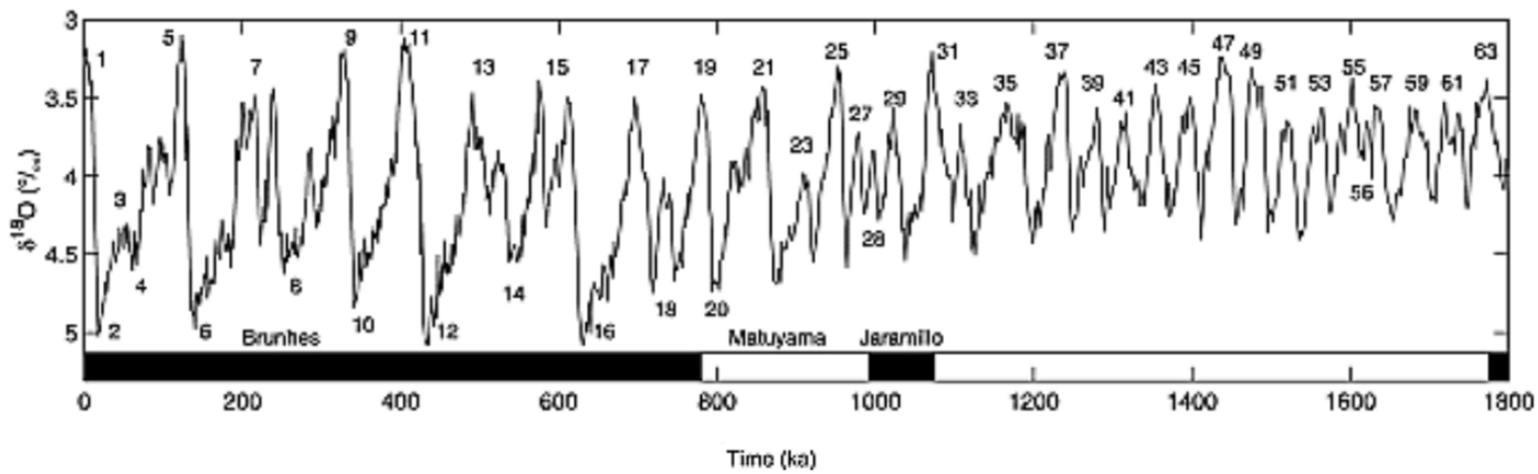

Figure 2.4. *Benthic δ^{18}O curve, showing time in thousands of years and δ^{18}O levels in per mil, calculated using benthic foraminifera from 57 globally distributed deep-sea sediment cores. Marine isotope stages are numbered, with even numbers representing glacial periods (colder) and odd numbers representing interglacial periods (warmer) (Lisiecki and Raymo, 2005).*

In the Barents Sea, glaciations that reached the western continental shelf edge (west of Svalbard) align with global glacial-interglacial cycles, and can be illustrated with a glaciation curve (Figure 2.5). The extent of the glaciations are based on records of IRD from sediment cores west of Svalbard, shown covering the last ~150,000 years (Ingólfsson and Landvik, 2013). However, the purpose of this study is to examine the ice-sheet advance during the onset of glaciation much further back in time, and will therefore require the use of seismic data to study ice sheet advance from subsurface features.

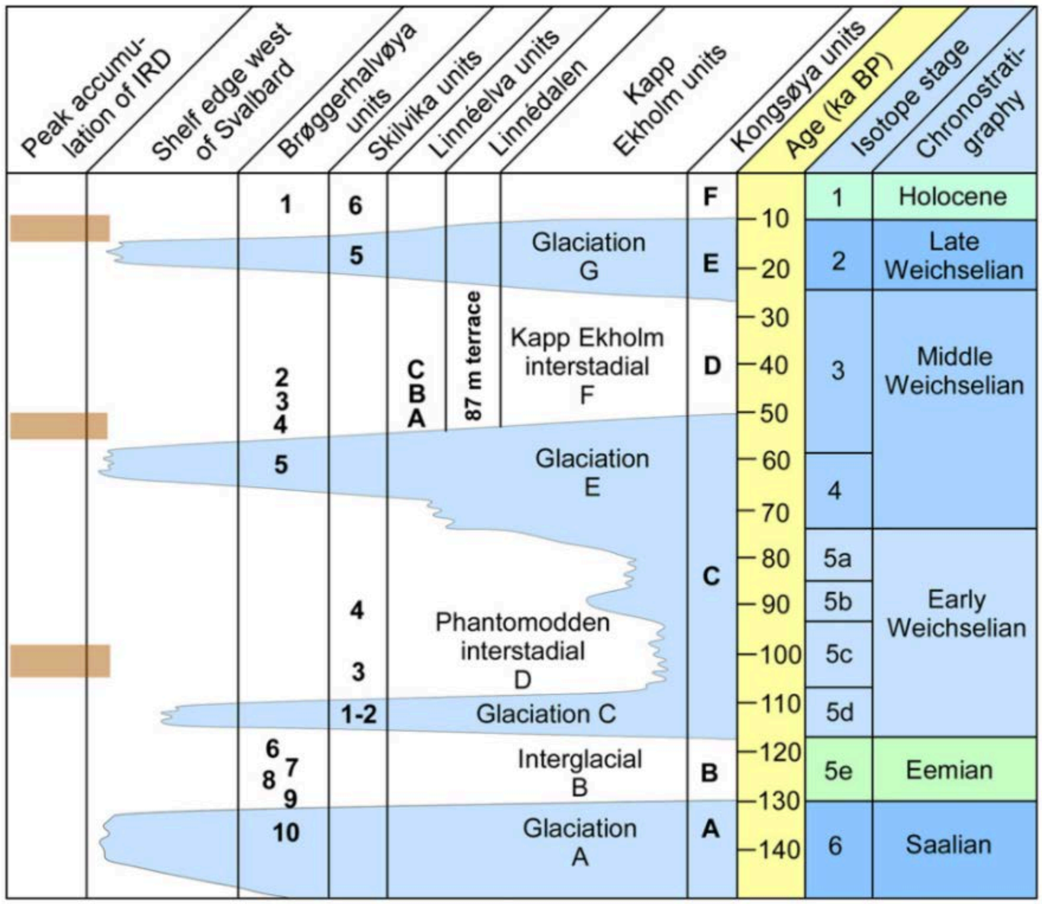

Figure 2.5. *Glaciation curve showing time-distance relationship of ice extent in the northern Barents Sea (close to Svalbard). Glaciation G matches up with MIS2, or the LGM (from Ingólfsson and Landvik et al., 2013, modified after Mangerud et al., 1998).*

2.2.2 Ice-sheet History in the Barents Sea

The study area is located in the southwestern Barents Sea, which was influenced by the growth of three different ice sheets, the Fennoscandian ice sheet, Barents Sea ice sheet, and Kara Sea ice sheet (Svendsen et al., 2004; Larsen et al., 2006). The Fennoscandian ice sheet began growing from the northern, mountainous region of mainland Norway, and the first large-scale glaciation in the Northern Hemisphere (~1.0 Ma) might be around the time the ice sheet first expanded to the shelf edge (Knies et al., 2009). The Barents Sea ice sheet started from the Norwegian archipelago of Svalbard. At its largest, this ice sheet expanded and reached the continental shelf break, increasing sediment delivery and creating large, submarine trough mouth fans to the north and west of the Barents Sea (Ottesen et al., 2005; Knies et al., 2009). The Kara ice sheet covers the Russian archipelago of Novaya Zemlya; at the maximum extent during the Quaternary, this ice sheet may have covered parts of European Russian and Western Siberia (Mangerud et al., 2002; Knies et al., 2009).

The Barents Sea experienced three different major phases of ice growth in the last 3.5 million years (Sejrup et al., 2005; Knies et al., 2009). Phase 1 (3.5 - 2.4 Ma) was an initial growth phase where the three ice sheets began to grow on mainland Scandinavia, Svalbard, and Novaya Zemlya, respectively. During this phase, ice began growing in the mountainous regions of the subaerially exposed Barents Sea, ranging in elevation from 1,000 to 2,500 km, which corresponds to the onset of Northern Hemisphere Glaciation (Knies et al., 2009), and illustrated by frequent pulses of iceberg-rafted debris in borehole data (Sættem et al., 1992).

Phase 2 (2.4 - 1.0 Ma) was a transitional growth phase in which colder, more intense glaciations alternated with warmer, longer interglacial cycles. The western Svalbard margin shows a decrease in IRD, which has been interpreted as partial disintegration of the ice margins (Knies et al., 2009). During this transitional period, the Barents Sea ice sheet grew considerably and reached the northern Kara Sea, possibly merging to form an even large ice sheet, and a global shift in cyclicity from 100,000 years to 40,000 years occurred; this switch from 100,000 year glacial cycles to 40,000 year glacial cycles is attributed to changes in Earth's obliquity and variations in Earth's orbit (Faleide et al., 1996; Knies et al., 2009; Huybers, 2009).

The third phase (<1.0 Ma) represented a large-scale intensification of glaciation where the ice sheets not only expanded but also converged and covered the entire Barents Sea (Knies et al., 2009) (Figure 2.5). Modellers suggest that around ~1 Ma, large parts of the previously subaerially exposed Barents Sea first became a submarine shelf sea (Dimakis et al., 1998; Butt et al., 2002). This phase marks the onset of full-scale glaciation in the Barents Sea, when grounded ice advanced to the northern and western shelf break, and can be used to study the processes that form subglacial geomorphic features in the Arctic.

2.3 Upper Regional Unconformity (URU)

Since the early Pleistocene, glacial ice has extended multiple times to the continental shelf break off the northern coast of Norway and western coast of Svalbard (Sættem et al., 1992; Faleide et al., 1996; Landvik et al., 1998). These repeated glaciations eroded sediment from the surface of the continental shelf, and deposited these sediments in TMFs located at the continental shelf break (Solheim et al., 1996; Ottesen et al., 2005). A regional unconformity, commonly referred to as the Upper Regional Unconformity (URU), carved by ice sheets developed over the entire shelf from repeated cycles of ice sheet advance and retreat, and represents the erosional base of continental shelf glaciations in the Barents Sea (Solheim and Kristoffersen, 1984; Vorren et al., 1989; Vorren et al., 2011).

In the southwestern Barents Sea, glacigenic sediments are 0-300 meters thick on the shelf, and thicken westwards towards the shelf break, where sediments can be as thick as 900-1000 meters (Vorren et al., 1991; Solheim et al., 1996). In seismic data, the URU is a bright reflector that separates variously dipping stratified bedrock below from a relatively thin and continuous cover of sub-horizontal glacigenic and glaciomarine Quaternary sediments (Vorren et al., 1991; Solheim et al., 1996; Andreassen et al., 2008). This unconformity is interpreted to represent the base of glacial sediments in the Barents Sea, separating pre-glacial bedrock from a cover of glacial deposits, and likely represents the erosional base for several continental shelf glaciations from which large volumes of sediment were eroded and deposited in submarine depocenters off the western continental shelf break (Faleide et al., 1996; Andreassen et al., 2008; Smelror et al., 2009).

Previous studies by Sættem et al. (1992) measured the paleomagnetic polarity of glacigenic and glaciomarine sediments from shallow boreholes close to the western continental shelf break. The magnetization direction of the upper sediments were all the same and all positive, implying that these sediments were deposited after the Bruhnes Normal Polarity Chron (Sættem et al., 1992). Because these sediments all have the same normal polarity above the unconformity, the oldest age for these sediments above the URU was tentatively dated at the Bruhnes-Matuyama boundary (790 ka) (Sættem et al., 1992). In the global sea-level curve, the Bruhnes-Matuyama boundary correlates roughly to MIS 20.

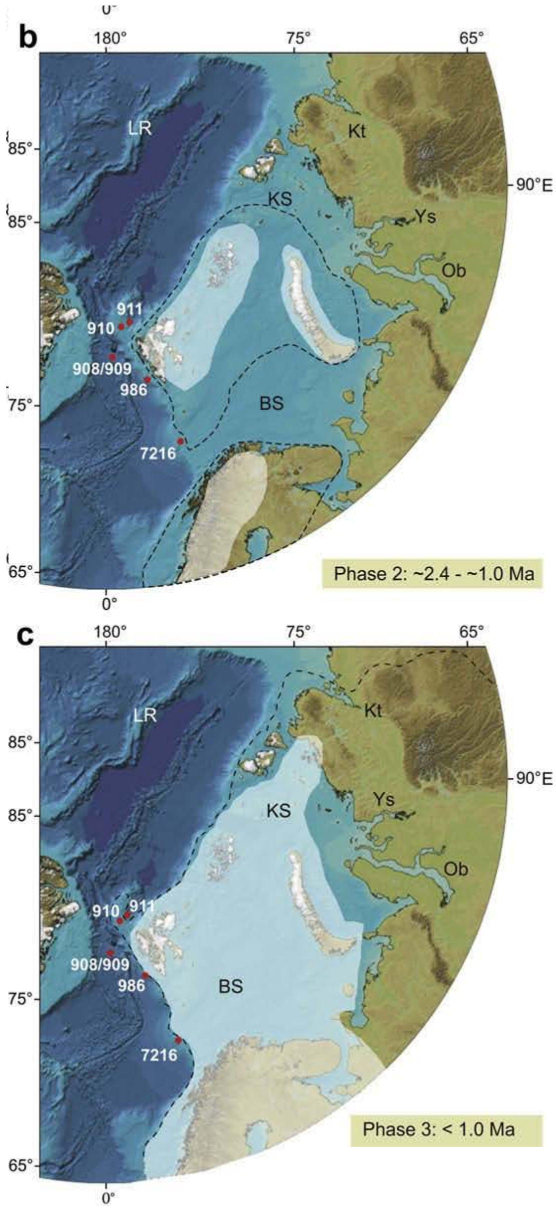

Figure 2.5. *Schematic drawing of the three different phases of ice sheet growth in the Barents Sea (BS) during the Plio-Pleistocene, where white polygons show interpreted ice sheet minimums, while black dashed lines show inferred maximums. Red dots are shallow boreholes from Knies et al., 2009. (a) Phase 1 (~3.5-2.4 Ma) is representative of an initial growth period (b) Phase 2 (~2.4-1.0 Ma) shows the transitional period and (c) Phase 3 (<1.0 Ma) marks the first large-scale glaciation when ice first converged and covered the entire Barents Sea (modified from Knies et al., 2009).*

Additionally, amino acid analyses were conducted to examine the carbonate fossil ages in order to estimate more accurate sediment dates. A measured aIle/Ile ratio was ultimately compared to similar ratios from foraminifera in Eemian sediments in the Norwegian trench, which estimate an age of 290-440 ka (Sættem et al., 1992; Sejrup et al., 1989). This led Sættem et al. (1992) to determine the oldest age of the sediments above the URU to be ~440 ka.

2.4 Glacial Processes and Landforms

Glacial ice has extended multiple times to the continental shelf break of the Barents Sea since the early Pleistocene (Sættem et al., 1992; Faleide et al., 1996; Sejrup et al., 2005; Andreassen et al., 2008; Knies et al., 2009; Jakobsson et al., 2014). This repeated process of ice sheet growth and retreat causes sub-glacial erosion beneath the ice sheet, and continuously carves glacial geomorphic features into the underlying sediment or bedrock (Ottesen et al., 2005; Dowdeswell et al., 2007; Andreassen et al., 2008; Dowdeswell and Ottesen, 2013). The presence of these features, can provide detailed information regarding past ice sheet behavior, and play a critical role in understanding future behavior (Andreassen et al., 2004; Dowdeswell et al., 2007; Andreassen et al., 2008; Laberg et al., 2009; Hogan et al., 2010).

Previous studies have used swath bathymetry images, 2D, and 3D-seismic data to examine submarine glacial geomorphology on the seafloor off the western and northern coasts of Norway (Andreassen et al., 2004; Dowdeswell et al., 2007; Andreassen et al., 2008; Hogan et al., 2010). Glacial geomorphology includes the study of different glaciallycarved landforms, which are then used to interpret processes regarding how ice sheets and glaciers move, and how these ice masses transport, erode, and deposit sediment (Menzies, 2009). Among these different types of glacial geomorphic landforms include MSGLs, grounding-zone wedges, transverse ridges, and iceberg ploughmarks (Dowdeswell et al., 2007) (Figure 2.6).

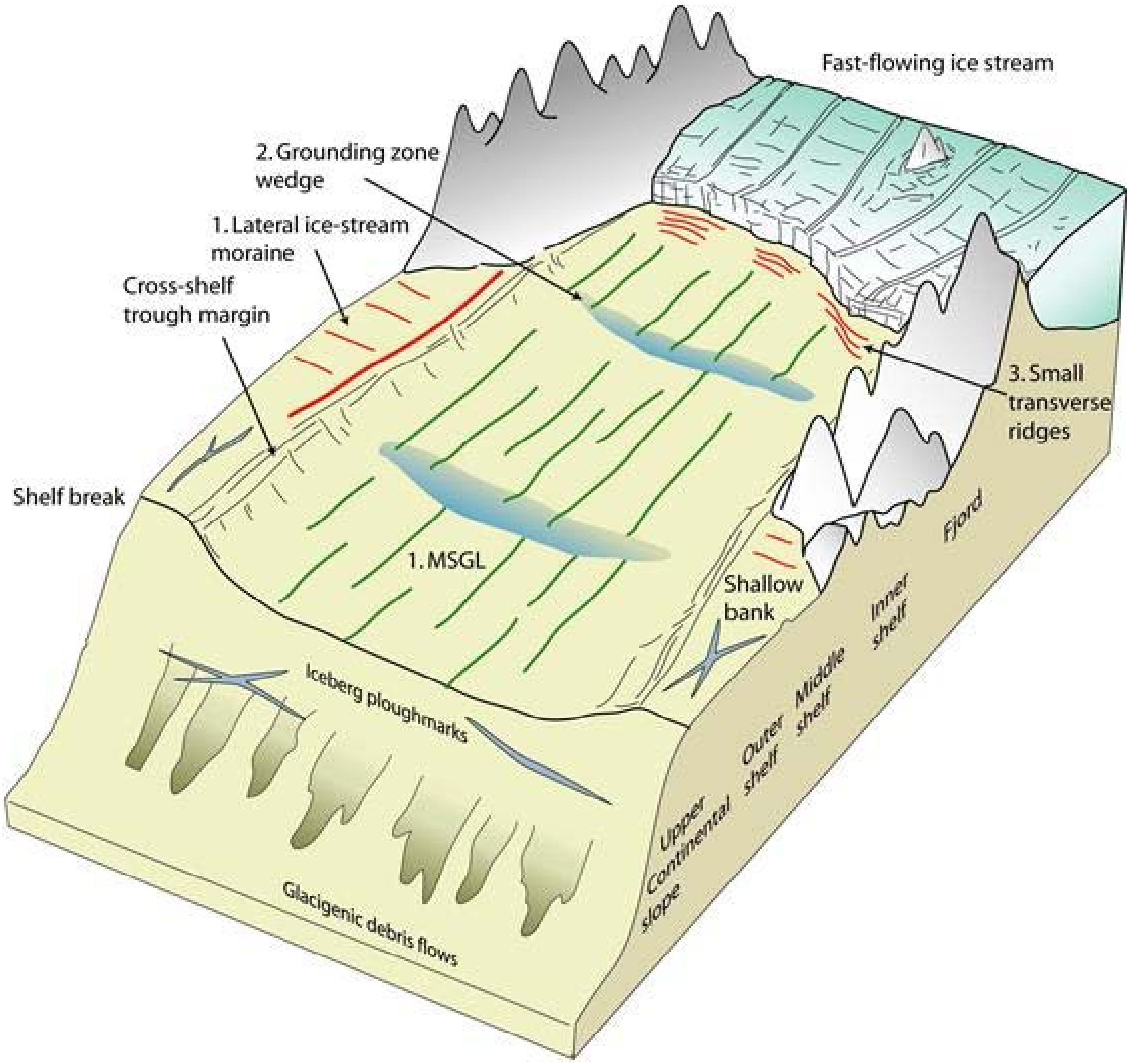

Figure 2.6. *Ice stream assemblage of glacial geomorphic features across a continental shelf (from Dowdeswell et al., 2016). Both iceberg ploughmarks and MSGLs will be analyzed further in the discussion.*

While seafloor landforms can reveal information regarding ice flow patterns at the LGM, preserved subsurface glacial landforms can provide more information about the onset of glaciation at the beginning of ice expansion in the Barents Sea. In particular, examination of buried landforms that have been preserved through periods of deposition can indicate past ice-sheet activity on the continental shelf from the onset of glaciation, when the Fennoscandian, Barents Sea, and Kara Sea ice sheets first merged and covered the entirety of the Barents Sea (Svendsen et al., 2004; Larsen et al., 2006; Knies et al., 2009; Jakobsson et al., 2014). Buried landforms have been identified off the western coast of Norway on the Norwegian margin by tracing horizons using 3D-seismic data (Dowdeswell et al., 2007). The surfaces created were then used to identify many of the same features found on the seafloor in the southwestern Barents Sea, including streamlined MSGLs, and iceberg-keel produced ploughmarks (Dowdeswell et al., 2007). This method has proven to successfully identify glacial geomorphic features found beneath the seafloor, and can be applied to the study area in the southwestern Barents Sea in order to better understand the onset of glaciation in the Arctic Barents Sea.

3. Dataset and Method

3.1 Seismic Data

The 3D-seismic dataset used in this study was obtained from a larger university consortium known as the LoCrA Project (Lower Cretaceous basin studies in the Arctic), which is managed by Professor Alejandro Escalona at the University of Stavanger in Norway and Professor Snorre Olaussen at the University Centre in Svalbard. These data were acquired and processed by several petroleum companies and the Norwegian Petroleum Directorate for industry and university use. Extensive 2D-seismic lines were mapped to trace the regional extent of the URU. Additionally, two 3D-seismic grids, SG9810 and SG9804, were used to map both the seafloor and URU, and were ultimately used to identify glacial geomorphic features for further analysis (Figure 3.1).

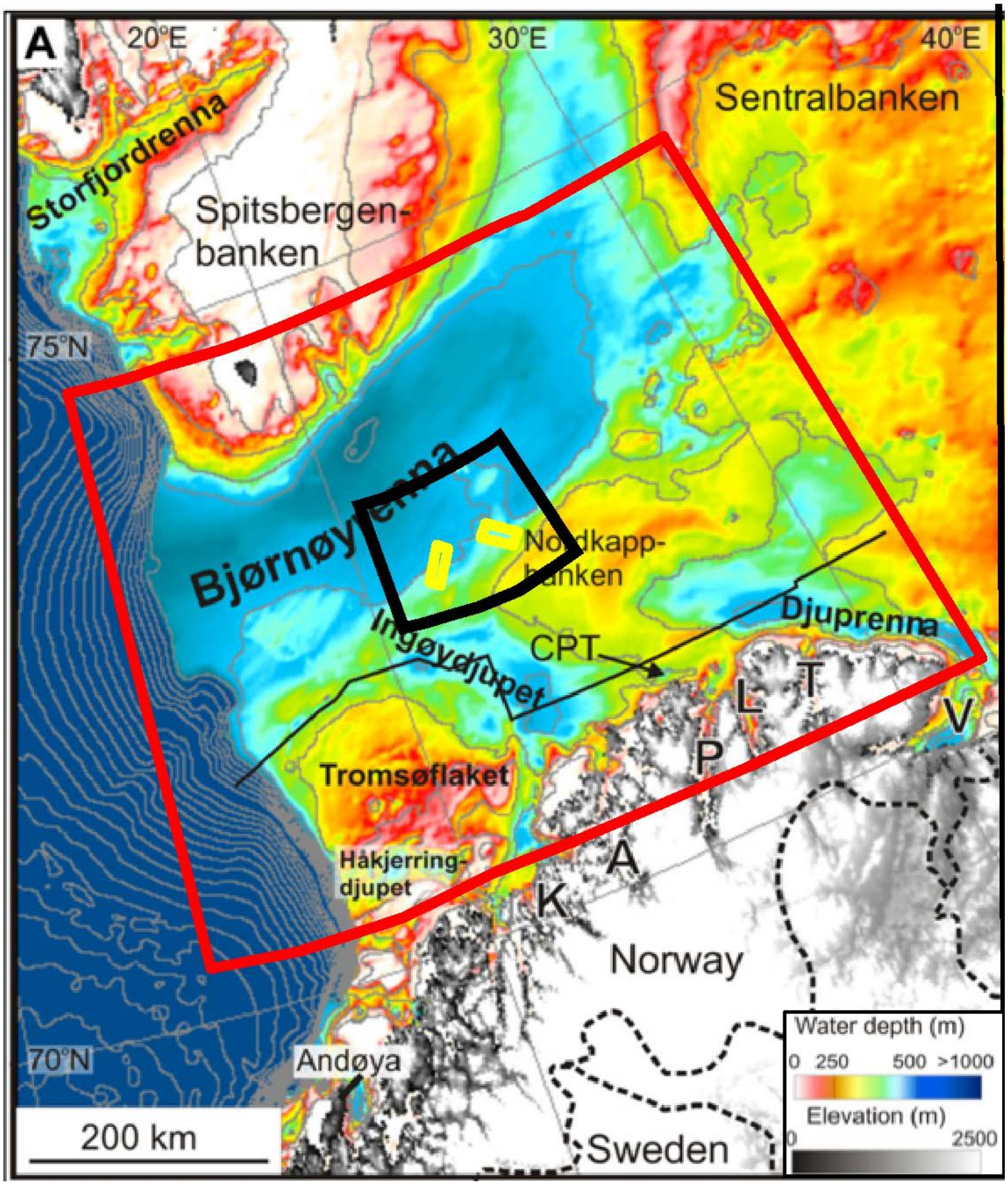

Figure 3.1. *(A) Bathymetry map of the Barents Sea, with the southwestern study area outlined in a red box (map modified from Winsborrow et al., 2010) and yellow boxes outlining 3D-seismic data used. Black box used in summary Figure 5.14. Figure continued on next page.*

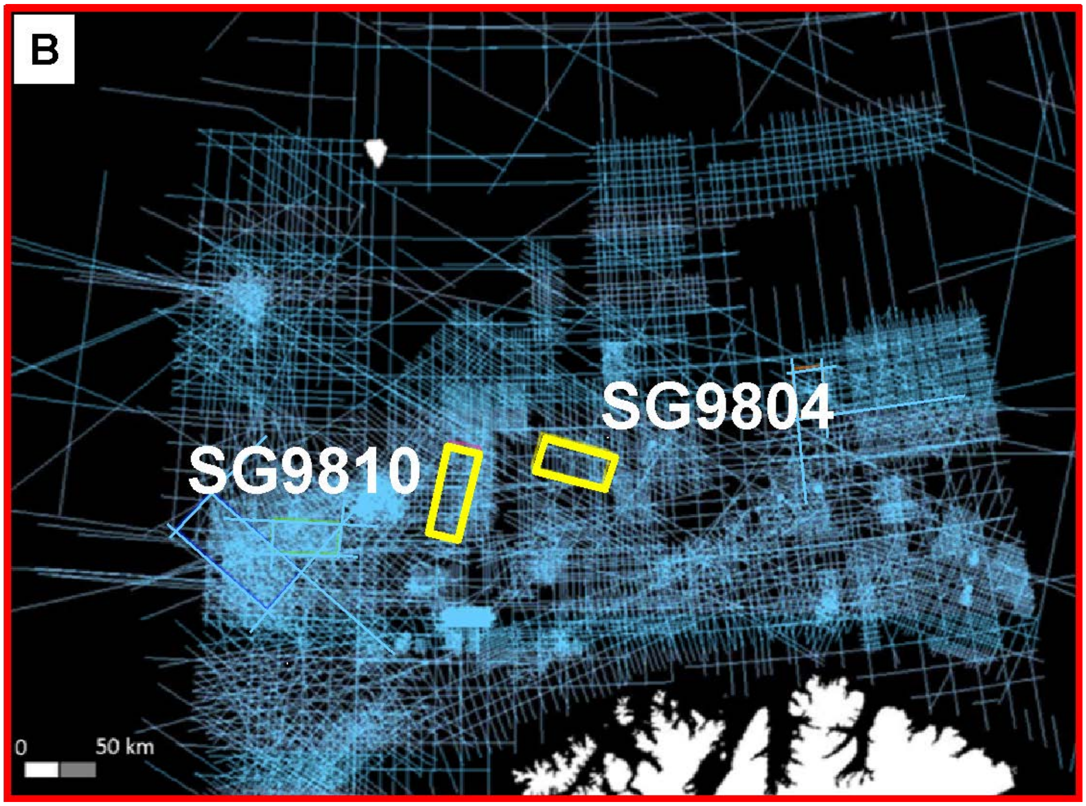

Figure 3.1. (continued) *(B) Inset of red box outlined in (A). Data used for interpretation included light blue lines (2D seismic lines), and yellow boxes (3D-seismic grids SG9810 (left) and SG9804 (right) used in this study).*

The western 3D cube, SG9810, covered a total area of roughly 970 km^2 (~371 mi^2) and is post-stack time-migrated (Carrillat et al., 2005; Sayago et al., 2012), collected in 1998 by Saga Petroleum ASA. This data is measured in two-way travel time (TWT) and has normal polarity, with a bin size of 25x25 m (82x82 ft) and a sampling interval of 4 ms (Rüther et al., 2011; Sayago et al., 2012). The inlines for this cube measure roughly 62 km, and crosslines about 21 km. A dominant frequency of 40 Hz provides a vertical resolution (one quarter of the wavelength) of roughly 11 m, and a spatial sampling distance of 12.5 m provides a horizontal resolution of roughly 12 m (Rüther et al., 2011). A sound velocity of 1800 m/s was used as a rough estimate to calculate the thickness of the glacigenic sediment overlying the unconformity and to convert TWT into depth in meters (Sættem et al., 1992).

3D-seismic cube SG9804 covers roughly 1020 km^2, and was collected in 1998 by Saga Petroleum ASA and measured in two-way travel time (TWT) (Rafaelsen et al., 2002; Rüther et al., 2011). In normal polarity the positive peak or increased acoustic impedance is represented in black, while the negative trough or decreased acoustic impedance is represented in red (Figure 3.3). A dominant frequency of 40 Hz provides a vertical resolution of roughly 11 m and a horizontal resolution of roughly 11 m (Rafaelsen et al., 2002; Khan, 2013). The inlines for 3D cube SG9804 measure roughly 25-48 km, and the crosslines range from 12-23 km (Figure 3.2). The dominant frequency of the glacigenic section above the URU is about 40 Hz in the shallower portion of the 3D-seismic grid. The same sound velocity, 1800 m/s, was used to calculate the thickness of the glacigenic and glaciomarine sediments as in grid SG9810 (Sættem et al., 1992; Rafaelsen et al., 2002).

3.2 Seismic Artifacts

Artifacts in seismic data are not representative of real geological structures, but are often created during seismic acquisition or seismic processing. One of the most commonly occurring artifacts is the acquisition footprint, which is defined as a noise pattern correlating to the position of sources and receivers on the earth during acquisition (Marfurt et al., 1998). These footprints can be created from various irregularities including seismic noise or inconsistent spatial patterns or geometries during acquisition (Marfurt et al., 1998, Bulat 2005). These acquisition footprints manifest as parallel ridges and grooves that run parallel to the inlines, and appear in every surface created using 3D-seismic (Figure 3.2).

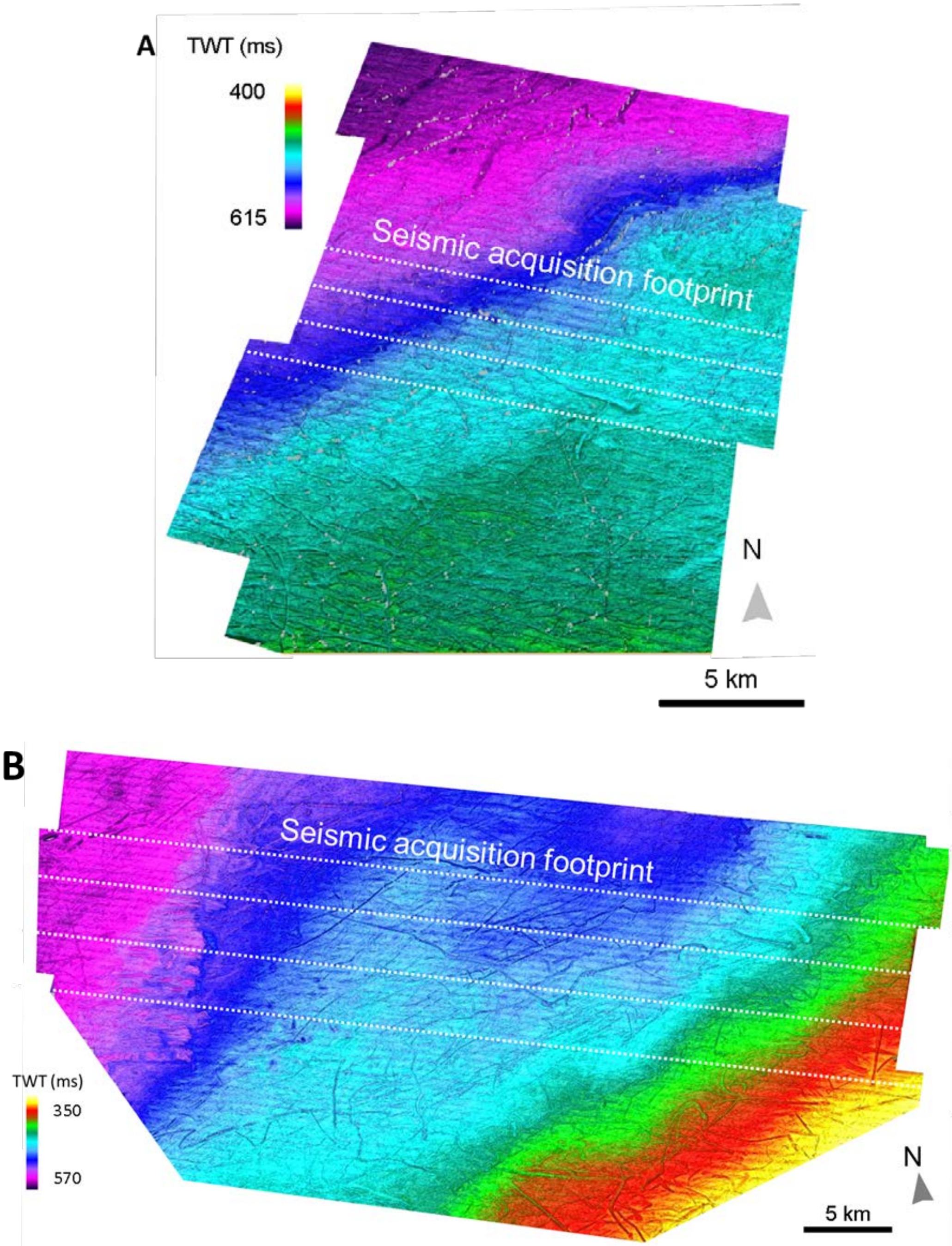

Figure 3.2. *Shaded bathymetry surfaces of the seafloor of 3D-seismic grid SG9810 (A) and SG9804 (B) showing seismic acquisition footprints (white dashed lines). These footprints run parallel to the inlines of the grid (trending northwest/southeast).*

3.3 Seismic Character

The seismic data were analyzed in the shallow portion of the both 3D-seismic grids and divided into three groups based on the characteristics of the reflectors within each section (Figure 3.3).

Semi-continuous chaotic weak to moderately strong reflectors beneath the URU indicate pre-glacial sedimentary units and bedrock. These reflectors are variously dipping, often heavily faulted, and can be seen truncating into the URU above it.

The URU is an erosional unconformity that is shown as a bright continuous strong reflector that runs mostly parallel, about 100 ms (180 m), beneath the seafloor. This unconformity marks the boundary between pre-glacial units and glacial and glaciomarine deposits across the Barents Sea continental shelf (Faleide et al., 1996). The URU clearly separates variously dipping strata below from parallel to sub-parallel reflectors above.

Above the URU and beneath the seafloor, a series of chaotic and discontinuous reflectors are relatively weak and laterally inconsistent. This section of parallel to sub-parallel reflectors is roughly 180 m thick, and are interpreted as glacigenic, glaciomarine, and marine sediment deposited after the onset of glaciation.

Description	Identification	Example
Chaotic, discontinuous, weak, parallel to sub-parallel reflectors	Glacigenic, glaciomarine, marine sediments	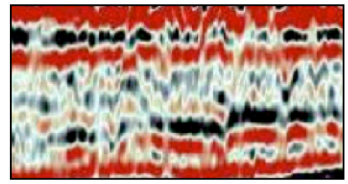
Bright, continuous, strong reflector that runs mostly parallel to the seafloor	Upper Regional Unconformity (URU)	
Semi-continuous, chaotic, weak to moderately strong reflectors	Pre-glacial sedimentary units and bedrock (heavily faulted)	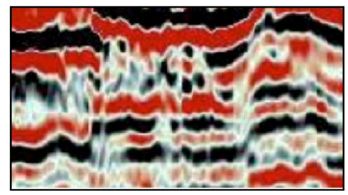

1 km

Figure 3.3. *Seismic character divided into three categories after analysis in the southwestern Barents Sea. The result separated glaciomarine sediments from pre-glacial bedrock by the URU.*

3.4 Seismic Attributes

A seismic attribute is a quantitative method of measuring seismic characteristics in an area of interest (Chopra and Marfurt, 2005). These attributes can be calculated from the seismic data in a window of interest and applied to the interpretation. The application of seismic attributes and amplitudes may enhance the visualization of geological and geomorphic features, as well as develop a better understanding of the seismic facies.

Root Mean Square (RMS) Amplitude Seismic Attribute

The RMS post-stack attribute calculates the square root of the sum of squared amplitudes, which is then divided by the number of samples used within the interval of interest (Chen and Sidney, 1997). Application of this amplitude may be able to highlight isolated anomalies found in the 3D-seismic data, and is particularly useful in identification of channels or gas sands (Chen and Sidney, 1997). RMS amplitude maps are a method of mapping the strength and distribution of amplitudes within a seismic volume, and are a potential method for visualizing internal features (Rüther et al., 2011).

3.5 Interpretation Tools

Seismic interpretation was carried out on UNIX workstations using Halliburton's Landmark DecisionSpace® software, from Landmark Graphic Corporation (LGC), at the University of Stavanger in Norway. Regional maps of the seafloor and URU were created using 2D-multi-channel seismic data to gain a broad understanding of the structure of the unconformity and seafloor across the southwestern Barents Sea. Higher-resolution surfaces of the both the seafloor and URU were created using a dense interpretation of 3D-seismic grids. The unconformity was delineated using horizon picking at an inline-by-inline grid density based on the erosive character of the unconformity. Additionally, ArcGIS 10, a geographic information system, was used to create maps and figures with the data provided.

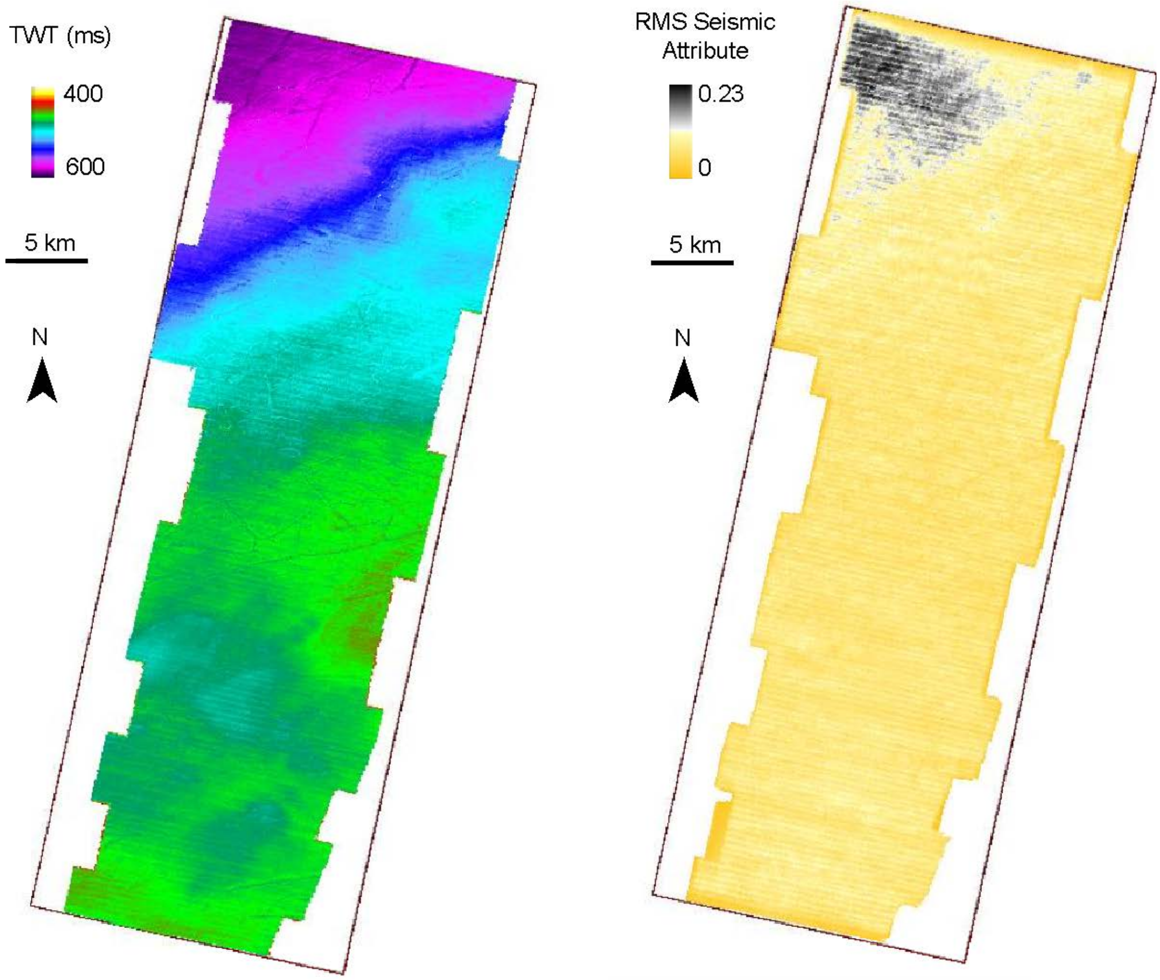

Figure 3.4. *3D grid SG9810 showing seafloor surface (left) and RMS amplitude seafloor surface (right), which was used to highlight glacial geomorphic figures.*

4. Results

In each of the following sections, a seismic line was used to illustrate the general character of the seafloor and URU, followed by 3D surfaces of both the seafloor and subsurface outlining different geomorphic features.

4.1 Results from 2D-Seismic Interpretation

2D-seismic lines were first interpreted in order to develop a better general understanding of the URU. The unconformity is roughly parallel to the seafloor and extends across the southwestern Barents Sea; the largest, most notable feature observed both in bathymetry data (Figure 1.2) and the URU (Figure 4.1) is the Bjørnøyrenna Trough, the deep, elongated trough that runs northeast-southwest across the Barents Sea. The two 3D-seismic grids used for this study are located near the southern edge of the trough.

4.2 Results from 3D-seismic Grid SG9810

A seismic inline of SG9810 is interpreted with two horizons outlined in light blue (seafloor) and yellow (URU) (Figure 4.2). Beneath the water column, a strong, continuous, black reflector is represented by a peak, indicating an increase in acoustic impedance in normal polarity data. This reflector is the seafloor and is marked in light blue in the seismic line at a water depth of ~410 meters. Below the seafloor, sub-parallel, horizontal reflectors are mainly weak, discontinuous, and often chaotic. The lowermost reflectors onlap onto the black reflector, which is strong and continuous throughout the seismic grid. This subsurface increase in acoustic impedance outlined in yellow is the URU, approximately 150 meters below the seafloor, and separates sub-horizontal reflectors above from variously dipping reflectors below. The underlying Cretaceous shale bedrock is marked by southwest-dipping reflectors that terminate into the overlying URU. Many of these reflectors are weak to moderately strong, and are often sub-parallel to each other. The southeast area of the grid shows more strongly dipping reflectors, while the northwest area shows gentler slopes.

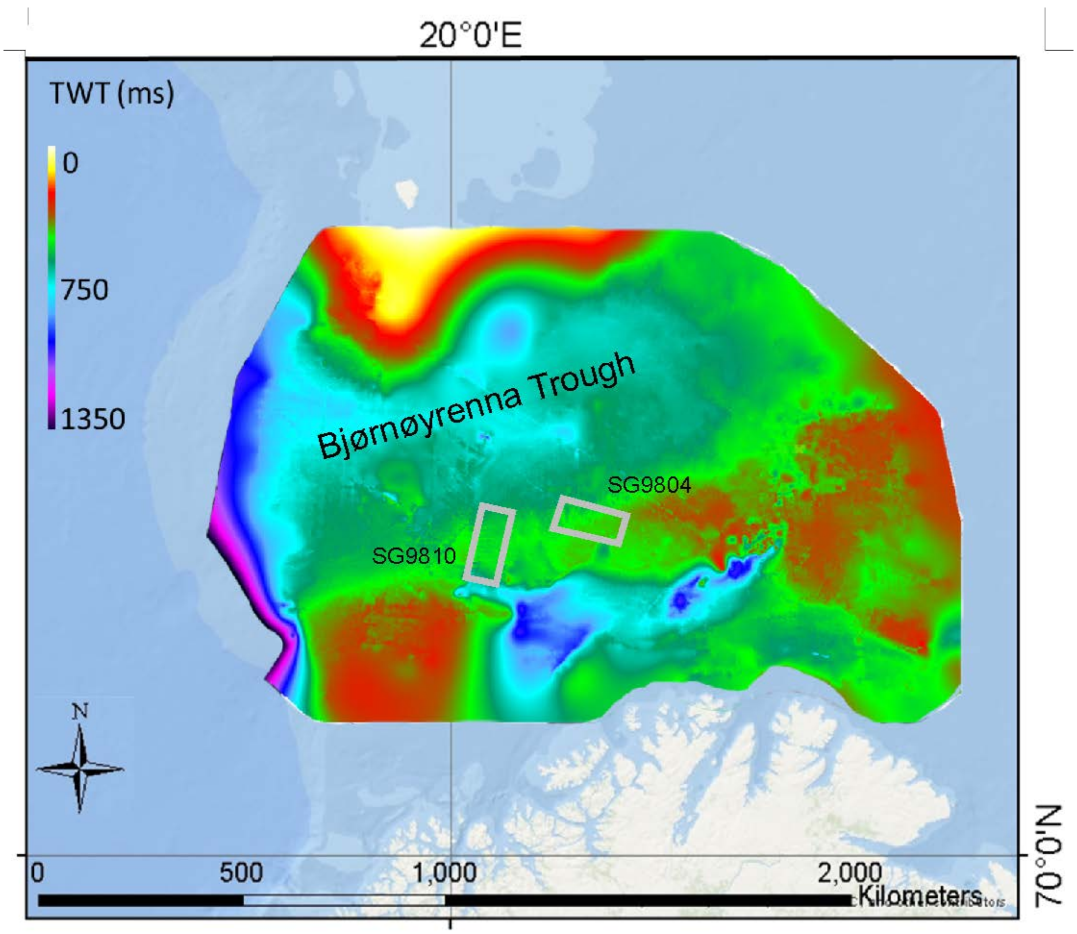

Figure 4.1. *Shaded time-relief map of the extent of the URU created from 2D seismic interpretation. Light gray boxes mark the locations of 3D-seismic grids SG9810 (left) and SG9804 (right), which were used to map and identify glacial geomorphic features from the seafloor and subsurface.*

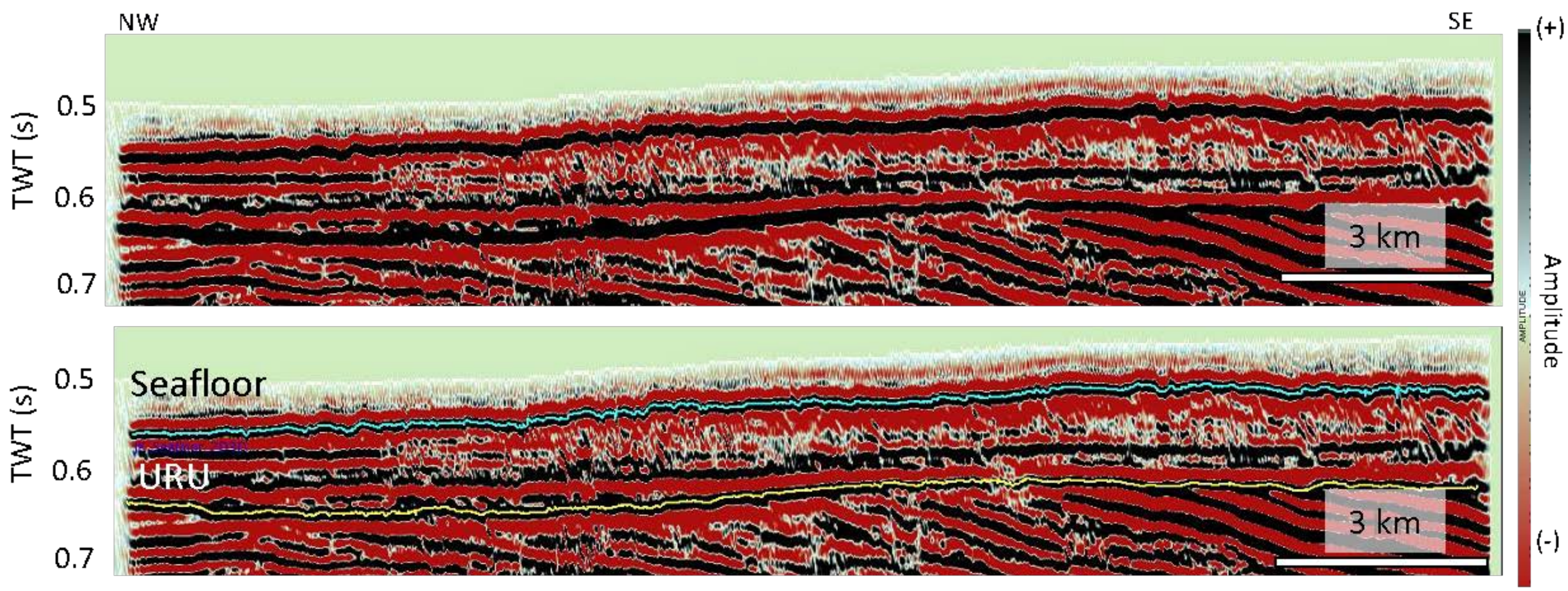

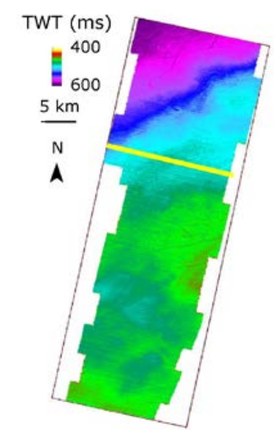

Figure 4.2. *Uninterpreted and interpreted seismic from 3D-seismic grid SG9810. The blue horizon marks the seafloor, while the yellow horizon marks the URU. The URU is roughly parallel to the seafloor and separates variously dipping strata below from unlithified, horizontal, sub-parallel sediments above. To the right, the seafloor surface shows the location of the seismic inline (yellow). Vertical exaggeration: 10x.*

4.2.1 SG9810 Seafloor

The 3D seafloor surface for SG9810 is covered with criss-crossing, curvilinear, irregular furrows that are u-shaped or v-shaped in seismic (Figure 4.3). The furrow widths, measured from edge-to-edge in seismic data, range from 93 – 375 meters wide, and the lengths measure up to several tens of meters, but likely continue past the boundaries of the 3D survey. The relief of the furrows measured from trough-to-crest is up to 17 m.

The furrows of varying widths and heights are distributed throughout the seafloor, and the distance between individual furrows also varies. Though some of the furrows are linear features, many of them are curved or oriented in different directions (Figure 4.4). In general, the furrows are more visible in the shallower, southern part of the survey than in the northwestern, deeper area.

4.2.2 SG9810 URU

Curvilinear furrows visible on the seafloor are absent on the 3D-URU surface. Instead, the subsurface shows elongated ridges covering the eastern and southeastern portions of the seismic grid are represented in seismic data as shallow, u-shaped dips (Figure 4.5). The erosional ridges are continuous throughout the seismic data and are often sub-parallel to each other.

The spacing of the ridges correlates to the dip of the underlying shale bedrock. Below the URU, shallow sands are represented by a decrease in acoustic impedance, and are troughs, or red truncating reflectors, in normal polarity data. Alternatively, shales are represented by an increase in acoustic impedance, indicated by peaks or black truncating reflectors. The dipping shales terminating into the URU are more eroded, manifesting as the shallow dips that create long, continuous ridges, while the dipping sandstones are less eroded, slightly protruding red reflectors between the alternating shale layers.

In 3D, the shallow u-shaped ridges are continuous from north to south across the URU surface (Figure 4.6). The ridges follow the dip of the underlying strata, which is dipping roughly ~15° towards the southwest. The more gradual, gentler sloping reflectors beneath the URU, with dips measuring 20-25°, do not create ridges, as seen in the northwestern corner of the 3D surface.

A small, circular depression found in the western part of this surface is located in an area unmarked by erosional ridges and can be seen in both seismic and the 3D surface (Figure 4.7). This depression measures about 1 km in length and 1.5 km in width, and is ~17 m deep at its deepest point. The bottom of the depression shows slightly different slopes: the western and northern edges of the depression indicate slightly steeper slopes, while the eastern and southern edges have gentler slopes. The depression has defined edges and a smooth, elliptical shape, and reflectors onlap onto the URU within the boundaries of the depression.

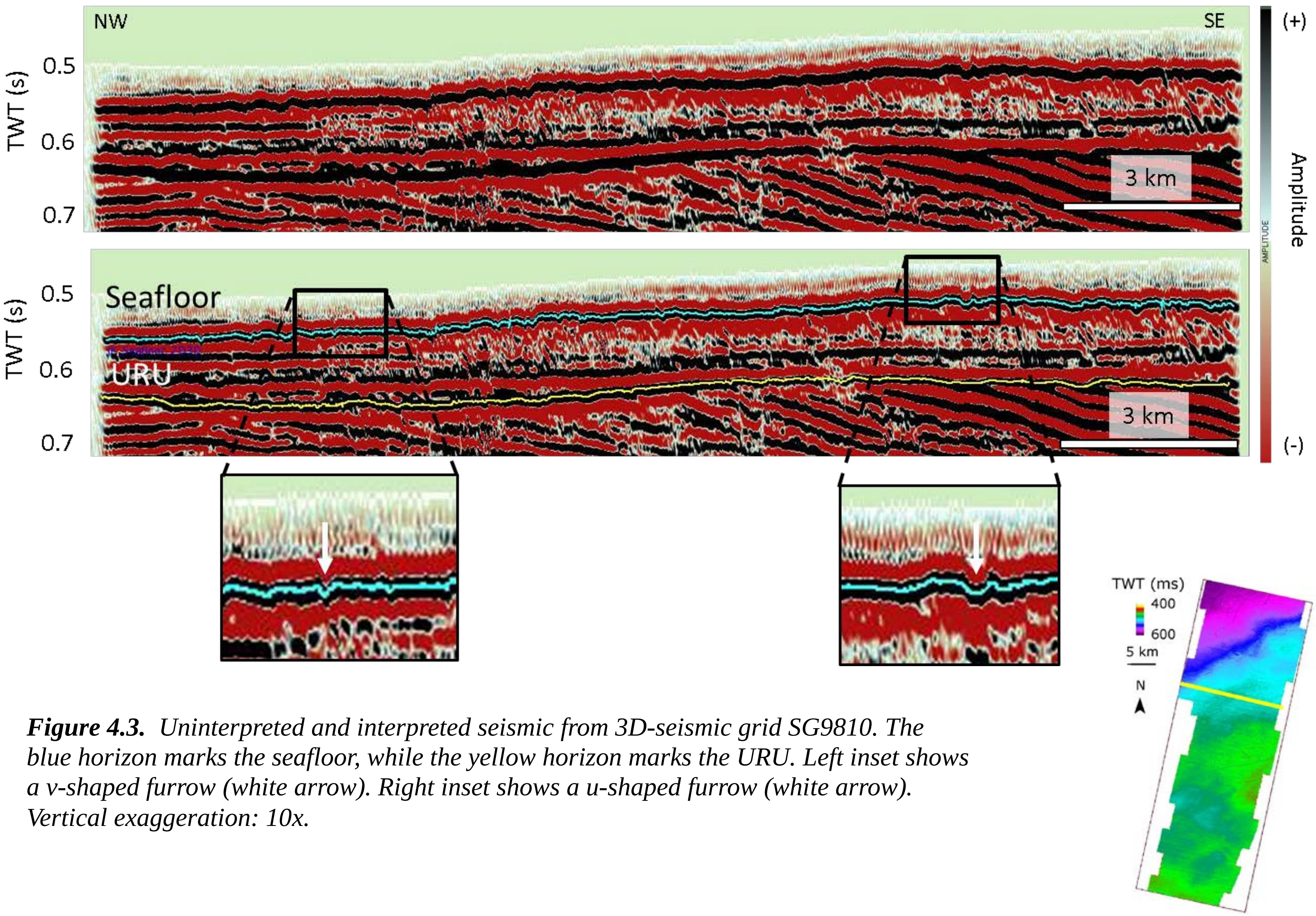

Figure 4.3. *Uninterpreted and interpreted seismic from 3D-seismic grid SG9810. The blue horizon marks the seafloor, while the yellow horizon marks the URU. Left inset shows a v-shaped furrow (white arrow). Right inset shows a u-shaped furrow (white arrow). Vertical exaggeration: 10x.*

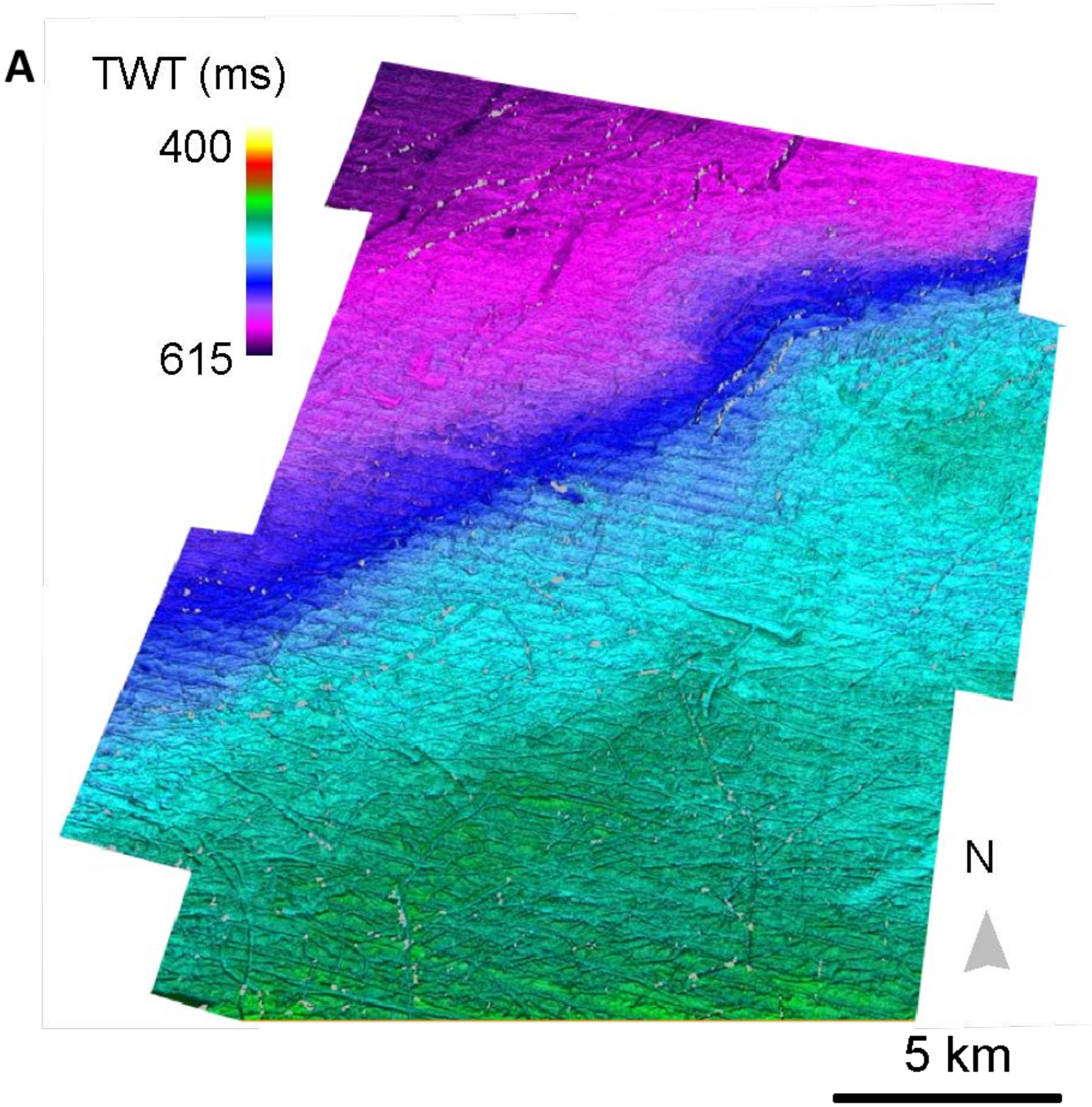

Figure 4.4. *(A) Uninterpreted seafloor surface of 3D-seismic grid SG9810. Interpreted seafloor surface (B) continued on next page.*

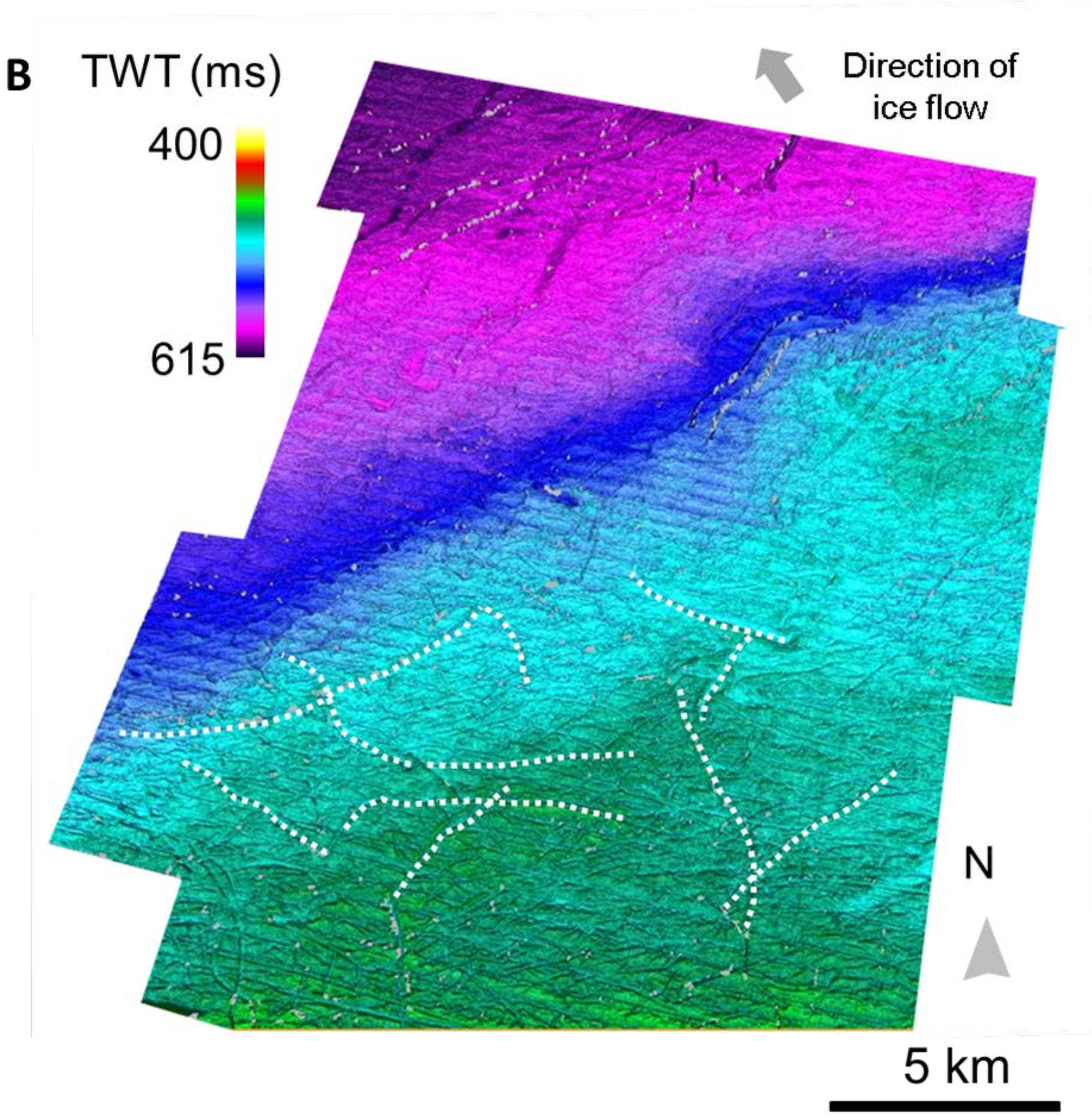

Figure 4.4. *(B) Interpreted seafloor surface of 3D-seismic grid SG9810, with white dashed lines outlining the curvilinear furrows carved into the seafloor. Furrows vary in width and length, and are randomly oriented. Fewer furrows are visible in the northwestern, deeper portion of the seismic grid than in the southeastern, shallower portion.*

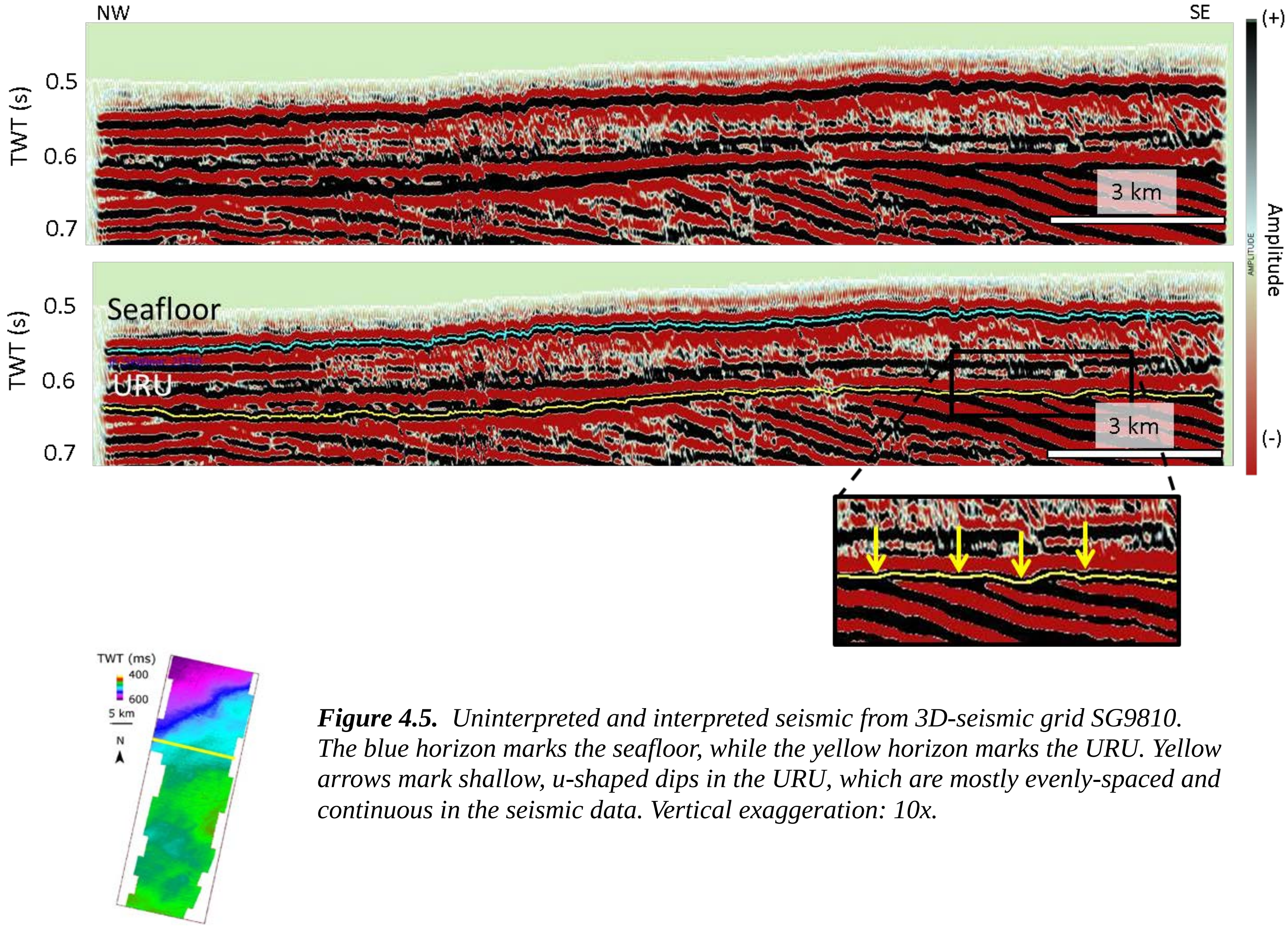

Figure 4.5. *Uninterpreted and interpreted seismic from 3D-seismic grid SG9810. The blue horizon marks the seafloor, while the yellow horizon marks the URU. Yellow arrows mark shallow, u-shaped dips in the URU, which are mostly evenly-spaced and continuous in the seismic data. Vertical exaggeration: 10x.*

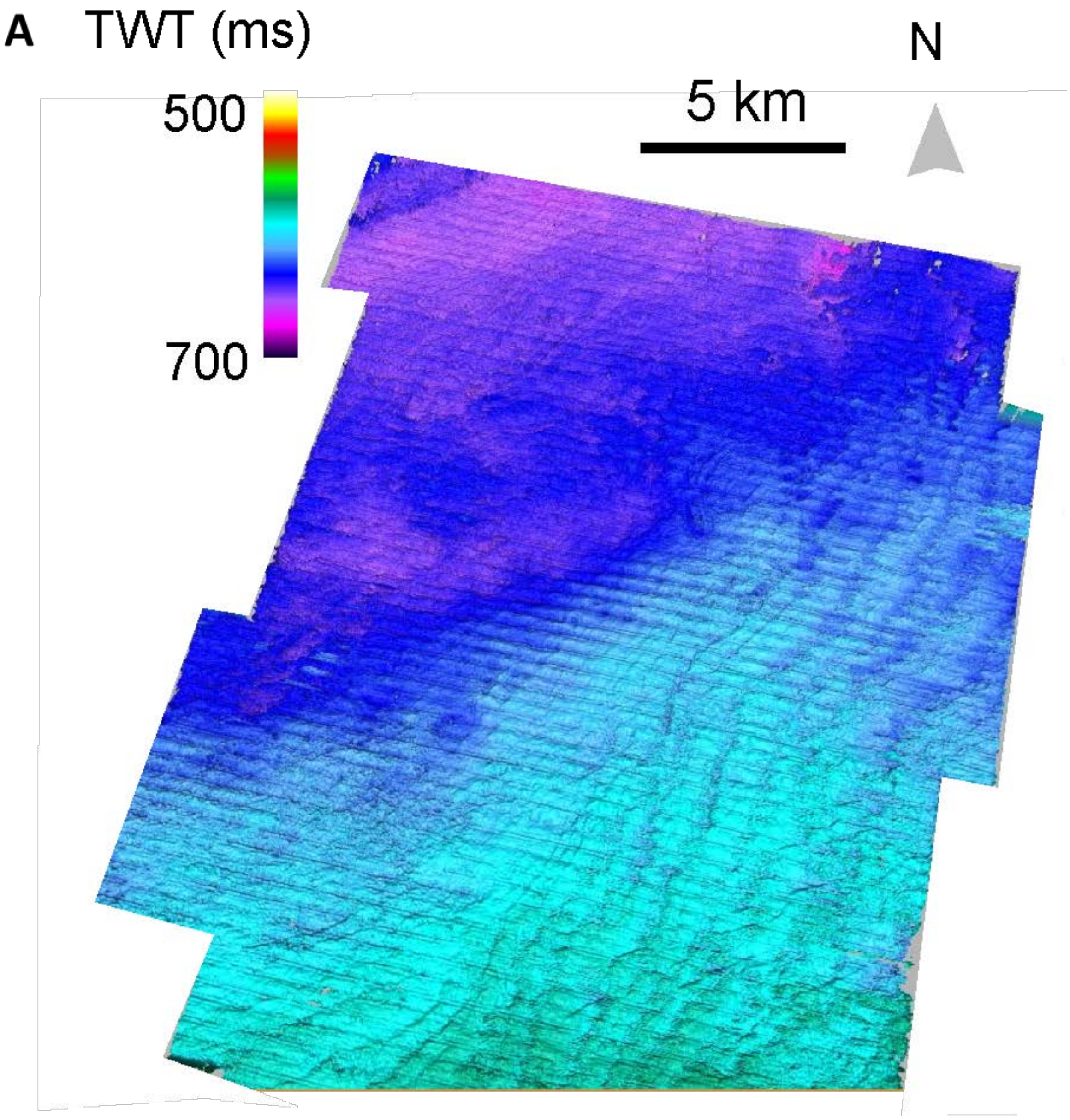

Figure 4.6. *(A) Uninterpreted URU surface of SG9810 showing several erosional grooves (eastern side of the surface). Interpreted surface continued on next page.*

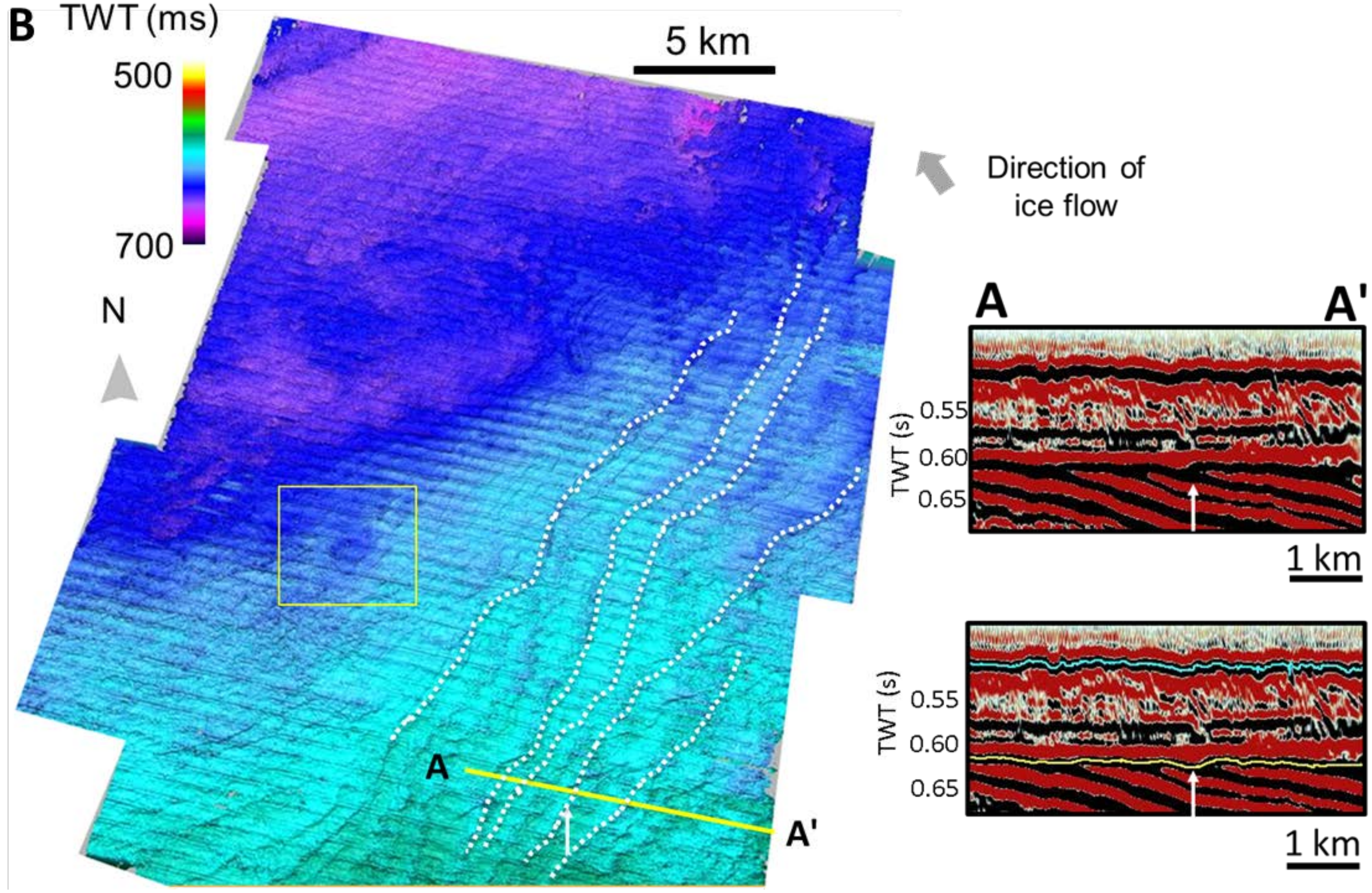

Figure 4.6. *(continued) (B) The interpreted URU surface uses white dotted lines to show the continuous ridges that appear as shallow u-shaped dips in seismic data. An uninterpreted and interpreted seismic line (A – A′) indicates the seafloor (light blue) and URU (yellow), with a white arrow marking the location of a u-shaped dip in both the 3D-surface and -seismic data. Yellow box outlines a circular depression, discussed in Figure 4.7. Dip of underlying bedrock caused by a Cretaceous tectonic event that caused regional uplift. Vertical exaggeration: 10x.*

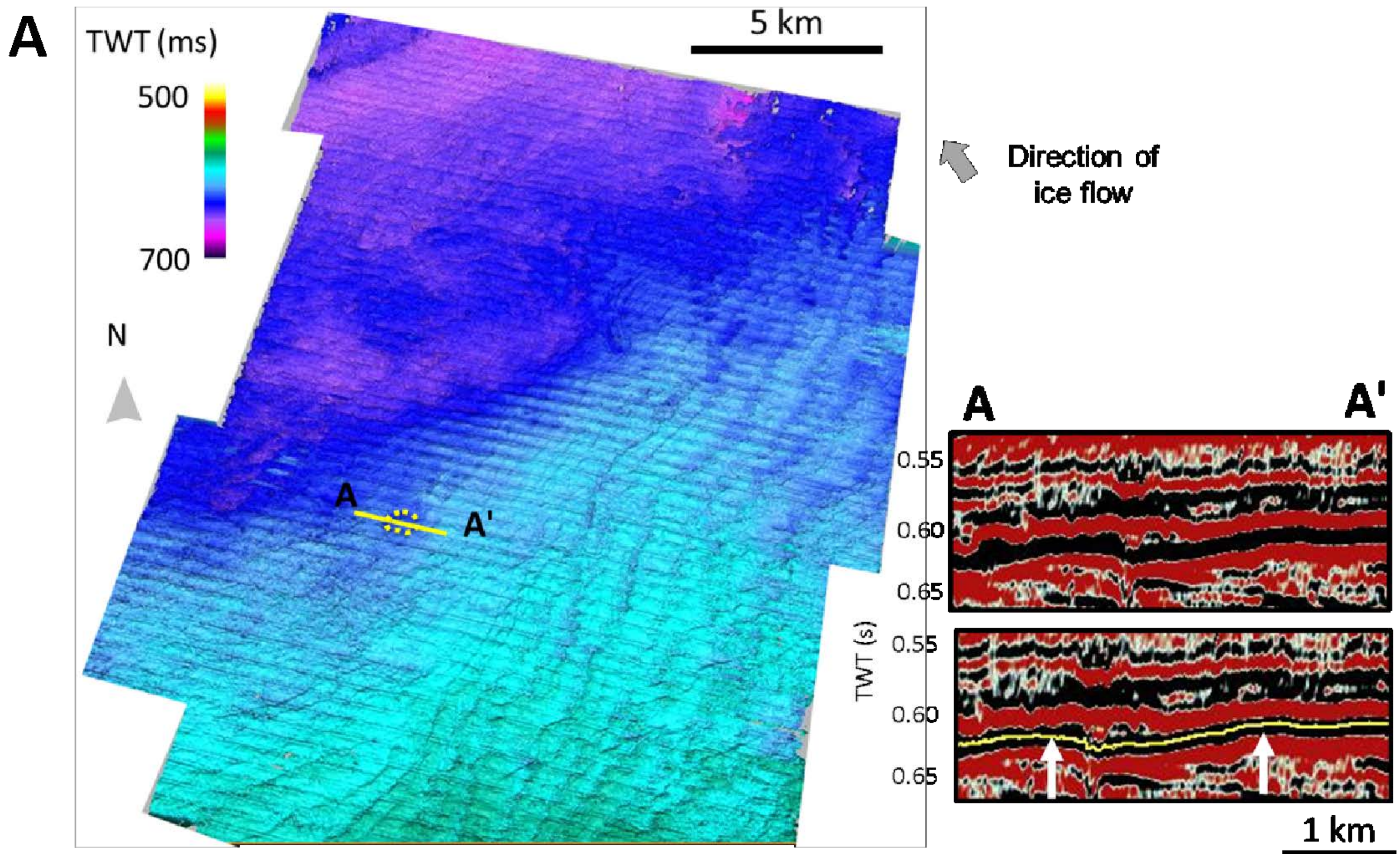

Figure 4.7. *(A) Seismic inline (A – A') through circular depression on SG9810 URU (yellow horizon). White arrows mark the edges of the depression, which is slightly steeper on west side, and more gently sloping on the west side. Vertical exaggeration: 10x. Figure continued on next page.*

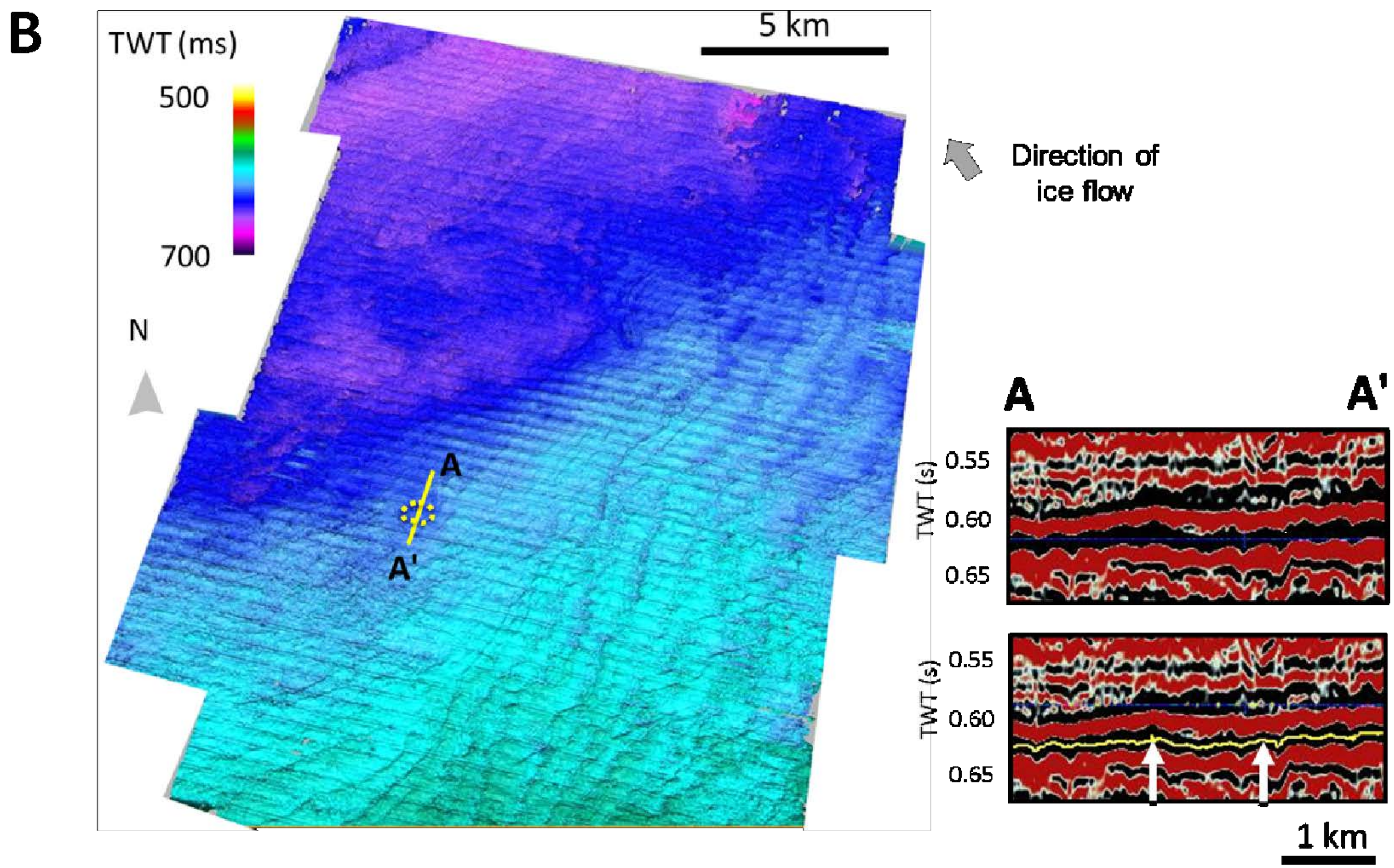

Figure 4.7. *(continued) (B) Seismic inline crossline (A – A') through circular depression on SG9810 URU (yellow horizon). White arrows mark the edges of the depression; the base of the depression is slightly steeper in the north than in the south. Vertical exaggeration: 10x.*

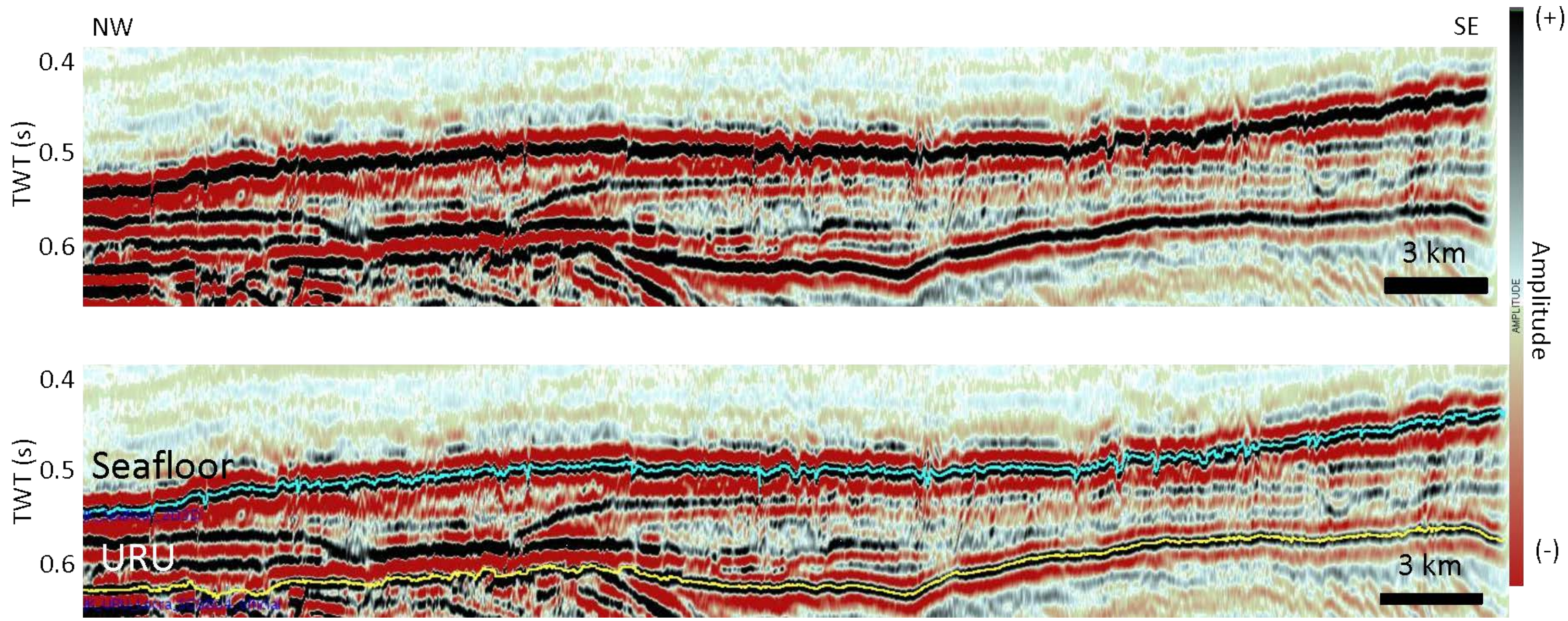

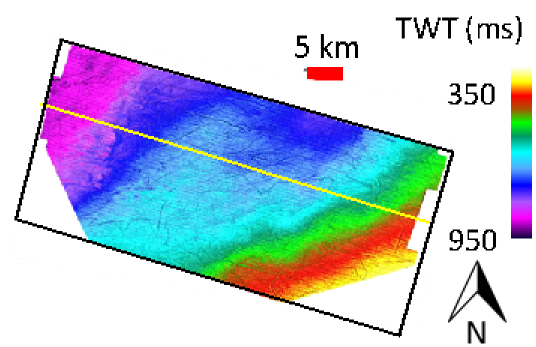

Figure 4.8. *Uninterpreted and interpreted seismic from 3D-seismic grid SG9804. The blue horizon marks the seafloor, while the yellow horizon marks the URU. The URU is roughly parallel to the seafloor and separates variously dipping strata below from unlithified, horizontal, sub-parallel sediments above. To the right, the seafloor surface shows the location of the seismic inline (yellow). Vertical exaggeration: 10x.*

4.3 Results from 3D-seismic Grid SG9804

Similar to SG9810, interpretation of horizons in seismic data of SG9804 shows the seafloor in light blue and the URU in yellow (Figure 4.8). The seafloor reflector, a peak and an increase in acoustic impedance, and is at a water depth of approximately 375-400 meters. Beneath the seafloor is a sequence of sub-parallel, horizontal, weak and discontinuous reflectors that are often chaotic in character. The URU, roughly 140 – 160 meters below the seafloor, separates the overlying horizontal reflectors from variously dipping, chaotic to moderately strong reflectors below, a few of which terminate into the overlying URU.

4.3.1 SG9804 Seafloor

Similar to SG9810, the seafloor surface of SG9804 is also covered with furrows that frequently cut across each other. Many of the furrows are v-shaped features identified in seismic data (Figure 4.9). The furrows range from 50 – 350 meters in width by measuring from edge-to-edge of the v-shaped incisions in seismic data. In relief, they measure up to 15 meters from trough-to-crest measurements. The lengths of the furrows are highly variable, with some a few meters and some tens of meters long, extending beyond the 3D surface grid.

The furrows are irregular, curvilinear features that vary in width, height, and length, and are distributed throughout the entire surface in random orientations (Figure 4.10). However, unlike SG9810, many of the furrows trend in an east-west direction across the seafloor, rather than complete random orientation.

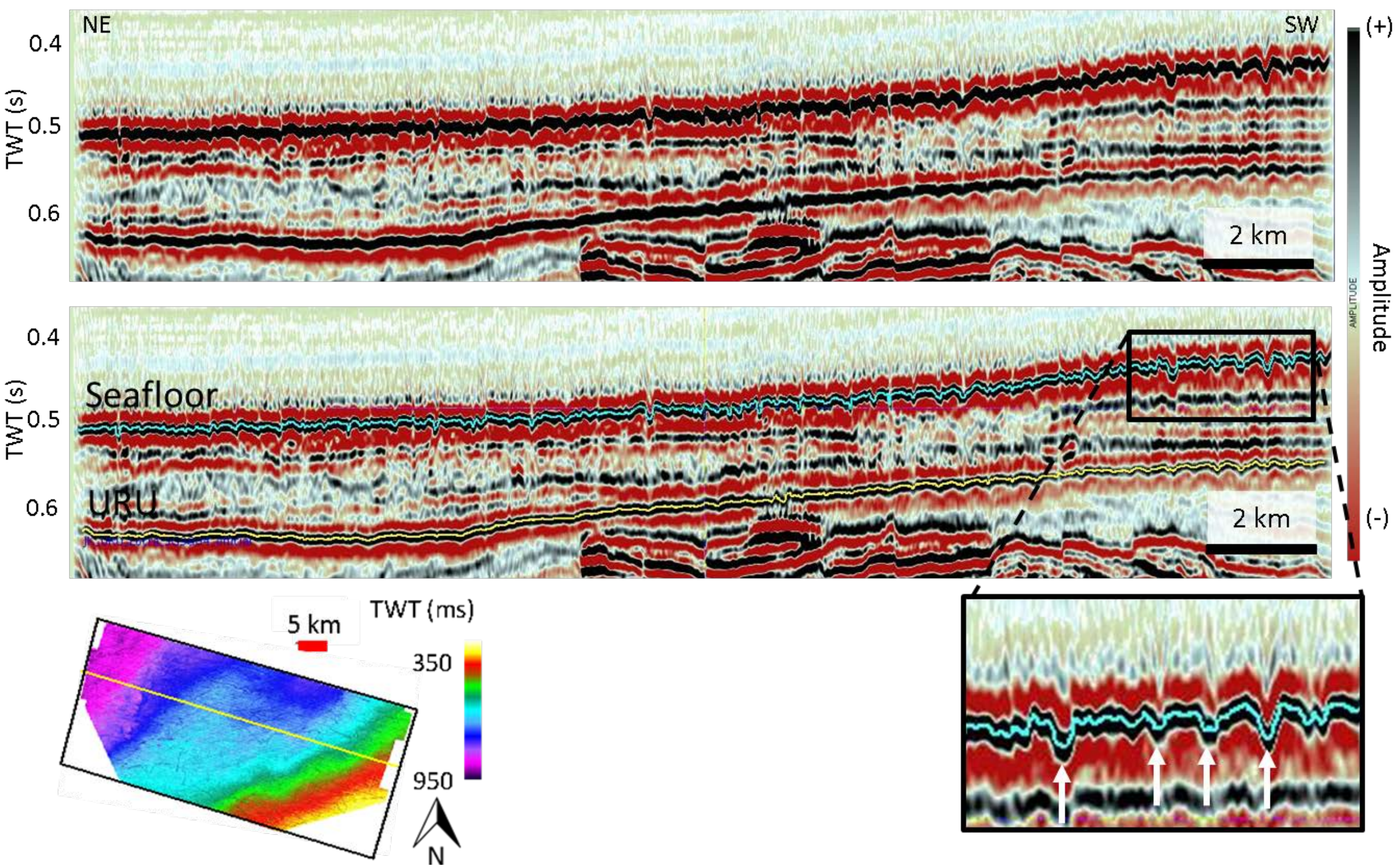

Figure 4.9. *Uninterpreted and interpreted seismic from 3D-seismic grid SG9804. The blue horizon marks the seafloor, while the yellow horizon marks the URU. White arrows in the inset (right) indicate several v-shaped furrows in seismic data. In the left corner, the location of the seismic line is shown in yellow. Vertical exaggeration: 10x.*

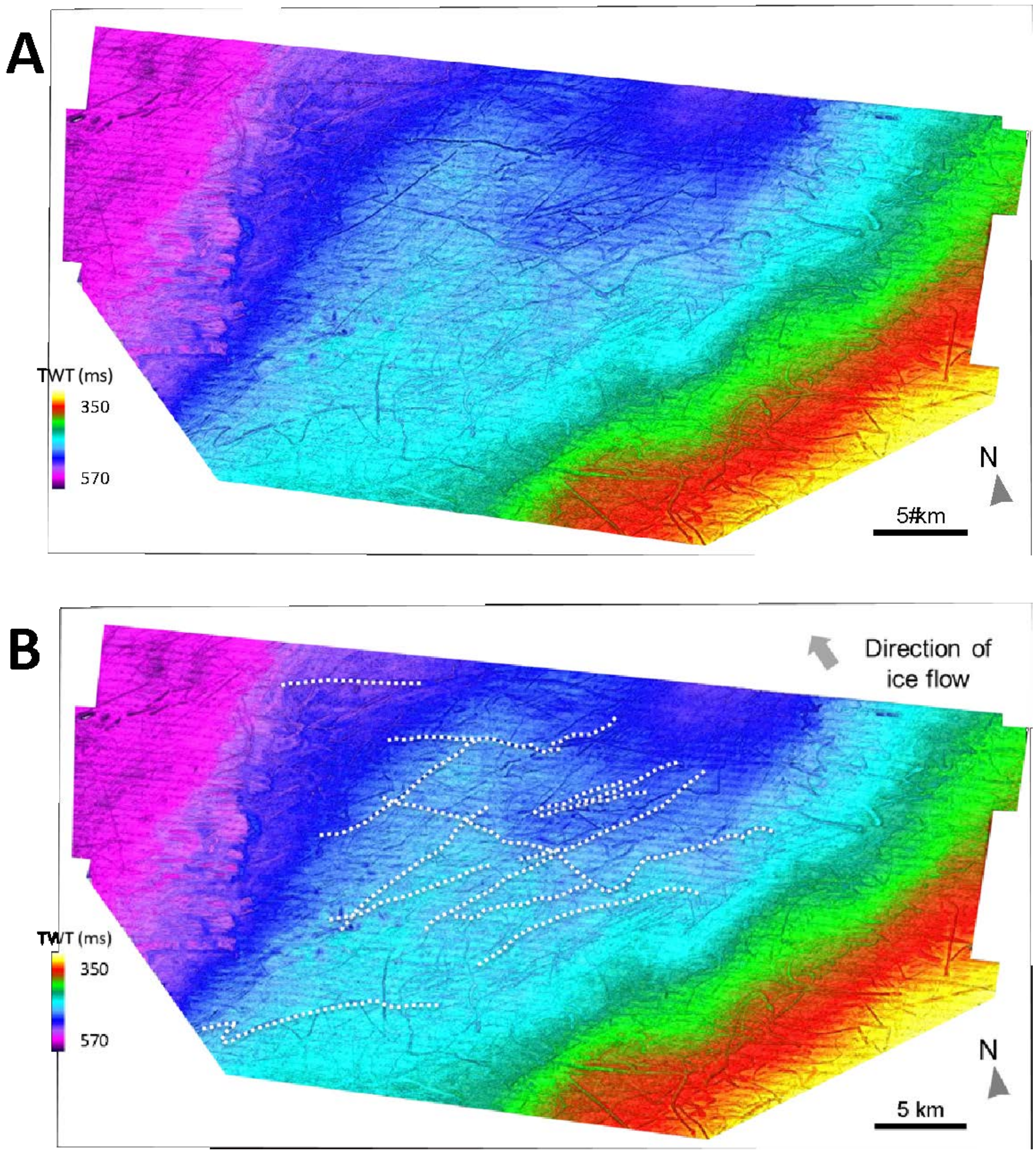

Figure 4.10. *Uninterpreted (A) and interpreted (B) seafloor surface for SG9804. Criss-crossing, curvilinear furrows outlined in dotted white lines – many furrows seem to trend in an east-west direction.*

4.3.2 SG9804 URU

A side-by-side analysis of the seafloor and URU shows that unlike the seafloor surface, the URU of SG9804 does not show evidence of curvilinear, irregular furrows, but does contain several straight linear features in the northern portion of the grid (Figure 4.11).

In a seismic inline, the linear features are represented by wavy, evenly-spaced and ridge-groove pairs of the same or similar amplitudes (Figure 4.12). In the 3D-seismic surface created from interpretation, the elongated and linear ridge-groove pairs have an exceptional parallel conformity. They are roughly 200 – 500 m wide, measured from crest-to-crest, and the relief of the linear features, measured from trough-to-crest, is up to 13 m in depth. The spacing is roughly 0.2 – 0.8 km apart, and have a minimum length of 2.0 – 6.5 km, although they may be longer by extending beyond the northern boundary of 3D acquisition.

From the 3D URU surface, the linear features are sub-parallel-to-parallel to each other, and all trend northwest-southeast (Figure 4.13). The average direction of the northwest-southeast-trending features is roughly 340° - 345°.

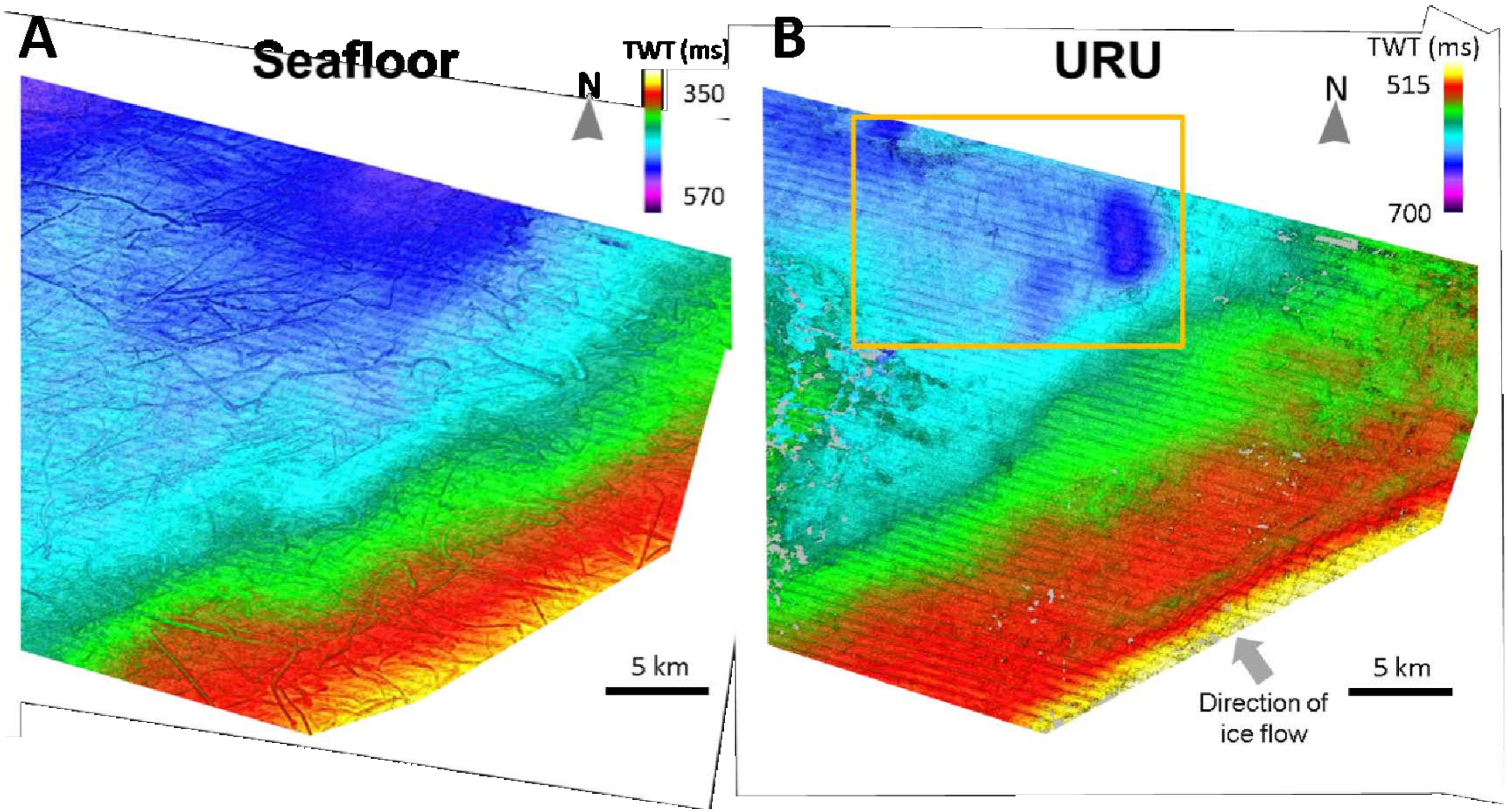

Figure 4.11. *Side-by-side analysis of SG9804 seafloor (A) and URU (B). While irregular furrows are clearly criss-crossing on the seafloor surface, similar features are not found on the URU. Instead, straight, linear features and a large depression (orange box) are visible and will be discussed below.*

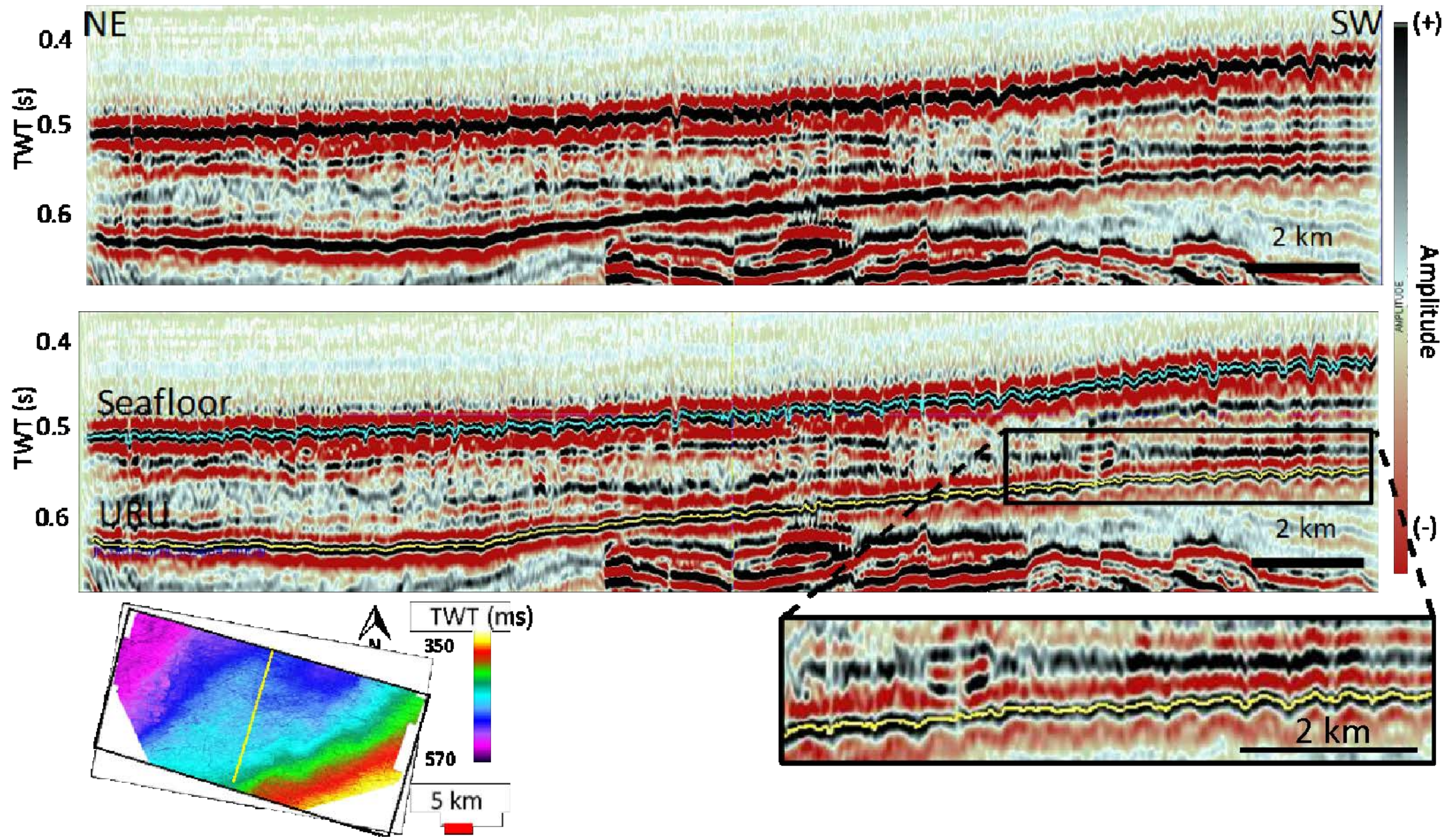

Figure 4.12. Uninterpreted and interpreted seismic from 3D-seismic grid SG9804 (location from crossline in lower left corner). The blue horizon marks the seafloor, while the yellow horizon marks the URU. In the right inset, the URU reflector shows evenly-spaced, wavy character that creates a ridge-groove pair. Vertical exaggeration: 10x.

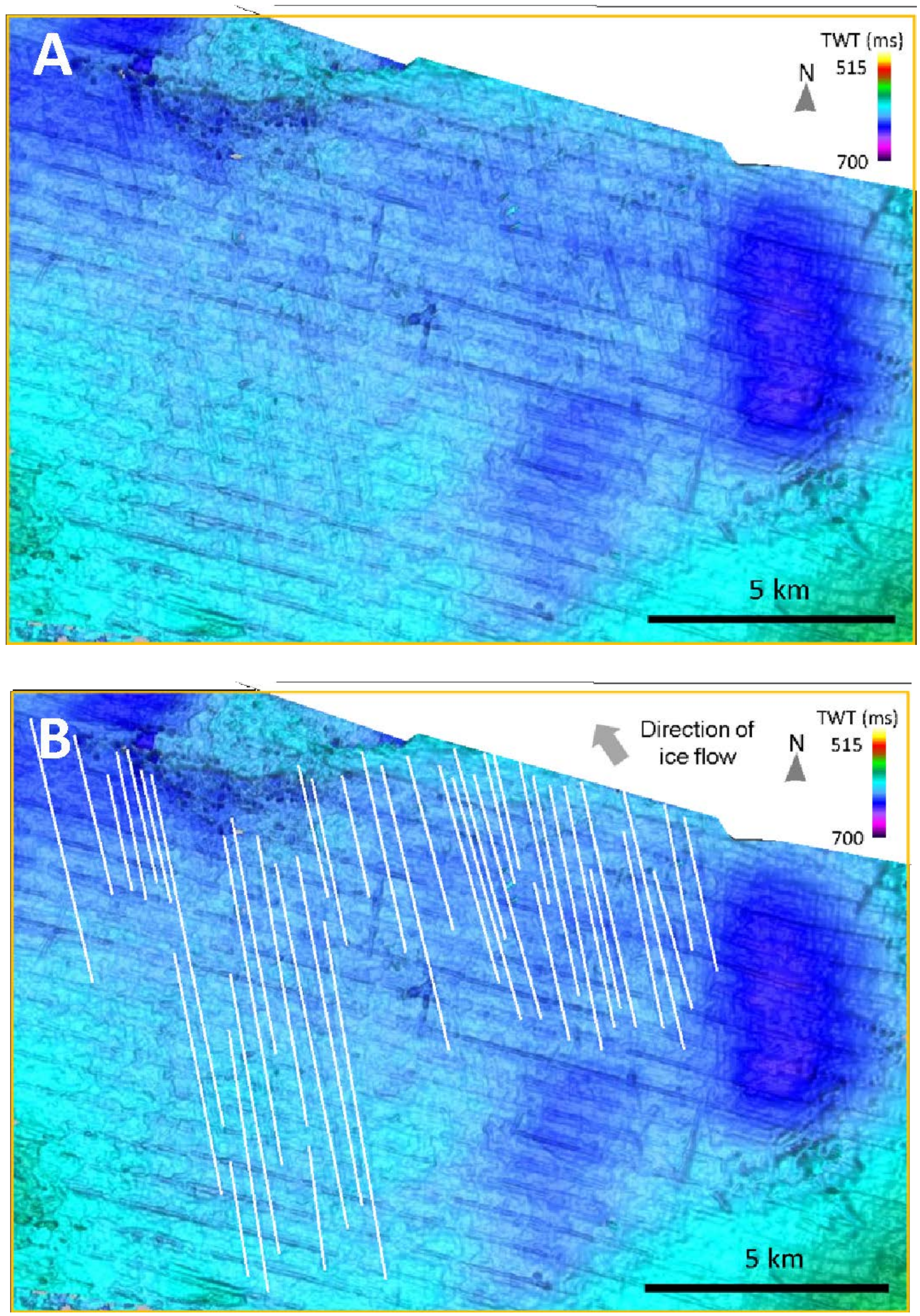

Figure 4.13. *Inset (orange box) from Figure 4.11, with uninterpreted surface (A) and interpreted surface (B). White lines outline several linear features, which are parallel or sub-parallel to each other and trend northwest-southeast.*

Cutting across the ridge-groove pairs are several straight grooves that trend northeast-southwest rather than northwest-southeast (Figure 4.14). Though the ridges are straight, they differ from the linear ridge-groove pairs because they are fewer, shorter, and spaced further apart than paired features. The ridges measure 1.7 – 2.5 km in length and are spaced roughly 1.3 – 6.1 km apart. The relief of the cross-cutting features is much smaller than the average relief of the white ridge-groove pairs (Figure 4.15).

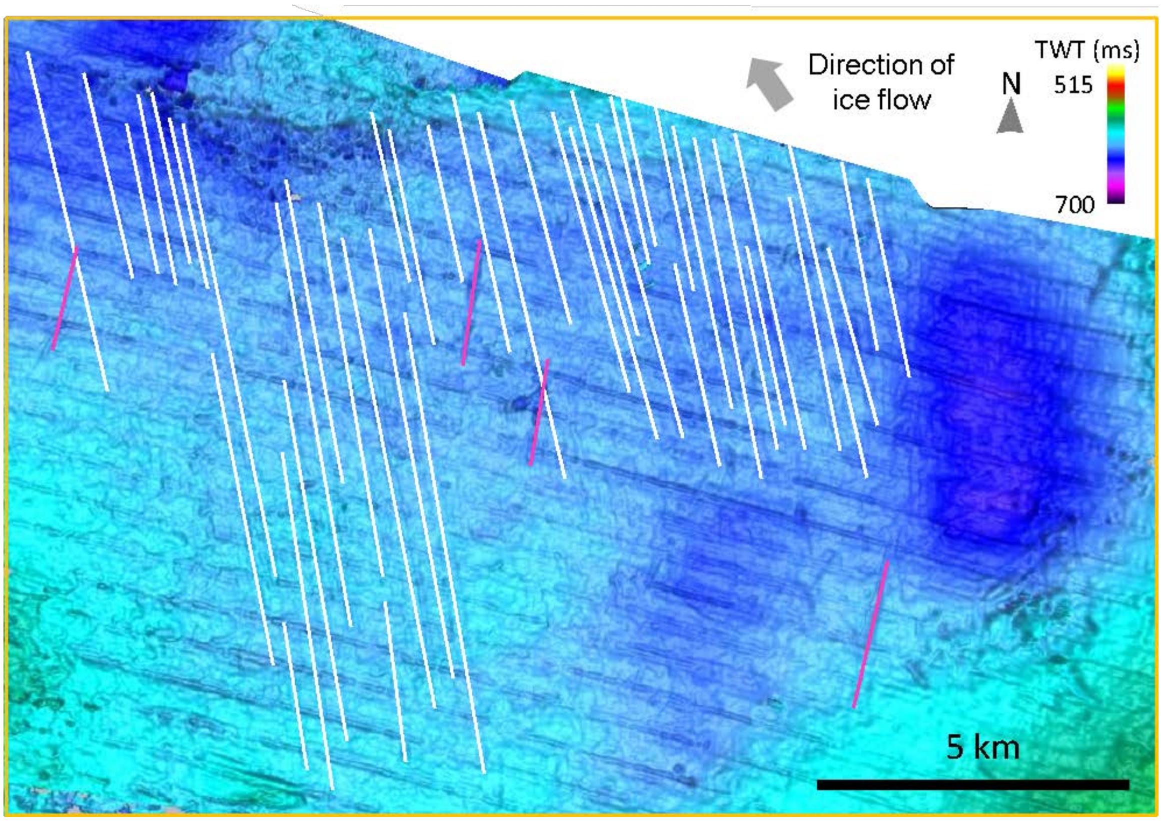

Figure 4.14. *3D surface of SG9804 URU, with inset location from Figure 4.11. Pink lines indicate straight grooves that cut across the ridge-groove pair features (white lines). The pink lines trend northeast-southwest, while the underlying white lines trend northwest-southeast.*

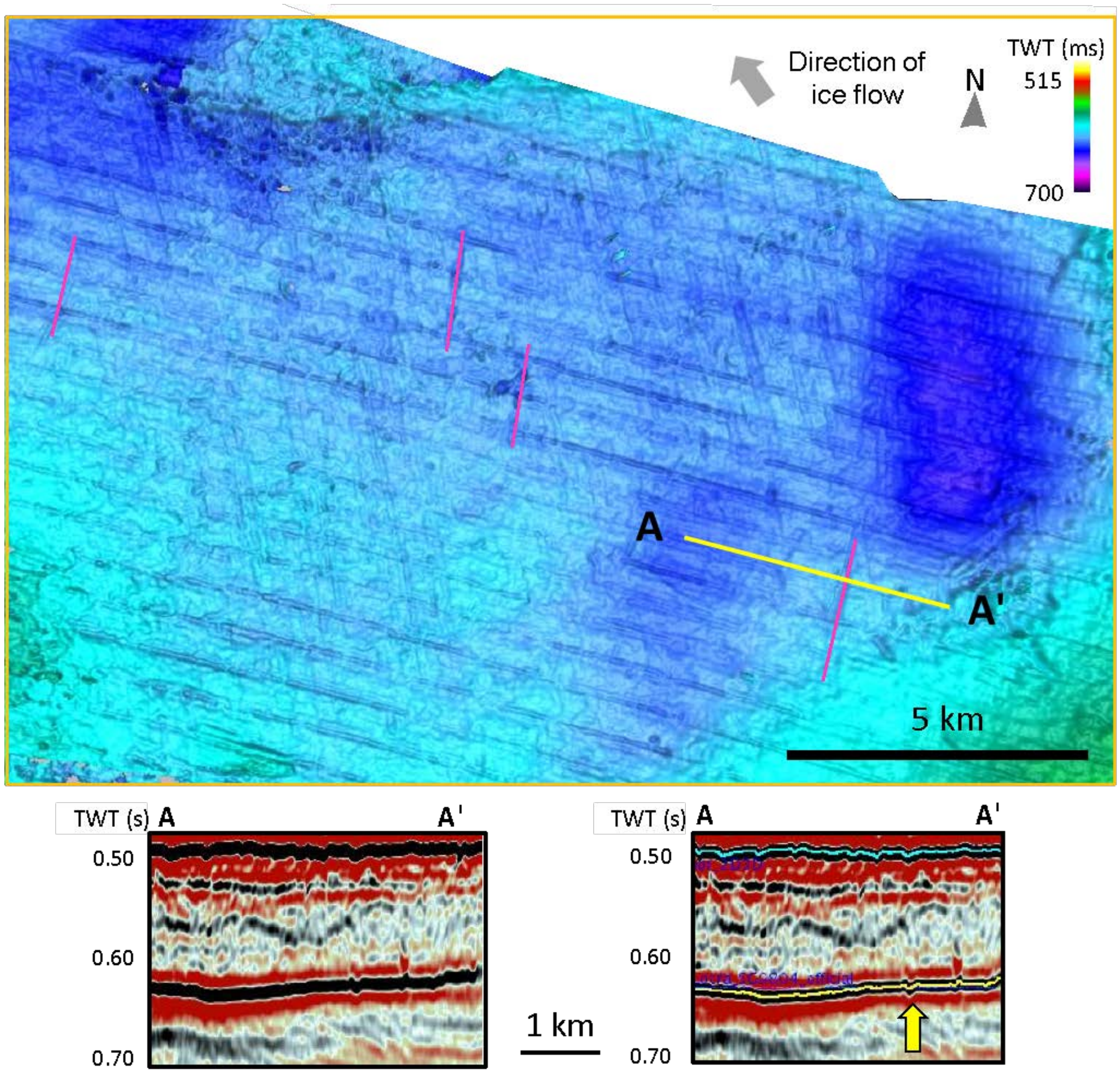

__Figure 4.15.__ Uninterpreted (left) and interpreted (right) seismic line drawn through the pink lineation, with the location of the pink lineation indicated by the yellow arrow. The small v-shaped indentation shows the relief of the pink linear feature.

In the eastern portion of the inset, a large, elliptical depression is visibly deeper than the rest of the URU (Figure 4.16). This depression has a diameter range of 2.8 km –

4.7 km and reaches depths of ~17 m. The sides of the depression are very gently dipping, as is visible in the seismic data (Figure 4.16).

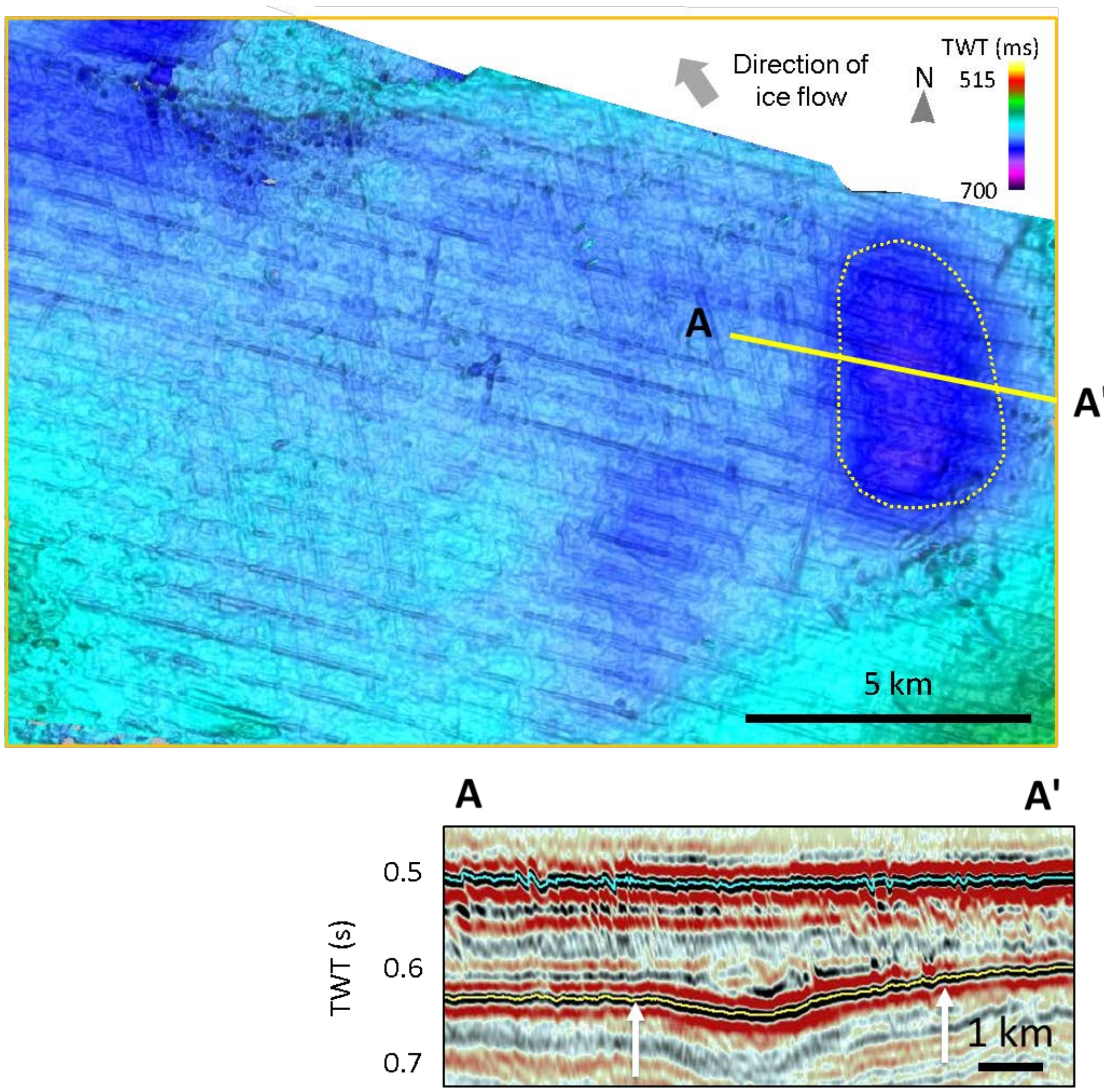

Figure 4.16. *SG9804 URU surface, with inset from Figure 4.11. Seismic inline (A – A′) across the depression is shown below. White arrows indicate the edges of the depression, which has very gently sloping edges to the deepest part of the depression (~17 meters). Vertical exaggeration: 10x.*

5. Discussion

5.1 Seafloor Interpretation

5.1.1. Iceberg-keel ploughmarks

The presence of cross-cutting, curvilinear furrows across the seafloor surfaces of both SG9810 and SG9804 are interpreted as iceberg-keel ploughmarks, which have been mapped using seismic data in previously glaciated margins such as the Norwegian-Greenland Sea (Dowdeswell et al., 2007), North Sea (Graham et al., 2007; Dowdeswell et al., 2013), and Barents Sea (Rafaelsen et al., 2002; Andreassen et al., 2004; Andreassen et al., 2008). Iceberg-keel ploughmarks, often known as iceberg scours, have also been mapped in Antarctica (Barnes and Lien, 1988; Lien et al., 1989; Dowdeswell and Bamber, 2007; López-Martinez et al., 2011).

Iceberg-keel ploughmarks are incisions formed by the gouging motion of drifting iceberg-keels and sea ice, which reworks sediments when the iceberg makes contact with the seafloor in submarine conditions (Stoker and Long, 1984; Barnes and Lien, 1988; Dowdeswell and Bamber, 2007) (Figure 5.1). They are common features in high-latitude regions, and are often found on the margins of ice sheets or fast-flowing ice streams, where outlet glaciers are common (Ottesen et al., 2005; Dowdeswell and Bamber, 2007). The detached iceberg, separated from the ice sheet or glacier terminus, can be carried in open marine waters by wind direction and water currents for long distances; the length of the ploughmark can extend several tens of kilometers before the iceberg melts (Andreassen et al., 2008).

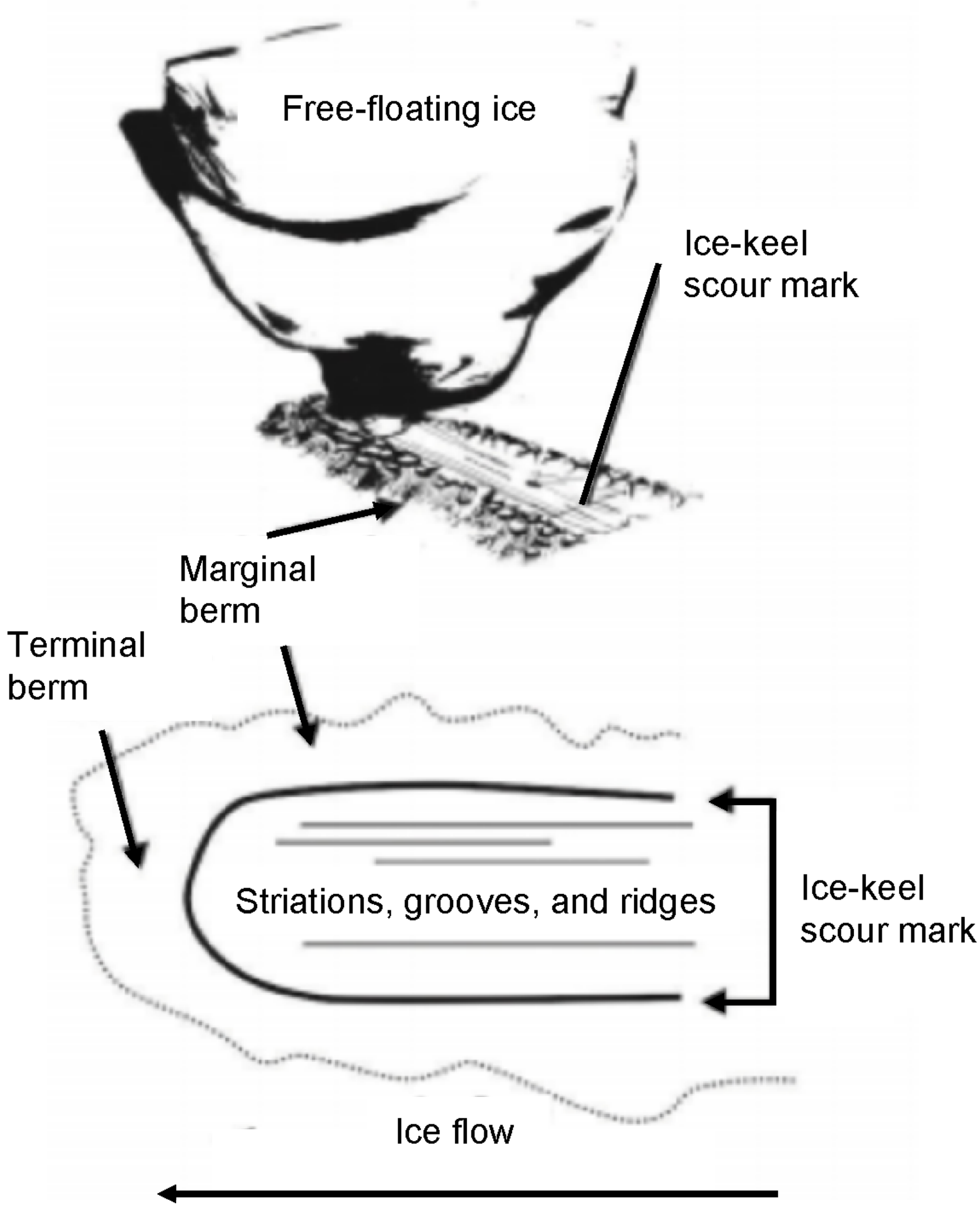

Figure 5.1. *Formation of iceberg-keel scours from free-floating ice in 3D and map view (Menozzo da Rosa et al., 2016, after Woodworth-Lynas and Dowdeswell, 1994 and Eyles et al., 2005). Marginal berms were used to measure widths of iceberg scours.*

The distribution of iceberg-keel ploughmarks is dependent on the changing flow and form of the ice sheets and glaciers from which the icebergs break off (Dowdeswell and Bamber, 2007). Additionally, the formation of iceberg scours depends on the water depth. Iceberg scouring is a process that is significant in water depths of less than 550 meters (Dowdeswell et al., 1993), though the features are found in present-day water depths of up to 848 m (Wise et al., 2017). Though the distribution of ploughmarks can be topographically dependent (Lien et al., 1989), the shallow continental shelf and roughly 375-450 m of water depth in the study area is well within the range established by Dowdeswell et al. (1993) for iceberg ploughmarks to cover the expanse of the seafloor.

A comparison of iceberg scour widths and reliefs between this study and other glaciated margins is shown below (Figure 5.2 and 5.3). The measurements of iceberg scour widths, measured from marginal berm to marginal berm of each v-shaped incision in cross profile, range from 93 – 375 meters in SG9810 and 50-350 meters in SG9804; these numbers are very close to scour measurements published in the Barents Sea by other authors, ranging from 65 – 300 meters (Andreassen et al., 2008; Esteves et al., 2017).

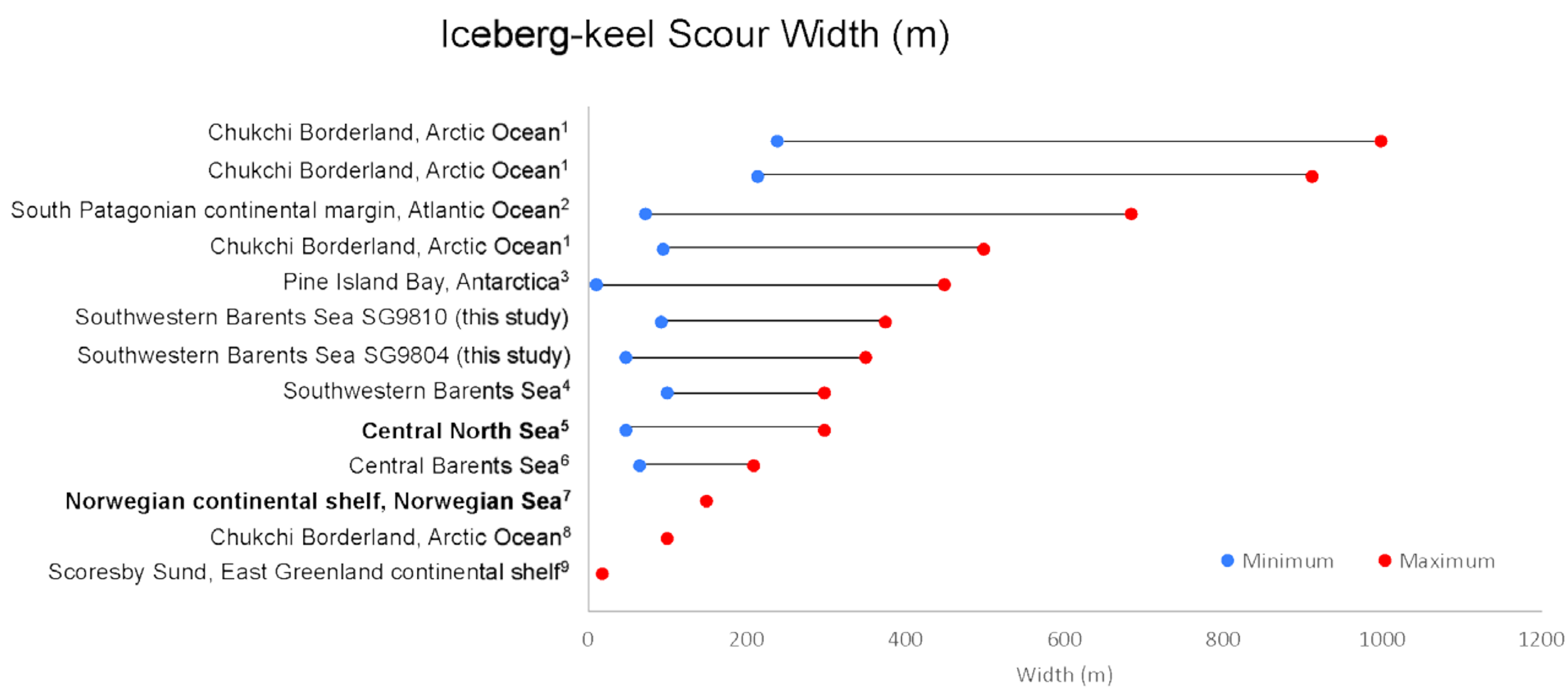

Figure 5.2. *Comparison of iceberg-keel scour widths measured from several glaciated margins, with blue markers indicating minimum widths and red markers indicating maximum widths (note: several locations only have maximum values). Most locations are seafloor surface measurementss, while subsurface measurements are bolded. Superscript numbers are references to published papers (1) Jakobsson et al., 2005 (2) López-Martínez et al., 2016 (3) Wise et al., 2017 (4) Andreassen et al., 2008 (5) Dowdeswell and Ottesen, 2013 (6) Esteves et al., 2017 (7) Ottesen et al., 2009 (8) Polyak et al., 2001 (9) Dowdeswell et al., 1993.*

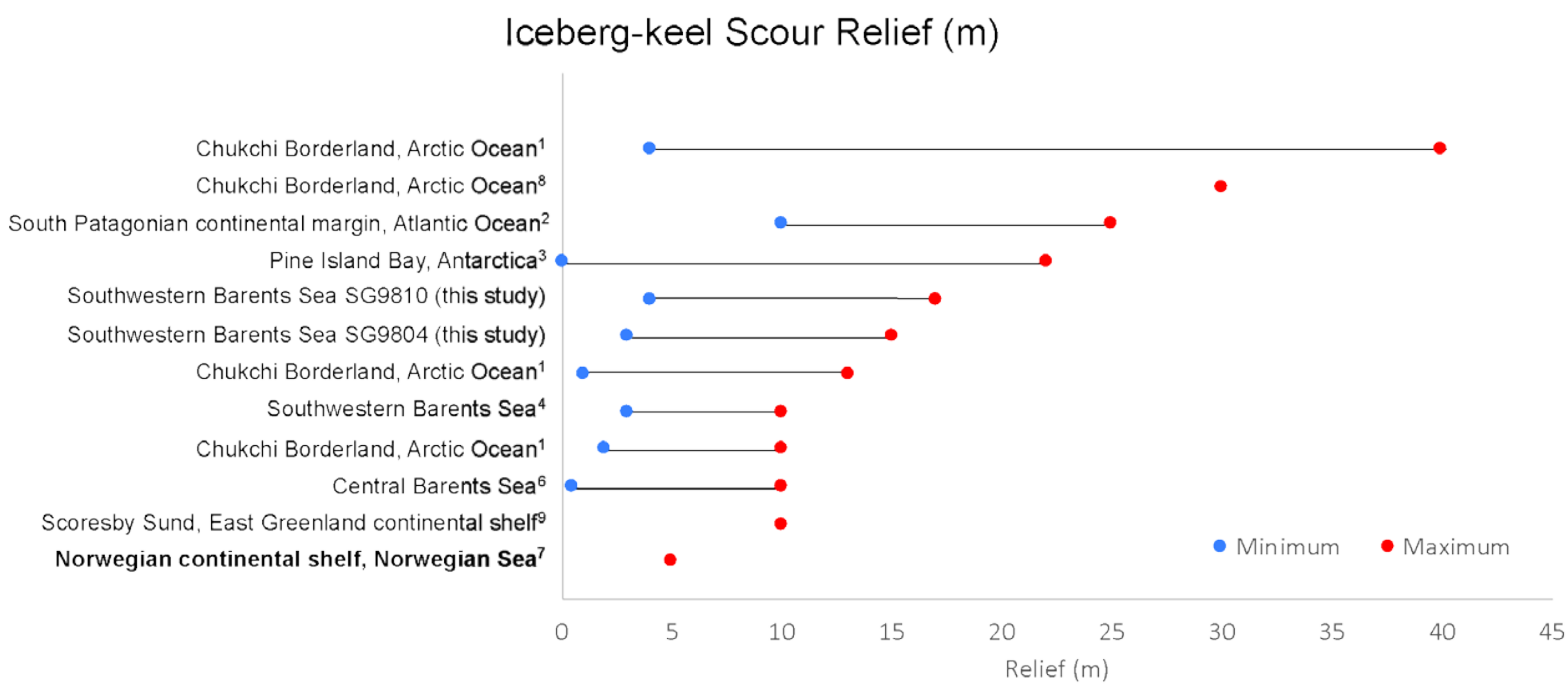

Figure 5.3. *Comparison of iceberg-keel scour relief measurements from several glaciated margins, with blue markers indicating minimum widths and red markers indicating maximum widths (note: several locations only have maximum values, no zero values used in graph). Bolded locations are subsurface measurements, while the rest are from seafloor measurements. Superscript numbers are references to published papers (references in Figure 5.2).*

The presence of iceberg scours on the seafloor is indicative of a glaciomarine-environment, as documented by many authors within the Barents Sea (Rafaelsen et al., 2002; Andreassen et al., 2008; Winsborrow et al., 2010; Andreassen et al., 2014; Piasecka et al., 2016; Piasecka et al., 2018). The slight east-west orientation of the iceberg scours, particularly visible in SG9804, suggests that wind direction and water currents may have been oriented towards the east or towards the west (Rafaelsen et al., 2002). The source of the icebergs that created the scours is most likely from the large ice sheets that retreated during the last major deglaciation during the LGM (~20,000 years ago) (Dowdeswell and Bamber, 2007). Intersecting ploughmarks may indicate slightly differing ages (Andreassen et al., 2014); however, lack of present-day ice sheets in the Barents Sea or northern Scandinavian region leads to the assumption that these iceberg-keel plough marks were formed following the melting and retreat of ice sheets following the LGM.

5.2 Subsurface Interpretation

5.2.1. Grooves from Differential Erosion

Long, continuous erosional grooves on the eastern side of the SG9810 URU are heavily influenced by the underlying bedrock and structural trends of the southwestern dipping beds. These grooves likely represent differential erosion of the bedrock beneath the URU.

The underlying bedrock is dominantly Cretaceous shale, or possibly a mix of sandstone and shale layers. If the bedrock consists mainly of shale, the differential erosion of the underlying substrate could mean that the long, continuous grooves were eroded from slightly less-resistant shale layers. In contrast, the more-resistant layers would protrude, creating the highs between each of the u-shaped lows.

If the substrate consisted of alternating, thick layers of sandstone and shale, the shale would be represented by increases in acoustic impedance or black reflectors, while the sandstone would be represented by decreases in acoustic impedance or red reflectors. In this case, the shale would be more easily eroded (lows) between the more-resistant sandstone (highs) creating u-shaped grooves that continue across the eastern portion of this seismic grid (Figure 5.4).

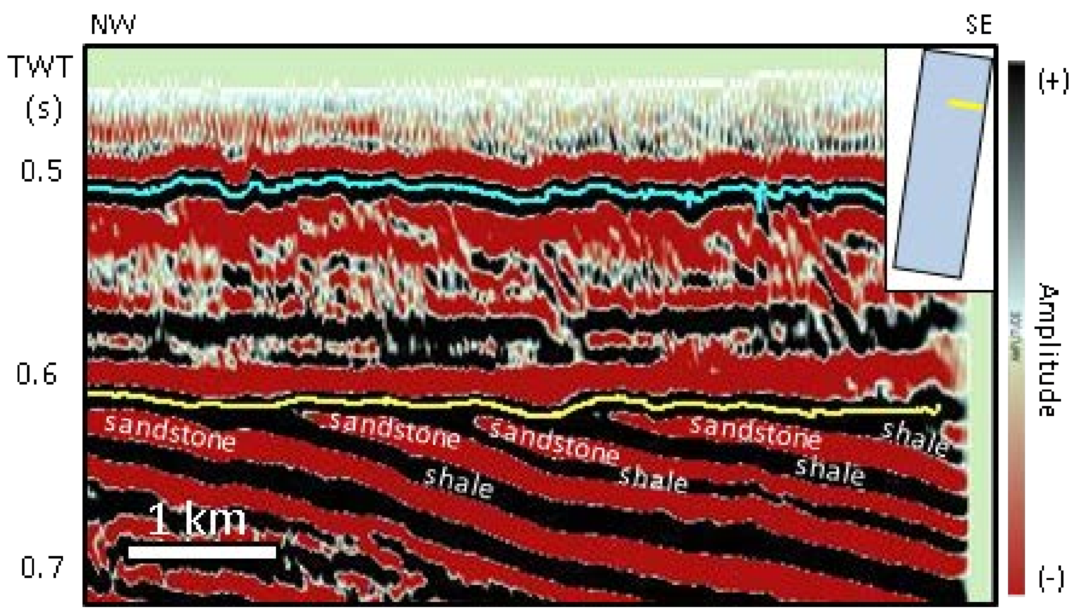

Figure 5.4. *Seismic line (location from inset in upper right corner) of SG9810 showing potential differential erosion of non-resistant shale (black reflectors) and the slight protrusion of more-resistant sandstone (red reflectors). Blue horizon represents seafloor, and yellow horizon represents URU. Vertical exaggeration: 10x.*

Lack of core data from this study area leads to an incomplete understanding of the Cretaceous bedrock, and therefore it is difficult to predict whether the reflectors beneath the URU represent exclusively shale or alternating layers of sandstone and shale. However, alternating sandstone and shale layers may be more plausible because it would take into account both the lithology of the bedrock and the polarity of the seismic data. In this case, a cross-profile view would show the shallow, u-shaped dips visible in the shale bedrock with alternating layers of sandstone and shale (Figure 5.5). Though the dip slope and scarp slope are not as easily discernable or as obvious in the seismic line as in Figure 5.5, much of the less-resistant, weaker shale layers have been eroded, creating shallow dips between erosion-resistant sandstone.

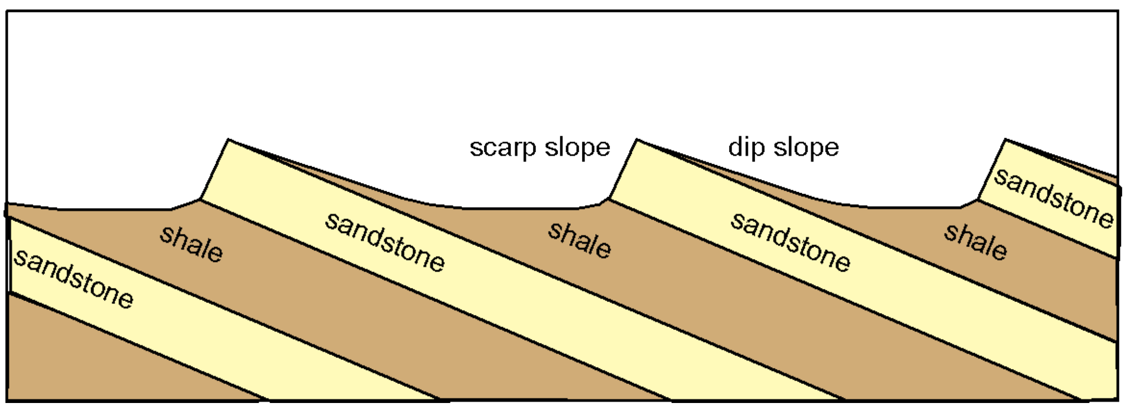

Figure 5.5. *Cross-profile view of tilted strata influenced by differential erosion. Valleys are created by erosion of non-resistant strata (e.g., shale) between ridges of more-resistant strata (e.g., sandstone). The asymmetrical valleys have a steeper side (scarp slope) and slightly more gentle side (dip slope). The direction of ice flow is towards the north-northwest, as indicated by the black arrow.*

The RMS seismic attribute was also applied to the URU surface in SG9810 for better analysis of the differential erosion. The amplitude values are generally low for the majority of the RMS map, but are slightly higher where the differential erosion is most prominent (Figure 5.6). The depths of the grooves measure up to 11 m in relief in the northeast section of the RMS surface.

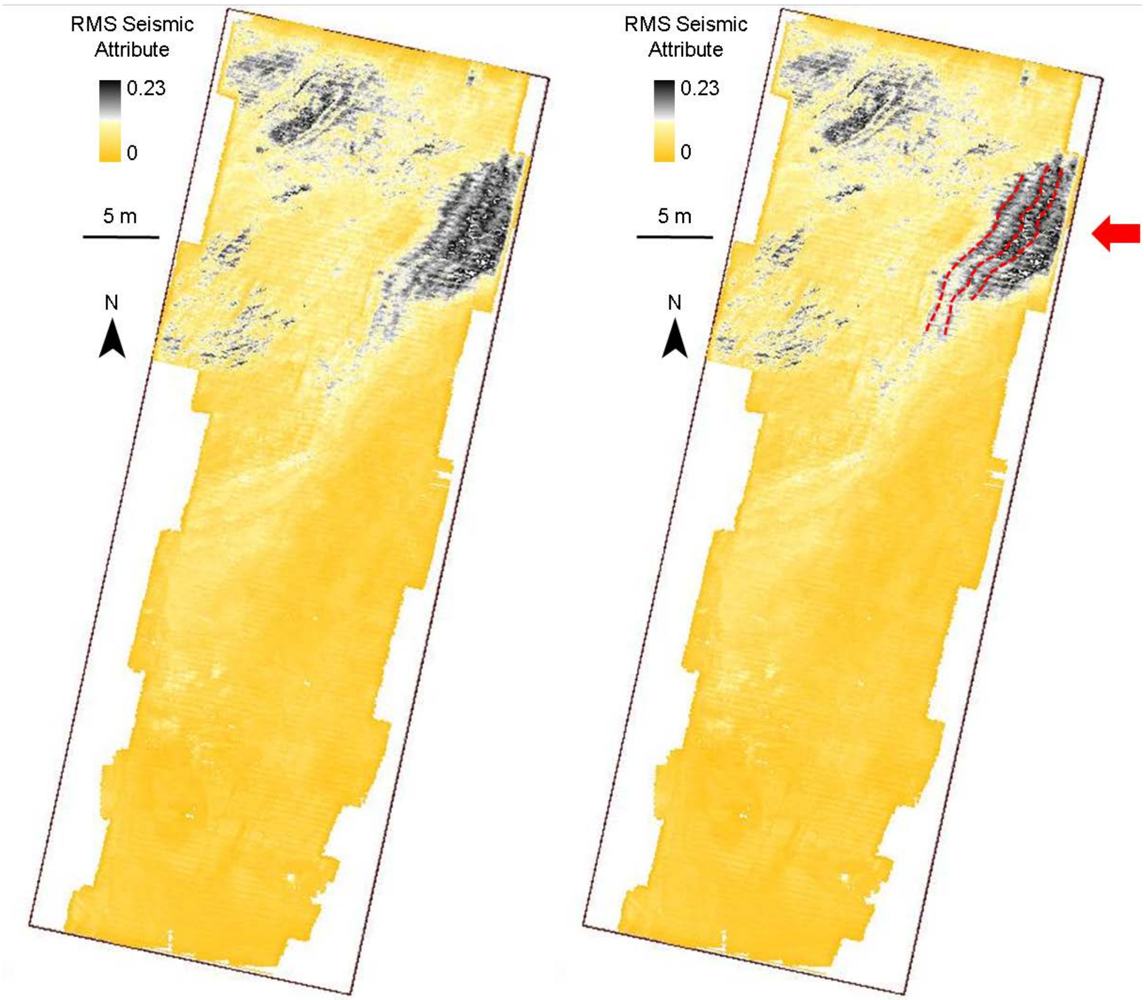

Figure 5.6. *Uninterpreted (left) and interpreted (right) RMS maps for SG9810 URU surface, showing the higher amplitude values in the northern section (red arrow), particularly concentrated in the upper right hand corner where differential erosion is most prominent (erosional grooves outlined in dashed red lines).*

5.2.2 Subglacially-eroded Depressions

Two erosional depressions are observed in the subsurface, one from each seismic grid. Previously, Rafaelsen et al. (2002) divided depressions found in the Barents Sea using 3D-seismic data into three different categories: type I (concentric depressions with a smooth surface and even edges), type II (elliptical shape with rough or indented edges), and type III (semi-circular depression with relatively smooth edges that formed in bedrock).

The subsurface, circular depression observed on the URU in SG9810 and the larger, slightly elliptical depression on the URU in SG9804 may both have formed from subglacial erosion of the Cretaceous bedrock. The small depression (SG9810) is more circular, located away from the erosional grooves, and has a slightly steeper slope on one side and gentler slope on the other. The larger depression (SG9804) has a slightly elongated northwest-southeast trend, an almost elliptical shape, and is not cut by the ridge-groove paired features that trend northwest-southeast. In SG9804, a differently oriented (northeast) 3D view of the depression shows ridge-groove paired features reaching the edge of the depression, but not visible within the edges, suggesting the linear features and depression may have formed at the same time (Figure 5.6). Both depressions have relatively smooth edges and circular to semi-circular shapes, and may have been formed beneath the ice sheet in locations where the bedrock was slightly easier to erode (Rafaelsen et al., 2002). The subsurface depressions might be classified as type III depressions for their shape (semi-circular with relatively smooth edges), depth (up to 15 meters), and location (erosion of underlying Cretaceous bedrock).

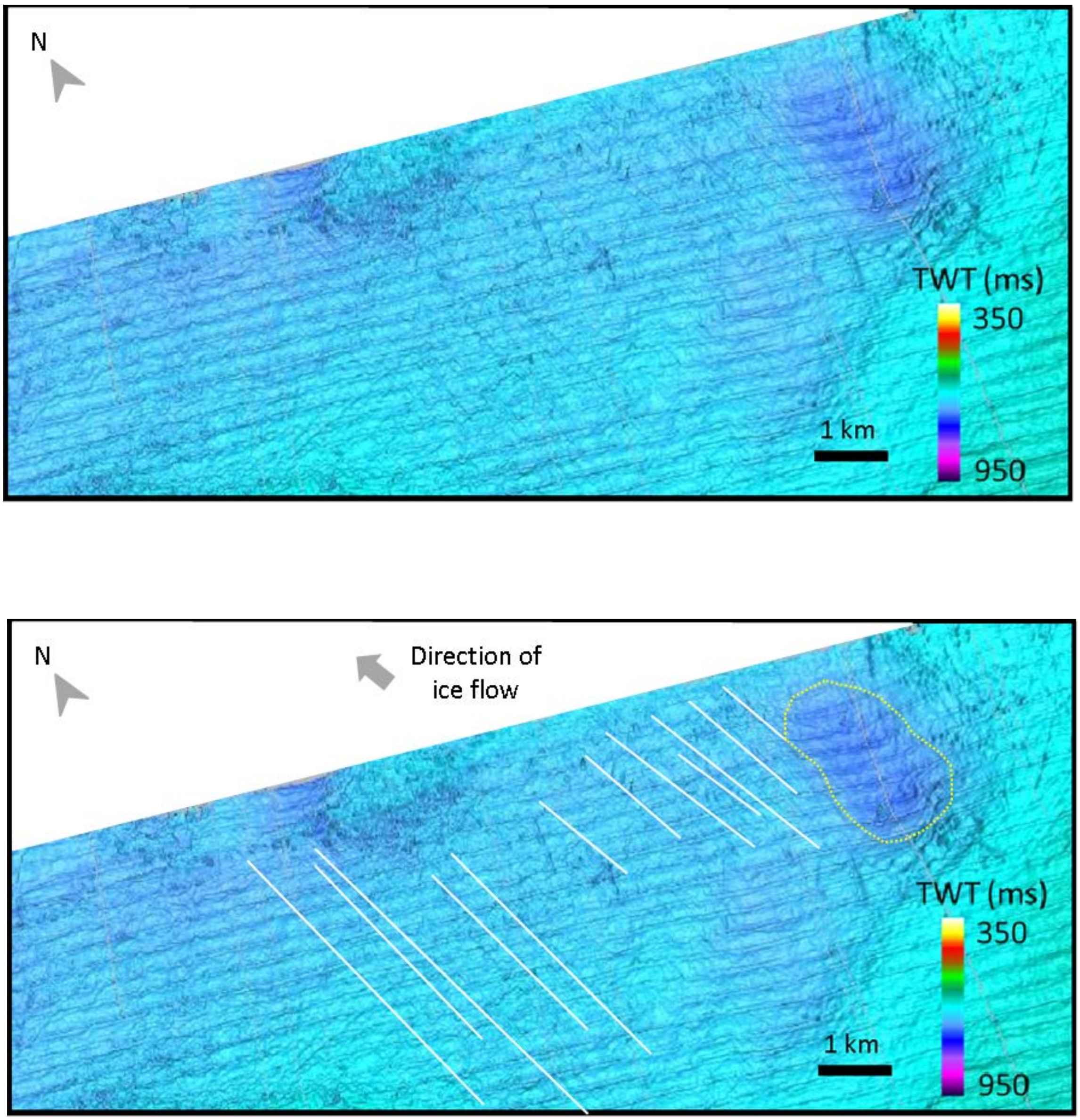

Figure 5.6. *Slightly angled view (north is now pointing towards the northwest) of depression on URU in seismic grid SG9804 uninterpreted (above) and interpreted (below) with a few linear ridge-groove pairs outlined in white lines, and the depression outlined in a yellow dashed line. White linear features are visible across the northern part of the grid, leading up to the edge of the depression, but not within the depression itself.*

Depressions that form in bedrock due to subglacial meltwater erosion have ranged in diameter from a few meters to several hundred meters (Bennett and Glasser, 2009). The effectiveness of the subglacial meltwater beneath the ice sheet would depend on three factors: the susceptibility of the underlying bedrock (e.g., structural weakness), the water discharged (e.g., water velocity of subglacial meltwater), and the quantity of transported sediment (Bennett and Glasser, 2009).

One possible explanation for the formation of the depressions could be that the depressions are similar to sculpted forms, or s-forms, which are described in Alberta, Canada, by Beaney and Shaw (2000). S-forms are eroded by subglacial meltwater and often form in different varieties of vorticies in turbulent flow (Beaney and Shaw, 2000). They form in broad areas of subglacial meltwater, which cause the coeval formation of large depressions (e.g., in SG9804) with the other features (e.g., ridge-groove pairs) which do not necessarily overlap or cross-cut each other because they were created by similar flow (Beaney and Shaw, 2000).

Another potential explanation would be that these depressions are evidence of plunge pools. These features are specific kinds of potholes that occur at the foot of a nearly vertical waterfall, creating a steeply sloping side of the depression (Elston, 1917). The depth and diameter of the depression would depend on the height of the waterfall and the volume of the water, respectively (Elston, 1917). An example from Niagara Falls describes a large plunge pool with a depth of 72 ft (21 m), which is close to the depths of the depressions in this study region (~17 m) (Elston, 1917). This interpretation would require that this specific area was subaerial at the time of plunge-pool formation;

however, there is no detailed information regarding which regions of the Barents Sea became submarine and which regions stayed a subaerial shelf sea around 1 Ma (Dimakis et al., 1998; Butt et al., 2002). Though plunge pools are a possibility, they cannot be proved with the current understanding of the Barents Sea at around 1 Ma, and even more so during the formation of the URU ~800,000 years ago.

The more likely explanation includes the formation of depressions in bedrock by subglacial meltwater erosion, potentially creating a subglacial lake beneath the ice. This could be due to increased melting in one particular spot, which caused meltwater to continuously erode the bedrock beneath. The depressions were mostly likely created at the same time as the other features (MSGLs and grooves) on the URU because they two structures do not overlap or cross-cut in any way. With the current understanding of the Barents Sea at this time, subglacial meltwater erosion is a likely interpretation for both of the depressions in SG9810 and SG9804.

5.2.3. Mega-scale Glacial Lineations

The linear, ridge-groove paired features observed in SG9804 that generally trend in the same direction differ from iceberg-keel scour marks in several ways: they have a clear preferred orientation, they are straight and appear parallel to one another, they do not vary widely in size or depth, and they have a distinct pattern of ridge-groove-ridge-groove topography covering an expansive area of the URU. Based on their description, and previously published glacial history of the region, lineations such as these ridge-groove pairs are interpreted as MSGLs (Clark, 1993), which are often observed within high-latitude troughs and fjords (Ottesen et al., 2005) (Figure 5.7).

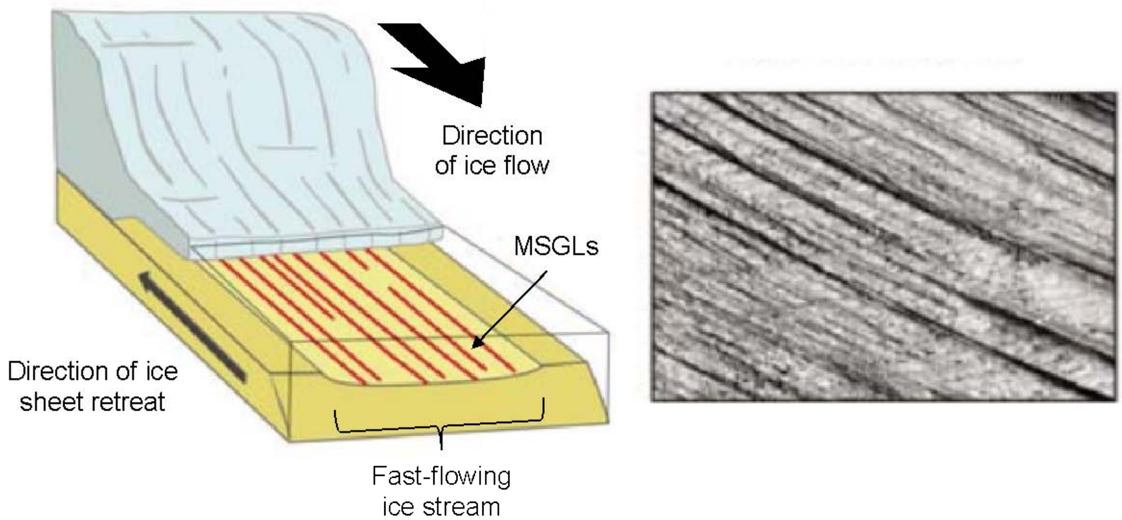

Figure 5.7. *(left) Schematic diagram of submarine MSGLs indicating fast flow of ice streams in a high-latitude region or continental shelf (right) swath bathymetric image example of MSGLs (scale across 15 km) (modified from Dowdeswell et al., 2008)*

MSGLs are streamlined, elongated glacial geomorphic features that form from subglacial sediment deformation at the base of fast-flowing ice streams under rapid flow in a layer of deforming till (Clark, 1993; Clark et al., 2003; Dowdeswell et al., 2008), and can extend as many as tens of kilometers with wavelengths of tens to hundreds of meters and up to a few meters of relief (Dowdeswell et al., 2008) (Figure 5.8). In this study area, much of the underlying bedrock or substrate was eroded by the ice stream, which carved parallel MSGLs in the direction of ice flow. The MSGLs measured in SG9804 are roughly 200 – 500 m in width and up to 13 m in relief, extending a minimum length of 2.5 km, falling well into the range for MSGLs.

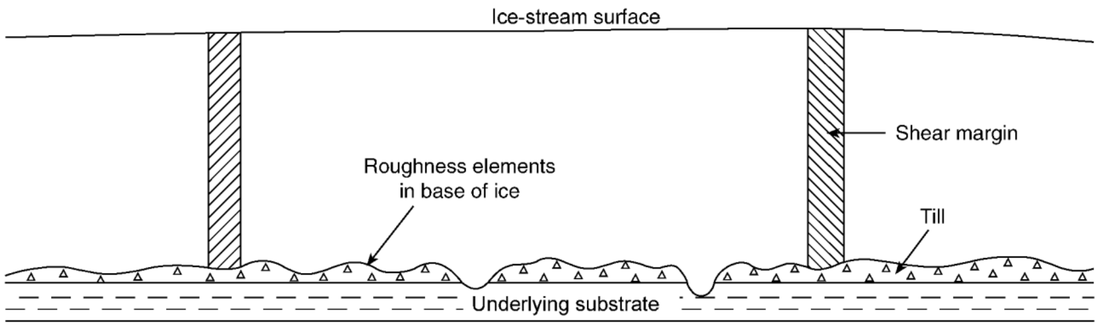

Figure 5.8. *Cross section of an ice stream showing the deformation of the underlying till layer, creating the groove-ridge pair features, or MSGLs (from Clark et al., 2003). Certain areas of larger keels can erode through the till into the underlying substrate, which is then eroded and adds to the sediment supply of the overlying till layer.*

MSGLs are particularly useful for examining paleo-ice flow direction, because the streamlined features form parallel to the direction of ice flow. In seismic grid SG9804, the subsurface MSGLs are trending northwest-southeast (see Figure 4.13). However, in order to determine the exact direction of ice flow, the features must be compared to seafloor studies of the Barents Sea. Inferred ice flow direction of former ice streams in the southwestern Barents Sea, from MSGLs mapped on the seafloor, show that much of the ice from the LGM flowed out the deep Bjørnøyrenna Trough off the western Barents Sea continental margin (Figure 5.9)

The location of SG9804 is close to the edge of Nordkappbanken (Figure 3.1A), and by extrapolating from the direction of ice flow from the LGM (Figure 1.2), MSGLs observed on the URU are more likely to flow towards the northwest, as those found on the seafloor, rather than towards the southeast. This is additionally supported by the glacial history of the region, where the ice sheets began growing on the mountainous regions of mainland Norway, then advanced out into the ocean, suggesting ice flowed away from the continent rather than towards it (Knies et al., 2009). The trend of the MSGLs, towards the northwest, are roughly 340°-345°. Additionally, the presence of MSGLs, but lack of retreat moraines or sedimentary wedges, not only indicates fast flowing ice through ice streams in this area (Andreassen et al., 2004; Andreassen et al., 2008), but also are indicative of rapidly or continuously retreating ice (Dowdeswell et al., 2008).

MSGLs have been mapped extensively in the Barents Sea (Rafaelsen et al., 2002; Andreassen et al., 2004; Ottesen et al., 2005; Dowdeswell et al., 2008; Andreassen et al., 2008; Winsborrow et al., 2010; Rüther et al., 2011; Piasecka et al., 2018), but have also been observed in many other glaciated margins including Canada (Clark et al., 1993), Newfoundland (Jakobsson et al., 2005), and Antarctica (Shipp et al., 1999; Wellner et al., 2001; Dowdeswell et al., 2004; Campo et al., 2017). Measurements of the MSGLs observed in SG9804 can be compared to similar measurements in other locations (Figure 5.10), a few of which are labelled in the histogram from a more comprehensive study of MSGL dimensions (Spagnolo et al., 2014).

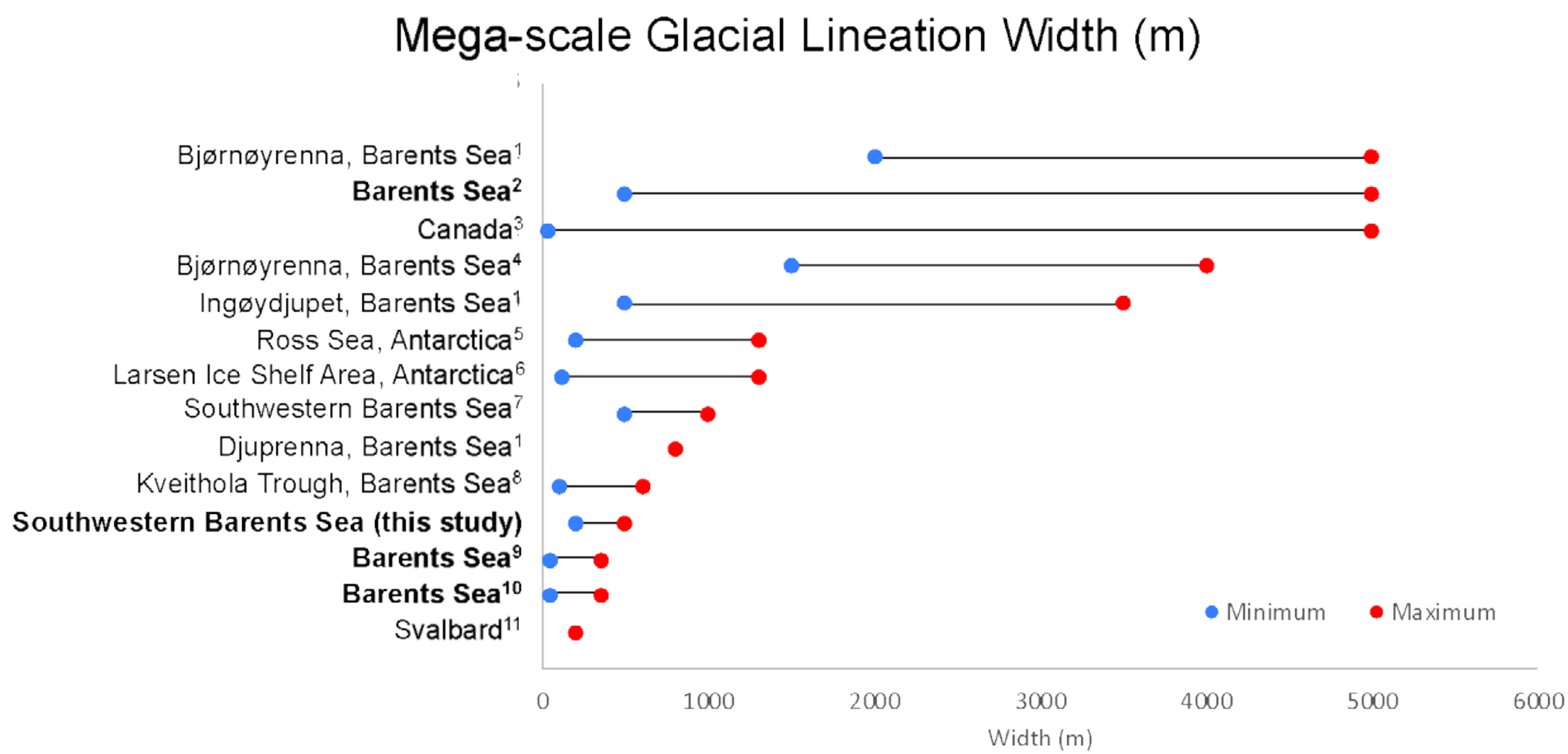

Figure 5.10 *Comparison of MSGL widths from several glaciated margins, with blue markers indicating minimum widths and red markers indicating maximum widths (note: some measurements include only maximums, no zero values used in graph). Bolded locations are subsurface measurements, and all others are seafloor measurements. Superscript numbers are references to published papers (1) Andreassen et al., 2008 (2) Andreassen et al., 2007 (3) Clark et al., 1993 (4) Rüther et al., 2011 (5) Shipp et al., 1999 (6) Campo et al., 2017 (8) Rebesco et al., 2011 (9) Andreassen et al., 2004 (10) Andreassen and Winsborrow, 2009 (11) Ottesen et al., 2008.*

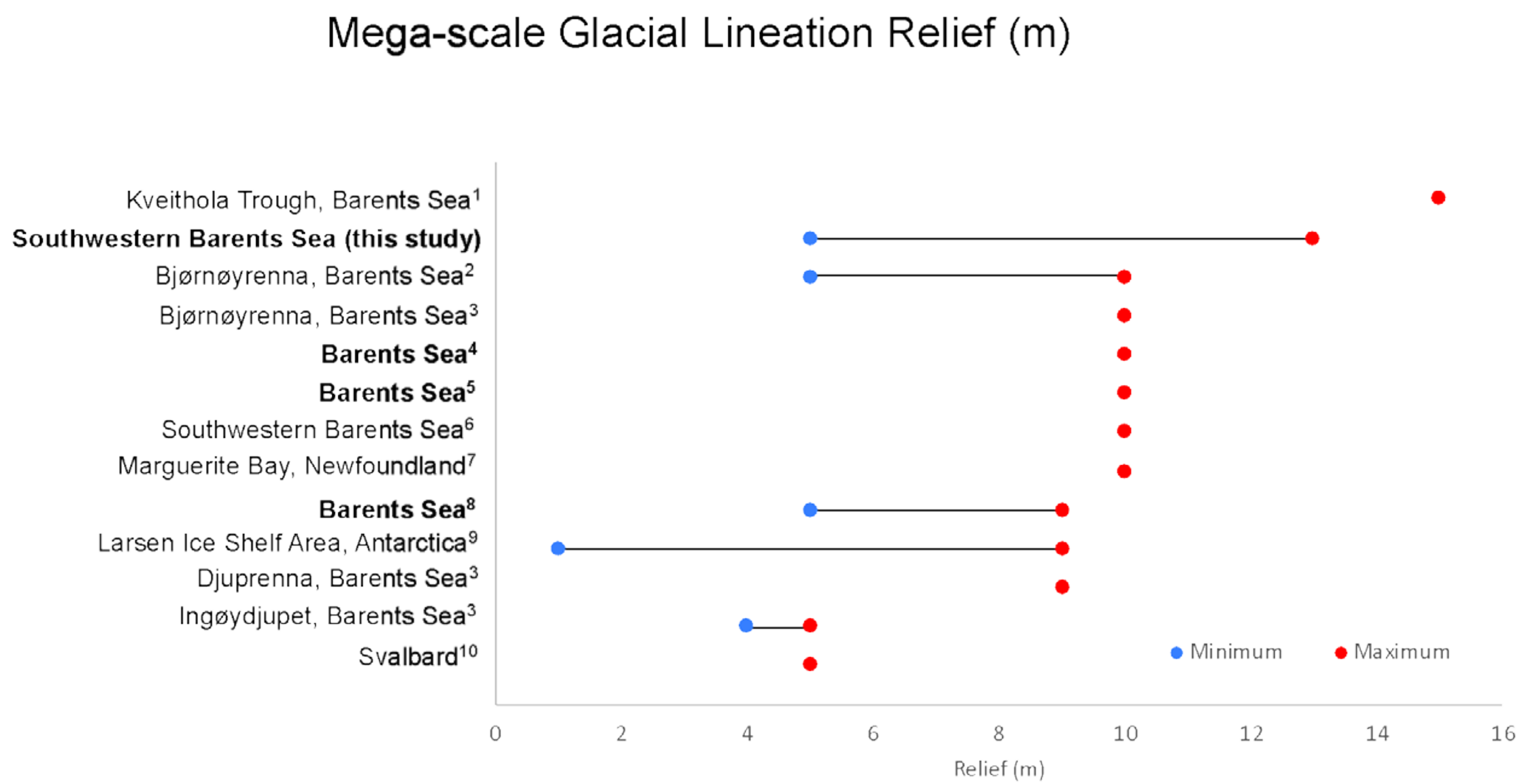

Figure 5.11 *Comparison of MSGL relief measurements from several glaciated margins, with blue markers indicating minimum widths and red markers indicating maximum widths (note: some measurements include only maximums, no zero values used in graph). Bolded locations are subsurface measurements, and all others are seafloor measurements. Superscript numbers are references to published papers (1) Rebesco et al., 2011 (2) Rüther et al., 2011 (3) Andreassen et al., 2008 (4) Andreassen et al., 2004 (5) Andreassen and Winsborrow, 2009 (6) Winsborrow et al., 2012 (7) Jakobsson et al., 2005 (8) Andreassen et al., 2007 (9) Campo et al., 2017 (10) Ottesen et al., 2008.*

Ultimately, a large scale comparison of MSGLs in the southwestern Barents Sea would contrast MSGL directions from the seafloor (LGM) with MSGL directions from the URU (~800,000 years ago) (Figure 5.12). Although the seafloor surface shows more mapping of MSGLs, the subsurface MSGLs that have been identified seem to trend in the same directions as those found from the LGM – particularly, most of the MSGLs indicate ice that was flowing out of the smaller troughs to reach the large, deep Bjørnøyrenna Trough and flow westwards towards the Norwegian-Greenland Sea.

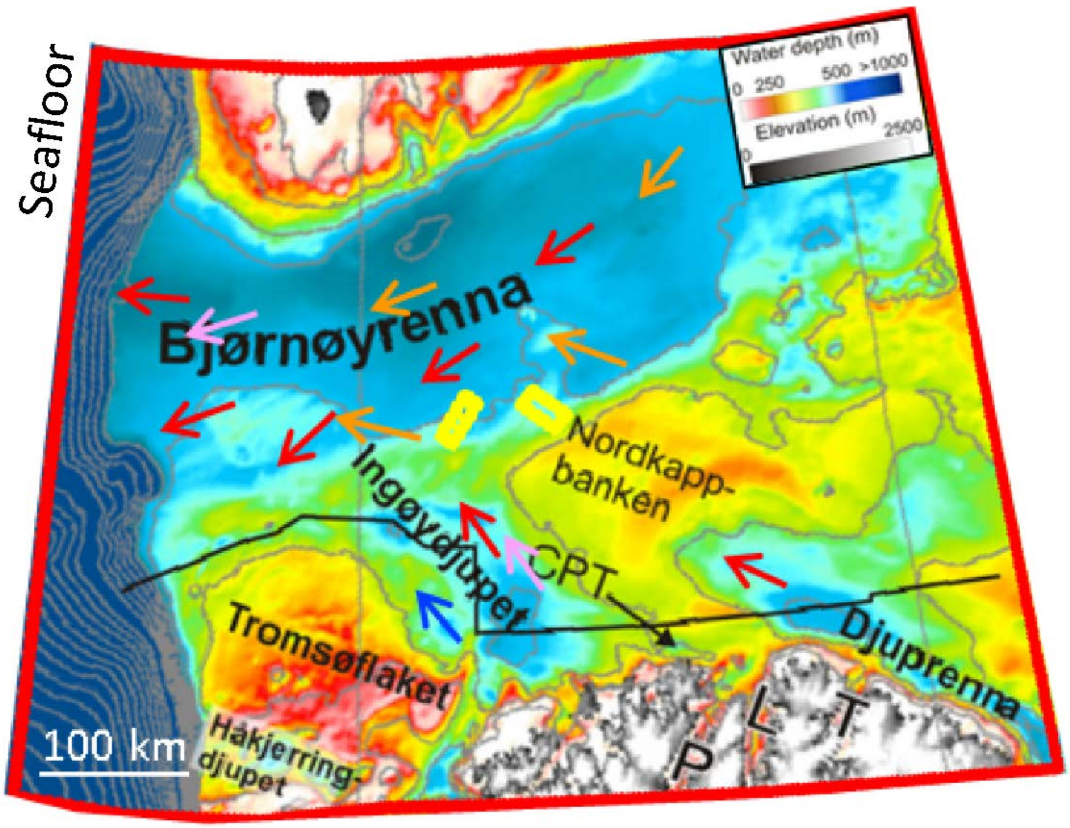

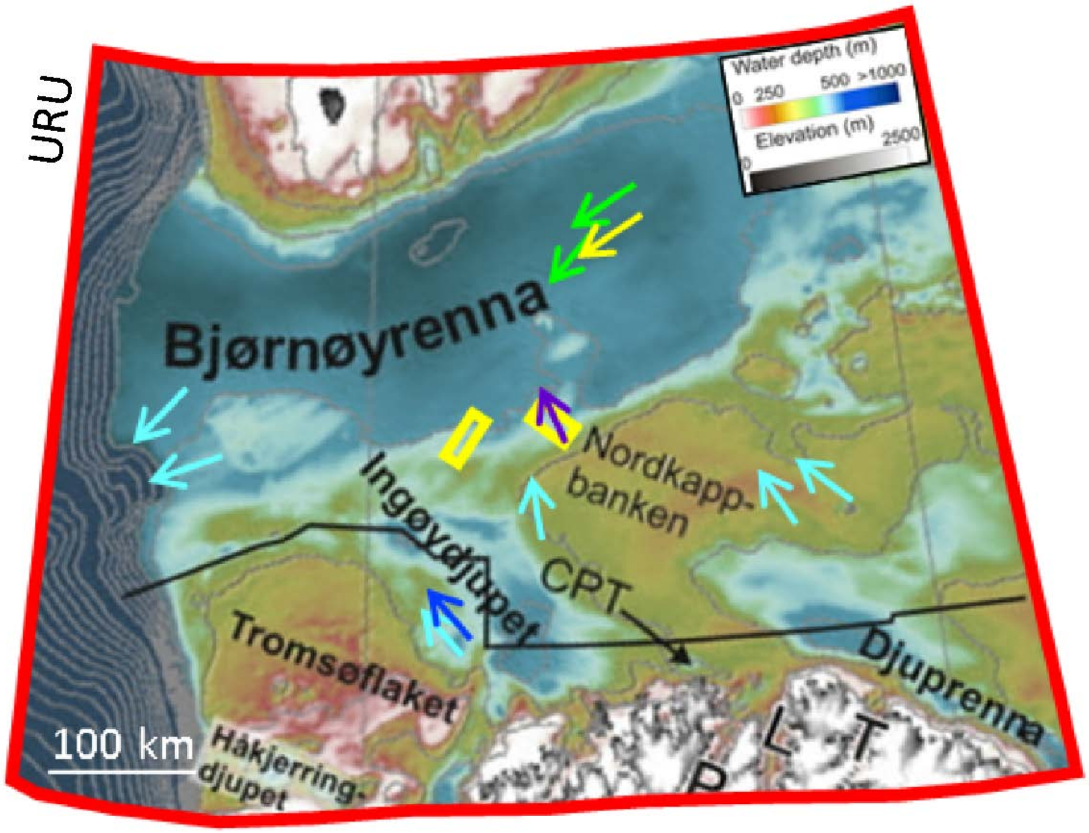

Figure 5.12. *Comparison of MSGL directions from the seafloor (above) and URU (below), with study area 3D grids outlined in yellow. Bathymetry map from Winsborrow et al., 2010. Different colored arrows are from published papers; pink arrow represents paleo-ice flow direction from this study, which is only visible in the subsurface. For seafloor arrows: Dark blue = Ostanin et al., 2005, Red = Winsborrow et al., 2010; Light green = Rebesco et al., 2011, and Purple = Laberg et al., 2012. For URU arrows: Light blue = Larsen et al., 2003, Dark blue = Ostanin et al., 2005; Dark green = Khan 2013; and Orange = Piasecka et al., 2016.*

5.2.4. Iceberg Break-up near the Grounding Zone

Four linear, erosional furrows cut across the MSGLs on the URU surface of SG9804 (Figure 4.2.7). Though parallel to each other and also linear, they differ from MSGLs in length, spacing, and direction – the younger features, cutting across older MSGLs, are much shorter (1.7-2.5 km), spaced unevenly (ranging from 1.3-6.1 km apart), and trend northeast-southwest, unlike the northwest-trending MSGLs. Additionally, these features are erosional rather than the depositional/deformational formation of MSGLs, and do not contain topographic ridges, only furrows.

The furrows are interpreted to be ice-marginal features that form close to the grounding line – specifically, linear iceberg furrows (Halberstadt et al., 2016). This type of furrow is different from an iceberg scour because they are created very close to the grounding line, or at the edge of a large ice mass, where permanently grounded ice transitions into a floating or calving ice shelf (Jakobsson et al., 2011; Halberstadt et al., 2016). The proximity to the grounding line would allow for the furrows to be parallel, but unevenly spaced depending on the size of the glaciers calving off from the main ice mass.

The relief of this lineation very shallow and much smaller than the MSGLs. Depending on the varying changes in ice sheet advance and retreat, and the merging of several ice sheets, the younger features may have been created by glaciers during a period of relative ice sheet retreat, causing icebergs to break off and erode towards the northeast rather than flow in the same northwest direction of the MSGLs (Figure 5.13).

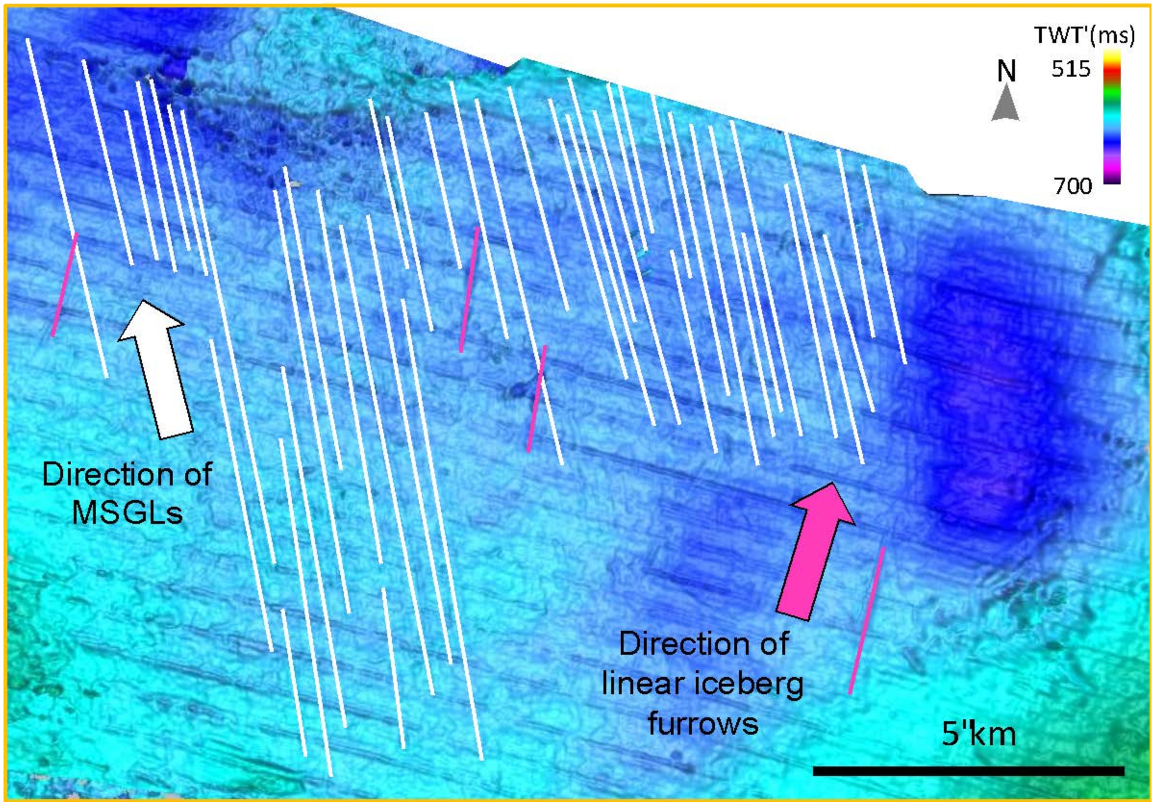

Figure 5.13. *Interpreted direction of older MSGLs compared to the direction of younger, linear iceberg furrows that cut across the lineations.*

5.3 Summary of Glacial Geomorphic Features

For both SG9810 and SG9804, iceberg-keel ploughmarks covered the expanse of the seafloor. Ploughmarks are good indicators of depositional environment, and in this case represent a glaciomarine to open marine environment following ice sheet retreat of the LGM. However, for the two 3D-seismic grids in this study, no features on the seafloor showed evidence of ice flow direction from the LGM.

In the subsurface, a collection of different ice-related features were mapped and analyzed. In SG9810, several long, continuous grooves are present, likely eroded by several cycles of advancing and retreating ice sheets during the onset of glaciation. A small depression found on the URU carved into the underlying bedrock may be evidence of subglacial meltwater erosion, possibly from pooling meltwater beneath the ice sheet (Figure 5.14).

In SG9804, several elongated, ridge-groove paired features are interpreted as MSGLs, which indicate northwest-flowing ice from ~800,000 years ago. A large, ~17 m deep subglacially-carved depression identified next to the MSGLs has the same northwest-southeast orientation, and was likely formed by the same flowing ice that carved the MSGLs. This is particularly emphasized by the direction of the depression's long axis as well as the lack of MSGLs within the depression. Cross cutting the northwest-flowing MSGLs are several short, northeast-trending furrows, which indicate a potential change in environment of this specific spot from a subglacial environment (which carved the MSGLs and depression) to a proximal glaciomarine environment close to the grounding zone (which carved the short furrows). The furrows, which cross-cut the MSGLs but not the depression, may have been created by icebergs that calved off in the same, northeast direction, but were not deep enough to scour the bottom of the depression (Figure 5.15).

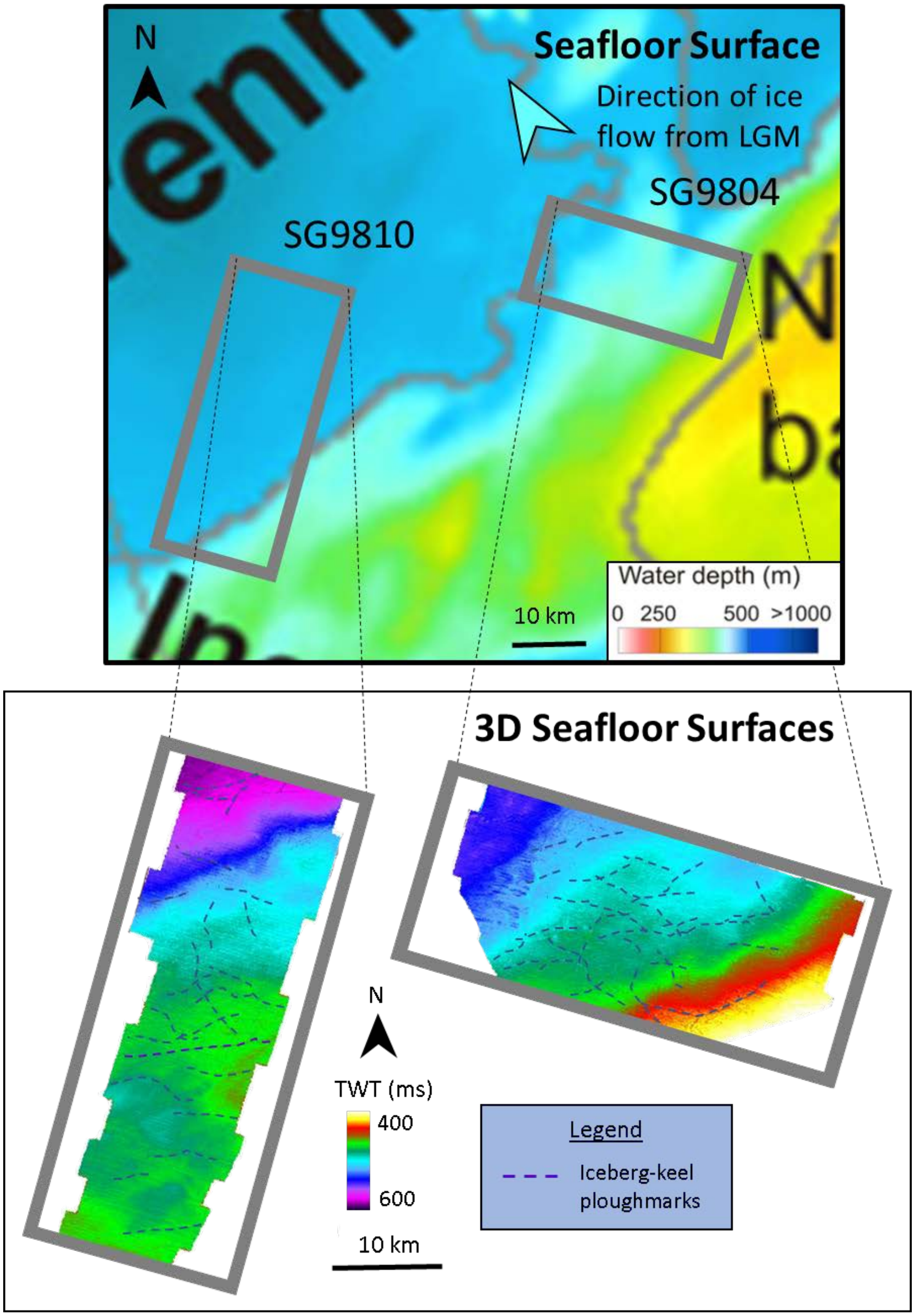

Figure 5.14. *Summary figure of seafloor glacial geomorphic features in SG9810 and SS9804 (bathymetry inset from Figure 3.1, from Winsborrow et al., 2010). Direction of ice flow indicated by light blue arrow. 3D surfaces show iceberg-keel ploughmarks outlined in dashed purple lines covering the expanse of the seafloor in both seismic grids, indicating a glaciomarine or open marine environment.*

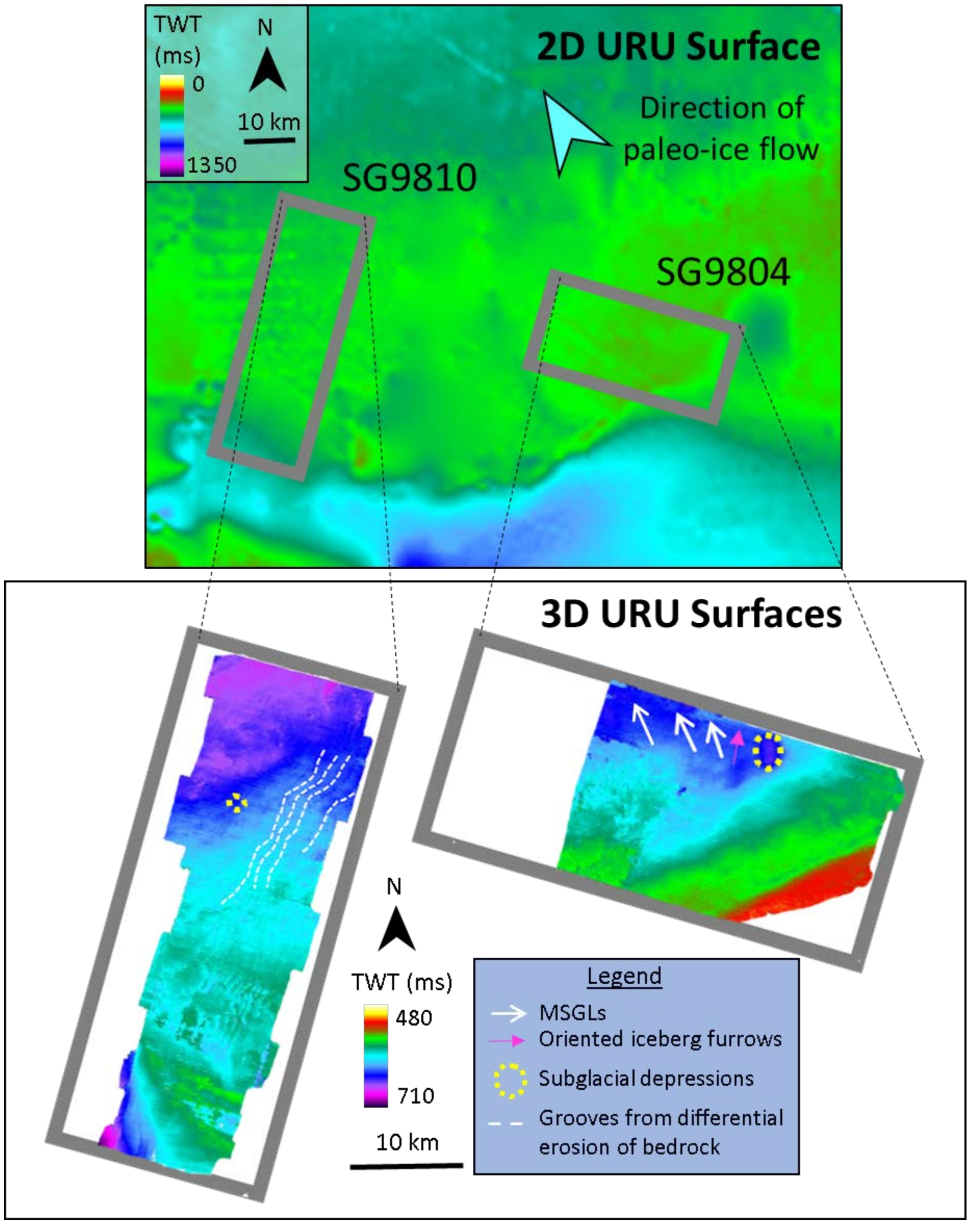

Figure 5.16. . *Summary figure of URU glacial geomorphic features in SG9810 and SS9804 (background from 2D seismic data in Figure 4.1). Direction of ice flow indicated by light blue arrow. 3D surface of SG9810 shows several long grooves from differential erosion of tilted strata below carved by cycles of ice sheet advance and retreat. A subglacial meltwater-carved depression (dotted yellow circle) is located away from the continuous grooves. SG9804 shows MSGLs indicating northwest paleo-ice flow, which likely also formed the subglacial meltwater-carved depression, which has an axis that also trends in the same northwest direction. The MSGLs are cross-cut by short, northeast-trending furrows that may indicate a change in environment from subglacial to proximal glaciomarine, which would form short furrows trending in the same direction.*

6. Conclusions

The resolution and density of 3D-seismic data allow for the creation of detailed, high-resolution surfaces that are able to image features >10 m in size and relief both in the seafloor and subsurface. Though certain features were only found subsurface, or only found on the seafloor, comparison to previously published papers creates the opportunity to determine the direction of paleo-ice flow in the Barents Sea, as well as identify depositional environments and examine geomorphic features carved by subglacial erosion in the study area.

The northwest-trending MSGLs identified in the subsurface (URU) and the comparison to seafloor studies of MSGLs suggest that paleo-ice flow was in the same direction as ice flow during the LGM. In comparison to other studies in the region (Figure 5.10), though the width of these MSGLs fall well within the range for the Barents Sea, the relief of the subsurface features in this study is slightly larger than some other published measurements. Though the gap between the subsurface (800,000 years ago) and LGM (20,000 years ago) is quite large, the paleo-record for ice flow implies that ice sheets most likely follow a pattern of behavior for growth and retreat. This is particularly useful in examining current glaciated margins, such as Greenland and Antarctica, to map MSGL locations and measurements in order to examine where fast-flowing ice is most dynamic and predicting future ice sheet retreat across a continental shelf can be studied using seafloor geomorphology (Muñoz and Wellner, 2018).

Though several authors have used MSGLs to examine changes in paleo-ice flow patterns in the Barents Sea (Andreassen et al., 2004; Andreassen et al., 2008; Rüther et al., 2011; Winsborrow et al., 2012), the presence of cross-cutting features may not be younger MSGLs, which would indicate a change in paleo-ice flow direction, but potentially iceberg-keel ploughmarks cross-cutting the older MSGLs. This may indicate a change in the environment of the region, which would have been subglacial during the formation of MSGLs, but proximal to the grounding line for iceberg scours that moved towards the northeast rather than the northwest.

The depressions and iceberg-keel ploughmarks are indicative of depositional environments in the Barents Sea. The depressions eroded into the underlying bedrock most likely occurred from subglacial meltwater erosion, while the presence of iceberg-keel ploughmarks across the seafloor of both 3D grids indicates a glaciomarine environment following subglacial conditions during the LGM ~20,000 years ago. Using seismic data to study glacial geomorphology is particularly useful in examining past glacial activity by imaging geomorphic features, such as MSGLs and iceberg-keel ploughmarks, in order to develop a better understanding of present-day ice sheet dynamics.

References Cited

Andreassen, K., Nilssen, L. C., Rafaelsen, B., and Kuilman, L. Three-dimensional seismic data from the Barents Sea margin reveal evidence of past ice streams and their dynamics. *Geology* 32: 729–732 (2004).

Andreassen, K., Laberg, J. S., and Vorren, T. O. Seafloor geomorphology of the SW Barents Sea and its glaci-dynamic implications. *Geomorphology*, 97: 157-177 (2008).

Andreassen, K., Nilssen, E. G., and Ødegaard, C. M. Analysis of shallow gas and fluid migration within the Plio-Pleistocene sedimentary succession of the SW Barents Sea continental margin using 3D-seismic data. *Geo-Marine Letters* 27: 155-171 (2007).

Andreassen, K., and Winsborrow, M. Signature of ice streaming in Bjørnøyrenna, Polar North Atlantic, through the Pleistocene and implications for ice-stream dynamics. *Annals of Glaciology* 50: 17-26 (2009).

Andreassen, K., Winsborrow, M. C. M., Bjarnadóttir, L. R., and Rüther, D. C. Ice stream retreat dynamics inferred from an assemblage of landforms in the northern Barents Sea. *Quaternary Science Reviews* 92: 246-257 (2014).

Barnes, P., and Lien, R. Icebergs rework shelf sediments to 500 m off Antarctica. *Geology* 16: 1130-1133 (1988).

Beaney, C. L., and Shaw, J. The subglacial geomorphology of southeast Alberta: evidence for subglacial meltwater erosion. *Candian Journal of Earth Sciences* 37: 51-61 (2000).

Bennet, M. R. and Glasser, N. F. Glacial geology – Ice sheets and landforms. *Wiley-Blackwell* 2nd edition (2009).

Breivik, A. J., Faleide, J. I., and Gudlaugsson, S. T. Southwestern Barents Sea margin: late Mesozoic sedimentary basins and crustal extension. *Tectonophysics* 293: Issues 1-2: 21-44 (1998).

Bulat, J. Some considerations on the interpretation of seabed images based on commercial 3D-seismic in the Faroe-Shetland Channel. *Basin Research* Vol. 17 Issue 1: 21-42 (2005).

Butt, F. A., Drange, H., Elverhøi, A., Otterå, O. H., and Solheim, A. Modelling Late Cenozoic isostatic elevation changes in the Barents Sea and their implications for oceanic and climatic regimes: preliminary results. *Quaternary Science Reviews* 21: 1643-1660 (2002).

Campo, J. M., Wellner, J. S., Domack, E., Lavoie, C., and Yoo, K. Glacial geomorphology of the northwestern Weddell Sea, eastern Antarctic Peninsula continental shelf: Shifting ice flow patterns during deglaciation. *Geomorphology* 280: 89-107 (2017).

Carrillat, A., Hunt, D., Randen, T., Sonneland, L., and Elvebakk, G. Mapping carbonated build-ups from seismic data. *Petroleum Geology: North-West Europe and Global Perspectives – Proceedings of the 6th Petroleum Geology Conference* 6: 1595-1611 (2005).

Chen, Q. and Sidney, S. Seismic attribute technology for reservoir forecasting and monitoring. *The Leading Edge* 16: 445-448 (1997).

Chopra, S. and Marfurt, K. J. Seismic attributes – A historical perspective. *Geophysics* Vol. 70 No. 5: 3SO-28SO (2005).

Clark, C. D. Mega-scale glacial lineations and cross-cutting ice-flow landforms. *Earth Surface Processes and Landforms* 18: 1-29 (1993).

Clark, C. D., Tulaczyk, S. M., Stokes, C. R., and Canals, M. A groove-ploughing theory for the production of mega-scale glacial lineations, and implications for ice-stream mechanics. *Journal of Glaciology* 49: 240-256 (2003).

Dimakis, P., Braathenb, B. I., Faleide, J. I., Elverhøid, A. E., and Gudlaugssone, S. T. Cenozoic erosion and the preglacial uplift of the Svalbard-Barents Sea region. *Tectonophysics* 300: Issues 1-4: 311:327 (1998).

Dokken, T. M., and Jansen, E. Rapid changes in the mechanism of ocean convection during the last glacial period. *Nature* 401: 458-461 (1999).

Dowdeswell, J. A. and Bamber, J. L. Keel depths of modern Antarctic icebergs and implications for sea-floor scouring in the geological record. *Marine Geology* 243: 120-131 (2007).

Dowdeswell, J. A., Canals, M., Jakobsson, M., Todd, B. J., Dowdeswell, E. K., and Hogan, K. A. Atlas of submarine glacial landforms: Modern, Quaternary, and Ancient. *Geological Society, London, Memoirs* 46 (2016).

Dowdeswell, J. A., Cofaigh, C. Ó., and Pudsey, C. J. Thickness and extent of the subglacial till layer beneath an Antarctic paleo-ice stream. *Geology* 32: 13-16 (2004).

Dowdeswell, J. A. and Ottesen, D. Buried iceberg ploughmarks in the early Quaternary sediments of the central North Sea: A two-million year record of glacial influence from 3D-seismic data. *Marine Geology* 344: 1-9 (2013).

Dowdeswell, J. A., Ottesen, D., Evans, J., Cofaigh, C. Ó., and Anderson, J. B. Submarine glacial landforms and rates of ice-stream collapse. *Geology* 36: 819-822 (2008).

Dowdeswell, J. A., Ottesen, D., and Rise, L. Landforms characteristic of inter-ice stream settings on the Norwegian and Svalbard continental margins. *Geological Society of London* 46: 437-444 (2016).

Dowdeswell, J. A., Ottesen, D., Rise, L., and Craig, J. Identification and preservation of landforms diagnostic of past ice-sheet activity on continental shelves from three dimensional seismic evidence. *Geology* 35: 359-362 (2007).

Dowdeswell, J. A., Villinger, H., Whittington, R. J., and Marienfeld, P. Iceberg scouring in Scoresby Sund and on the East Greenland continental shelf. *Marine Geology* 111: 37-53 (1993).

Esteves, M., Bjarnadóttir, L. R., Winsborrow, M. C. M., Shackleton, C. S., and Andreassen, K. Retreat patterns and dynamics of the Sentralbankrenna glacial system, central Barents Sea. *Quaternary Science Reviews* 169: 131-147 (2017).

Eyles, N., Elyes, C. H., Woodworth-Lynas, C. M. T., and Randall, T. A. The sedimentary record of drifting ice (early Wisconsin Sunnybrook deposit) in an ancestral ice-dammed Lake Ontario, Canada. *Quaternary Research* 63: 171-181 (2005).

Faleide, J.I., Solheim, A., Fiedler, A., Hjelstuen, B. O., Andersen, E. S., and Vanneste, K. Late Cenozoic evolution of the western Barents Sea–Svalbard continental margin. *Global Planetary Change* 12: 53-74 (1996).

Faleide, J. I., Gudlaugsson, S. T., and Jacquart, G. Evolution of the western Barents Sea. *Marine and Petroleum Geology* 1: 123-150 (1984).

Faleide, J. I., Vågnes, E., and Gudlaugsson, S. T. Late Mesozoic-Cenozoic evolution of the southwestern Barents Sea in a regional rift-shear tectonic setting. *Marine and Petroleum Geology* 10: 186-214 (1993).

Graham, A. G. C., Lonergan, L., and Stoker, M. S. Evidence for Late Pleistocene ice steram activity in the Witch Ground Basin, central North Sea, from 3D-seismic reflection data. *Quaternary Science Reviews* 26: 627-643 (2007).

Halberstadt, A. R. W., Simkins, L. M., Greenwood, S. L., and Anderson, J. B. Past ice-sheet behavior: retreat scenarios and changing controls in the Ross Sea, Antarctica. *The Cryosphere* 10: 1003-1020 (2016).

Hogan, K. A., Dowdeswell, J. A., Noormets, R., Evans, J., Cofaigh, O Cofaigh, C., and Jakobsson, M. Submarine landforms and ice-sheet flow in the Kvitøya Trough, northwestern Barents Sea. *Quaternary Science Reviews* 29: 3545-3562 (2010).

Huybers, P. Pleistocene glacial variability as a chaotic response to obliquity forcing. *Climate of the Past* 5: 481-488 (2009).

Ingólfsson, Ó. And Landvik, J. Y. The Svalbard-Barents Sea ice sheet – Historical, current, and future perspectives. *Quaternary Science Reviews* 64: 33-60 (2013).

Jakobsson, M., Anderson, J. B., Nitsche, F. O., Dowdeswell, J. A., Gyllencreutz, R., Kirchner, N., Mohammad, R., O'Regan, M., Alley, R. B., Anandakrishnan, S., Eriksson, B., Kirshner, A., Fernandez, R., Stolldorf, T., Minzoni, R., and Majewski, W. Geological recor of ice shelf break-up and grounding line retreat, Pine Island Bay, West Antarctica. *Geology* 39: 691-694 (2011).

Jakobsson, M., Andreassen, K., Bjarnadóttir, L. R., Dove, D., Dowdeswell, J. A., England, J. H., Funder, S., Hogan, K., Ingólfsson, Ó., Jennings, A., Larsen, N. K., Kirchner, N., Landvik, J. Y., Mayber, L., Mikkelsen, N., Möller, P., Niessen, F., Nilsson, J., O'Regan, M., Polyak, L., Nørgaard-Pedersen, N., and Stein, R. Arctic Ocean glacial history. *Quaternary Science Reviews* 92: 40-67 (2014).

Jakobsson, M., Gardner, J. V., Vogt, P. R., Mayer, L. A., Armstrong, A., Backman, J., Brennan, R., Calder, B., Hall, J. K., and Kraft, B. Multibeam bathymetric and sediment profiler evidence for ice grounding on the Chukchi Borderland, Arctic Ocean. *Quaternary Research* 63: 150-160 (2005).

Khan, M. I. Ice stream dynamics inferred from seismic geomorphology from the Bjørnøyrenna and Nordkappbanken area, SW Barents Sea. Master's thesis from the University of Tromsø: 1-121 (2013).

Knies, J., Matthiessen, J., Vogt, C., Laberg, J. S., Hjelstuen, B. O., Smelror, M., Larsen, E., Andreassen, K., Eidvin, T., and Vorren, T. O. The Plio-Pleistocene glaciation of the Barents Sea-Svalbard region: a new model based on revised chronostratigraphy. *Quaternary Science Reviews* 28: 812-829 (2009).

Laberg, J. S., Andreassen, K., and Vorren, T. O. Late Cenozoic erosion of the high-latitude southwestern Barents Sea shelf revisited. *GSA Bulletin* 124: 77-88 (2012).

Laberg, J. S., Eilertsen, R. S., and Vorren, T. O. The paleo-ice stream in Vestfjorden, north Norway, over the last 35 k.y.: Glacial erosion and sediment yield. *GSA Bulletin* 121: 434-447 (2009).

Landvik, J. Y., Bondevik, S., Elverhøi, A., Fjeldskaar, W., Mangerud, J., Salvigsen, O., Siegert, M. J., Svendsen, J., and Vorren, T. O. The last glacial maximum of Svalbard and the Barents Sea area: Ice sheet extent and configuration. *Quaternary Science Reviews* 17: 43-75 (1998).

Larsen, E., KJær, K. H., Demidov, I. N., Funder, S., Grøsfjeld, K., Houmark-Nielsen, M., Jensen, M., Linge, H., and Lysa, A. Late Pleistocene glacial and lake history of northwestern Russia. *Boreas* 35: 394-424 (2006).

Lien, R., Solheim, A., Elverhøi, A., and Rokoengen, K. Iceberg scouring and sea bed morphology on the eastern Weddell Sea shelf, Antarctica. *Polar Research* 7: 43-57 (1989).

Lisieki, L. E., and Raymo, M. E. A Pliocene-Pleistocene stack of 57 globally distributed benthic $\delta^{18}O$ records. *Paleoceanography* 20: 1-17 (2005).

Loeng, H. Features of the physical oceanographic conditions of the Barents Sea. *Polar Research* 10: 5-18 (1991).

López-Martínez, J., Muñoz, A., Dowdeswell, J. A., Linés, C., and Acosta, J. Relict sea-floor ploughmarks record deep-keeled Antarctic icebergs to 45°S on the Argentine margin. *Marine Geology* 288: 43-48 (2011).

López-Martínez, J., Rivera, J., Dowdeswell, J. A., and Acosta, J. Giant ploughmarks on the South Patagonian continental margin produced by Antarctic icebergs. *Geological Society Memoirs* 46: 273-274 (2016).

Mangerud, J., Astakhov, V., and Svendsen, J. The extent of the Barents-Kara ice sheet during the Last Glacial Maximum. *Quaternary Science Reviews* 21: 111-119 (2002).

Mangerud, J., Dokken, T., Hebbeln, D., Heggen, B., Ingólfsson, O., Landvik, J. Y., Mejdahl, V., Svendsen, J. I., and Vorren, T. O. Flucuations of the Svalbard-Barents Sea ice sheet during the last 150,000 years. *Quaternary Science Reviews* 17: 11-42 (1998).

Marfurt, K. J., Scheet, R. M., Sharp, J. A., and Harper, M. G. Suppression of the acquisition footprint for seismic sequence attribute mapping. *Geophysics* Vol. 63, No. 3: 1024-1035 (1998).

Menozzo da Rosa, E. L., Vesely, F. F., and França, A. B. A review on late Paleozoic ice-related erosional landforms in the Paraná Basin: origin and paleogeographical implications. *Brazilian Journal of Geology* 46: 147:166 (2016).

Menzies, J. Glacial geomorphology. In: Gornitz, V. (eds) Encyclopedia of paleoclimatology and ancient environments. *Encyclopedia of Earth Sciences Series.* Springer, Dordrecht (2009).

Munoz, Y. P., and Wellner, J. S. Seafloor geomorphology of western Antarctic Peninsula bays: a signature of ice flow behaviour. *The Cryosphere* 12: 205-225 (2018).

Ottesen, D., Dowdeswell, J. A., Benn, D. I., Kristensen, L., Christiansen, H. H., Christensen, O., Hansen, L., Lebesbye, E., Forwick, M., and Vorren, T. O. Submarine landforms characteristic of glacier surges in two Spitsbergen fjords. *Quaternary Science Reviews* 27: 1583-1599 (2008).

Ottesen, D., Dowdeswell, J. A., and Rise, L. Submarine landforms and the reconstruction of fast-flowing ice streams within a large Quaternary ice sheet: The 2500-km-long Norwegian-Svalbard margin (57°–80°N). *GSA Bulletin* 117: 1033-1050 (2005).

Ottesen, D., Rise, L., Andersen, E. S., Bugge, T., and Eidvin, T. Geological evolution of the Norwegian continental shelf between 61°N and 68°N during the last 3 million years. *Norwegian Journal of Geology* 89: 251-265 (2009).

Piasecka, E. D., Stokes, C. R., Winsborrow, M. C. M., and Andreassen, K. Relationship between mega-scale glacial lineations and iceberg ploughmarks on the Bjørnøyrenna Palaeo-Ice Stream bed, Barents Sea. *Marine Geology* (in press) (2018).

Piasecka, E. D., Winsborrow, M. C. M., Andreassen, K., and Stokes, C. R. Reconstructing the retreat dynamics of the Bjørnøyrenna Ice Stream based on new 3D-seismic data from the central Barents Sea. *Quaternary Science Reviews* 151: 212-227 (2016).

Polyak, L., Edwards, M. H., Coakley, B. J., and Jakobsson, M. Ice shelves in the Pleistocene Arctic Ocean inferred from glaciogenic deep-sea bedforms. *Nature* 410: 453-457 (2001).

Rafaelsen, B., Andreassen, K., Kuilman, L. W., Lebesbye, E., Hogstad, K., and Midtbø, M. Geomorphology of buried glacigenic horizons in the Barents Sea from three-dimensional seismic data. *Geological Society, London, Special Publications* Vol. 203: 259-276 (2002).

Raymo, M. E., Lisiecki, L. E., and Nisancioglu, K. H. Plio-Pleistocene ice volume, Antarctic climate, and the global $\delta^{18}O$ Record. *Science* 313: 492-495 (2006).

Rebesco, M., Liu, Y., Camerlenghi, A., Winsborrow, M., Laberg, J. S., Caburlotto, A., Diviacco, P., Accettella, D., Sauli, C., Wardell, N., and Tomini, I. Deglaciation of the western margin of the Barents Sea Ice Sheet – A swath bathymetric and sub-bottom seismic study from the Kveithola Trough. *Marine Geology* 279: 141-147 (2011).

Rohling, E. J., Fenton, M., Jorissen, F. J., Bertrand, P., Ganssen, G., and Caulet, J. P. Magnitudes of sea-level lowstands of the past 500,000 years. *Nature* 394: 162-165 (1998).

Rüther, D. C., Mattingsdal, R., Andreassen, K., Forwick, M., and Husum, K. Seismic architecture and sedimentology of a major grounding zone system deposited by the Bjørnøyrenna Ice Stream during Late Weichselian deglaciation. *Quaternary Science Reviews* 30: 2776-2792 (2011).

Sayago, J., Lucia, M. D., Mutti, M., Cotti, A., Sitta, A., Broberg, K., Przybylo, A., Buonaguro, R., and Zimina, O. Characterization of a deeply buried paleokarst terrain in the Loppa High using core data and multiattribute seismic facies classification. *AAPG Bulletin* Vol. 96. No. 10: 1843-1866 (2012).

Sættem, J., Poole, D. A. R., Ellingsen, L., Sejrup, H. P. Glacial geology of outer Bjørnøyrenna, southwestern Barents Sea. *Marine Geology* 103: 15-51 (1992).

Sejrup , H. P., Hjelstuen, B. O., Dahlgren, K. I. T., Haflidason, H., Kuijpers, A., Nygard, A., Praeg, D., Stoker, M. S., and Vorren, T. O. Pleistocene glacial history of the NW European continental margin. *Marine and Petroleum Geology* 22: 1111-1129 (2005).

Sejrup, H. P., Nagy, J., and Brigham-Grette, J. Foraminiferal stratigraphy and amino acid geochronology of Quaternary sediments in the Norwegian Channel, northern North Sea. *Norsk Geologisk Tidsskrift* 69: 111-124 (1989).

Shipp, S., Anderson, J., and Domack, E. Late Pleistocene-Holocene retreat of the West Antarctic Ice-Sheet system in the Ross Sea: Part 1 – Geophysical results. *GSA Bulletin* 111: 1486-1516 (1999).

Smelror, M., Petrov, O., Larssen, G. B., and Werner, S. (eds). Geological History of the Barents Sea. *Geological Survey of Norway, Trondheim* (2009).

Solheim, A., Andersen, E. S., Elverhøi, A., and Fiedler, A. Late Cenozoic depositional history of the western Svalbard continental shelf, controlled by subsidence and climate. *Global Planetary Change* 12: 135-148 (1996).

Solheim, A. and Elverhøi, A. Gas-related sea floor craters in the Barents Sea. *Geo-Marine Letters* 13: 235-243 (1993).

Solheim, A., Faleide, J. I., Andersen, E. S., Elverhøi, A., Forsberg, C. F., Vanneste, K., Uenzelmann-Neben, G., and Channell, J. E. Late Cenozoic seismic stratigraphy and glacial geological development of the East Greenland and Svalbard-Barents Sea continental margins. *Quaternary Science Reviews* 17: 155-184 (1998).

Solheim, A. and Kristoffersen, Y. Sediments above the upper regional unconformity: thickness, seismic stratigraphy, and outline of the glacial history. *Nor. Polarinst. Skr.* 179B:26 (1984).

Spagnolo, M., Clark, C. D., Ely, J. C., Stokes, C. R., Anderson, J. B., Andreassen, K., Graham, A. G. C., and King, E. C. Size, shape and spatial arrangement of mega-scale glacial lineations from a large and diverse dataset. *Earth Surface Processes and Landforms* 39: 1432-1448 (2014).

Stoker, M. S. and Long, D. A relict ice-scoured erosion surface in the central North Sea. *Marine Geology* 61: 85-93 (1984).

Svendsen, J. I., Alexanderson, H., Astakhov, V. I., Demidov, I., Dowdeswell, J. A., Funder, S., Gataullin, V., Henriksen, M., Hjort, C., Houmark-Nielsen, M., Hubberten, H. W., Ingólfsson, Ó., Jakobsson, M., Kjær, K. H., Larsen, E., Lokrantz, H., Lunkka, J. P., Lyså, A., Mangerud, J., Matiouchkov, A., Murray, A., Møller, P., Niessen, F., Nikolskaya, O., Polyak, L., Saarnisto, M., Siegert, C., Sigerg, M. J., Spielhagen, R. F., and Stein, R. Late Quaternary ice sheet history of northern Eurasia. *Quaternary Science Reviews* 23: 1229-1271 (2004).

Tütken, T., Eisenhaur, A., Wiegand, B., and Hansen, B. T. Glacial-interglacial cycles in Sr and Nd isotopic composition of Arctic marine sediments triggered by the Svalbard/Barents Sea ice sheet. *Marine Geology* 182: 351-372 (2002).

Vorren, T. O., Hald, M., and Lebesbye, E. Late Cenozoic environments in the Barents Sea. *Paleoceanography and Paleoclimatology* 3: 601-612 (1988).

Vorren, T. O., and Laberg, J. S. Trough mouth fans – Palaeoclimate and ice-sheet monitors. *Quaternary Science Reviews* 16: 865-881 (1997).

Vorren, T. O., Landvik, J. Y., Andreassen, K., and Laberg, J. S. Glacial History of the Barents Sea. *Quaternary Glaciations – Extent and Chronology: A Closer Look* Volume 15*:* 361:372 (2011).

Vorren, T. O., Lebesbye, E., Andreassen, K. and Larsen, K. B. Glacigenic sediments on a passive continental margin as exemplified by the Barents Sea. *Marine Geology* 85: 251-272 (1989).

Vorren, T.O., Richardsen, G., Knutsen, S. M., and Henriksen, E. Cenozoic erosion and sedimentation in the western Barents Sea. *Marine and Petroleum Geology* 8: 317-340 (1991).

Wellner, J. S., Heroy, D. C., and Anderson, J. B. The death mask of the Antarctic ice sheet: Comparison of glacial geomorphic features across the continental shelf. *Geomorphology* 75: 157-171 (2006).

Wellner, J. S., Lowe, A. L., Shipp, S. S., and Anderson, J. B. Distribution of glacial geomorphic features on the Antarctic continental shelf and correlation with substrate: implications for ice behavior. *Journal of Glaciology* 47: 397-411 (2001).

Winsborrow, M. C. M., Andreassen, K., Corner, G. D., and Laberg, J. S. Deglaciation of a marine-based ice sheet: Late Weichselian palaeo-ice dynamics and retreat in the southern Barents Sea reconstructed from onshore and offshore glacial geomorphology. *Quaternary Science Reviews* 29: Issues 3-4: 424-442 (2010).

Winsborrow, M. C. M., Stokes, C. R., and Andreassen, K. Ice-stream flow switching during deglaciation of the southwestern Barents Sea. *GSA Bulletin* 124: 275-290 (2012).

Wise, M. G., Dowdeswell, J. A., Jakobsson, M., and Larter, R. D. Evidence of marine ice-cliff instability in Pine Island Bay from iceberg-keel plough marks. *Nature* 550: 506-510 (2017).

Woodworth-Lynas, C. M. T., and Dowdeswell, J. A. Soft-sediment striated surfaces and massive diamicton facies produced by floating ice. *Atlantic Geology* 30: 241-259 (1994).

Worsley, D. The post-Caledonian development of Svalbard and the western Barents Sea. *Polar Research* 27: Issue 3: 298-317 (2008).